



QEX

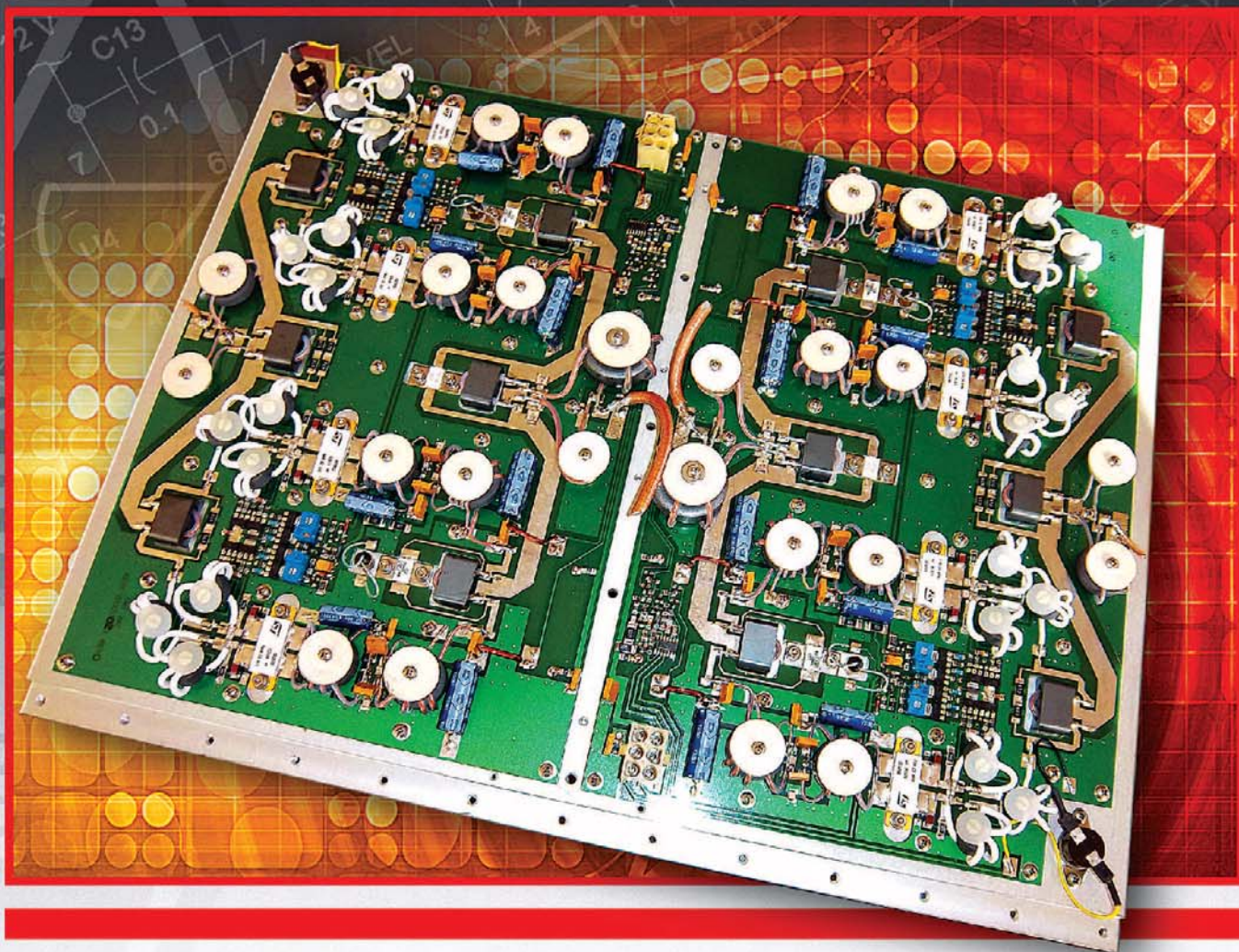
\$5

September/October 2015

www.arrl.org

A Forum for Communications Experimenters

Issue No. 292



WA1GFZ found this dual 80 MHz, 1200 W MRI amplifier board on eBay. He modified it to build a broadband linear amplifier for 160 through 6 meters.

Taking HF By Storm



The TS-480HX

KENWOOD

Customer Support: (310) 639-4200
 Fax: (310) 537-8235



Scan with your phone to
 download TS-480HX brochure.

www.kenwood.com/usa



ISO9001 Registered
 JVC/KENWOOD Corporation

ADS#27315



QEX (ISSN: 0886-8093) is published bimonthly in January, March, May, July, September, and November by the American Radio Relay League, 225 Main Street, Newington, CT 06111-1494. Periodicals postage paid at Hartford, CT and at additional mailing offices.

POSTMASTER: Send address changes to: QEX, 225 Main St, Newington, CT 06111-1494 Issue No 292

Harold Kramer, WJ1B
Publisher

Larry Wolfgang, WR1B
Editor

Lori Weinberg, KB1EIB
Assistant Editor

Zack Lau, W1VT
Ray Mack, W5IFS
Contributing Editors

Production Department

Steve Ford, WB8IMY
Publications Manager

Michelle Bloom, WB1ENT
Production Supervisor

Sue Fagan, KB1OKW
Graphic Design Supervisor

David Pingree, N1NAS
Senior Technical Illustrator

Brian Washing
Technical Illustrator

Advertising Information Contact:

Janet L. Rocco, W1JLR
Business Services
860-594-0203 – Direct
800-243-7768 – ARRL
860-594-4285 – Fax

Circulation Department

Cathy Stepina, QEX Circulation

Offices

225 Main St, Newington, CT 06111-1494 USA
Telephone: 860-594-0200
Fax: 860-594-0259 (24 hour direct line)
e-mail: qex@arrl.org

Subscription rate for 6 issues:

In the US: ARRL Member \$24,
nonmember \$36;

US by First Class Mail:
ARRL member \$37, nonmember \$49;

International and Canada by Airmail: ARRL member
\$31, nonmember \$43;

Members are asked to include their membership control number or a label from their QST when applying.

In order to ensure prompt delivery, we ask that you periodically check the address information on your mailing label. If you find any inaccuracies, please contact the Circulation Department immediately. Thank you for your assistance.



Copyright © 2015 by the American Radio Relay League Inc. For permission to quote or reprint material from QEX or any ARRL publication, send a written request including the issue date (or book title), article, page numbers and a description of where you intend to use the reprinted material. Send the request to the office of the Publications Manager (permission@arrl.org).

About the Cover

Frank Garcia, WA1GFZ, found a dual 80 MHz, 1200 W MRI amplifier board on eBay. Frank modified the amplifier board to operate on the 160 m through 6 m bands. Read about his solid state broadband linear amplifier in this issue of QEX.



In This Issue

Features

3 High Power Solid State Broadband Linear Amplifiers, a Different Approach
Francis Garcia, WA1GFZ

13 3D Simulation of a Feed Horn for a Parabolic Antenna Using Circular Polarization
J.C. Hénaux, F. Daout, P. Grassin, G.Holtzmer, A. Janon, L. Paupert, M. Phelipon

24 Radiation and Ground Loss Resistances In LF, MF and HF Verticals: Part 2
Rudy Severns, N6LF

29 Quality Factor, Bandwidth, and Harmonic Attenuation of Pi Networks
Bill Kaune, W7IEQ

36 SDR Simplified
Ray Mack, W5IFS

40 Letters

43 Upcoming Conferences

Index of Advertisers

ARRL	42, 44	Nemal Electronics International, Inc:.....	35
Down East Microwave Inc:.....	35	Quicksilver Radio Products.....	Cover IV
Expert Linears America LLC:.....	Cover III	RF Parts:.....	39, 41
Kenwood Communications:.....	Cover II	Tucson Amateur Packet Radio:	39
M ² :.....	35		

The American Radio Relay League



The American Radio Relay League, Inc. is a noncommercial association of radio amateurs, organized for the promotion of interest in Amateur Radio communication and experimentation, for the establishment of networks to provide communications in the event of disasters or other emergencies, for the advancement of the radio art and of the public welfare, for the representation of the radio amateur in legislative matters, and for the maintenance of fraternalism and a high standard of conduct.

ARRL is an incorporated association without capital stock chartered under the laws of the state of Connecticut, and is an exempt organization under Section 501(c)(3) of the Internal Revenue Code of 1986. Its affairs are governed by a Board of Directors, whose voting members are elected every three years by the general membership. The officers are elected or appointed by the Directors. The League is noncommercial, and no one who could gain financially from the shaping of its affairs is eligible for membership on its Board.

"Of, by, and for the radio amateur," ARRL numbers within its ranks the vast majority of active amateurs in the nation and has a proud history of achievement as the standard-bearer in amateur affairs.

A *bona fide* interest in Amateur Radio is the only essential qualification of membership; an Amateur radio license is not a prerequisite, although full voting membership is granted only to licensed amateurs in the US.

Membership inquiries and general correspondence should be addressed to the administrative headquarters:

ARRL
225 Main Street
Newington, CT 06111 USA
Telephone: 860-594-0200
FAX: 860-594-0259 (24-hour direct line)

Officers

President: KAY C. CRAIGIE, N3KN
570 Brush Mountain Rd, Blacksburg, VA 24060

Chief Executive Officer: DAVID SUMNER, K1ZZ

The purpose of *QEX* is to:

- 1) provide a medium for the exchange of ideas and information among Amateur Radio experimenters,
- 2) document advanced technical work in the Amateur Radio field, and
- 3) support efforts to advance the state of the Amateur Radio art.

All correspondence concerning *QEX* should be addressed to the American Radio Relay League, 225 Main Street, Newington, CT 06111 USA. Envelopes containing manuscripts and letters for publication in *QEX* should be marked Editor, *QEX*.

Both theoretical and practical technical articles are welcomed. Manuscripts should be submitted in word-processor format, if possible. We can redraw any figures as long as their content is clear. Photos should be glossy, color or black-and-white prints of at least the size they are to appear in *QEX* or high-resolution digital images (300 dots per inch or higher at the printed size). Further information for authors can be found on the Web at www.arrl.org/qex/ or by e-mail to qex@arrl.org.

Any opinions expressed in *QEX* are those of the authors, not necessarily those of the Editor or the League. While we strive to ensure all material is technically correct, authors are expected to defend their own assertions. Products mentioned are included for your information only; no endorsement is implied. Readers are cautioned to verify the availability of products before sending money to vendors.

Larry Wolfgang, WR1B

Empirical Outlook

Where Will Our Next Amateur Radio Operators Come From?

How do you share your hobby with others? Do you think about recruiting new hams? What "tricks" do you use to catch a new person's interest? These may seem like strange questions for "A Forum for Communications Experimenters." After all, aren't we really just interested in our next project, or reading about someone else's project to gain ideas for our own projects? Isn't recruiting more in the realm of license class instructors, and Amateur Radio clubs, and maybe an ARES group or those otherwise interested in public service communications? After all, *QEX* readers are primarily interested in the technical side of the hobby, rather than the "human relations" side. Or are they?

New hams (young and old) can bring fresh ideas and technical innovation to all aspects of Amateur Radio. There are lots of technically savvy folks who are not currently involved with our hobby. How many of them might become interested if they were given the opportunity? We'll never know if we don't try. I know that sometimes the response can be delayed, and often we may not even realize the impact we have had on someone, to spur them into learning more about Amateur Radio, and perhaps earning their license.

In the past, I have written about my involvement with the Boy Scouts of America, and my efforts to teach Radio Merit Badge or just get Scouts on the air talking to other hams. In November 2014 we taught a Radio Merit Badge class here at ARRL Headquarters, as part of our local BSA Council's STEM Merit Badge Day. Council Staff makes an effort to recruit various industry "experts" to host a Merit Badge class at their facilities as a way of introducing Scouts to some new activities and possible career choices. We have held a Radio Merit Badge class here at ARRL Headquarters for the past several years. One Scout in the class last Autumn had already been studying for his Technician license. The class gave him an extra spark, and within a few weeks he had contacted me and asked if I could help him find an exam session. With several other Volunteer Examiners here on the HQ staff, we invited him to come in late one afternoon, and we administered his exam, which he passed easily.

It has been fun to watch his interest and experience flourish. Not only is he active on several local 2 m and 70 cm repeaters, but he has built a 10 m dipole and hung it in the attic of his house. He has also found a schematic diagram for a simple keying interface, located the necessary parts, and soldered them together to create his own interface. He is learning about the technical aspects of Amateur Radio, and is very interested in learning more. Will this lead to a technical education and career choice? Who knows? He is still several years away from making those decisions.

I also spend one evening each week during summer camp season at a local Scout Camp teaching the Amateur Radio portion of Radio Merit Badge and getting the Scouts on the air talking with hams. This summer I had several young Scouts introduce themselves and tell me they have their license. This is very exciting because it shows that an earlier exposure to the joys of Amateur Radio has enticed them to take that next step.

I recently had a conversation with a young adult who asked if I could answer a few questions about Amateur Radio. During our conversation, I learned that this person is an IT Security professional. He told me that he was scheduled to attend a security conference in Las Vegas recently, but then was unable to attend. He learned that the conference organizers had recorded all of the presentations and put them on line for anyone to view. He searched out a couple of the presentations that he had been most interested in, but in the process of scrolling through the list of programs he came across one with a title something like "I Love Ham Radio and You Should, Too!" That caught his attention, and he started to watch the presentation. He realized that this was something he might be interested in, so he watched the entire presentation, and then followed some links at the end of the program to learn more. Soon he was studying the question pool, and becoming more excited about earning his license.

Shortly after starting to study, he learned that there was a hamfest being held near his home in about 2 weeks. When he saw that license exams would be offered there, he decided to attend. As you have probably guessed, he took his Technician Class License exam, and passed. Then he also took the General Class License exam, and passed that as well! Now he just has to wait for the exam session to be processed and for the FCC to issue his license.

This almost-a-new-ham wants to learn more about how to actually become involved with our hobby. He wants to learn how to operate, and was looking to purchase his first radio. He is already aware of software defined radio, and is anxious to learn more. He is a technically savvy person, and is probably well on his way to becoming involved with technical aspects of Amateur Radio.

My point is that by simply sharing some of what you are doing, you may inspire an interest in Amateur Radio. Whether it is a presentation at a technical conference or another group, your enthusiasm can be just the spark that ignites that passion. We are all recruiters, whether or not we are specifically trying to sign up a new ham.

High Power Solid State Broadband Linear Amplifiers, a Different Approach

The author describes how he modified some surplus amplifier boards to create broadband RF linear amplifiers.

As a member of the High Performance Software Defined radio, (HPSDR) group I found myself in need of an HF amplifier strip when the PennyLane exciter was released. The PennyLane exciter produces a very clean $\frac{1}{2}$ W signal. A two-tone display yields IMD numbers below -50 dBc, measured per MIL-STD-1311. This test method is 6 dB more conservative than the PEP method by measuring the difference between the peaks of the two-tone signals and the distortion. The two-tone method adds 6 dB, accounting for the time when both of the two tones are in phase increasing the peak by 6dB. The plan was to take this transmit quality and amplify it to a usable level.

A friend found some amplifier modules made by Erbtec from surplus MRI equipment on eBay. They had a power MMIC driving three push pull FET stages of gain, ending in a pair of MRF150s. The price was very fair so we picked up a few of them. A schematic was purchased from Erbtec. Figure 1 shows a picture of the module as purchased from eBay.

It was clear that the heat sink was too small for linear use, and half the board was filled with digital bias control and step attenuators. The power MMIC was not needed since the HPSDR exciter power was close to the MMIC output rating. I carefully sawed the board in half and removed the power MMIC. Next I mounted the amplifier section on a $\frac{1}{4}$ inch copper plate attached

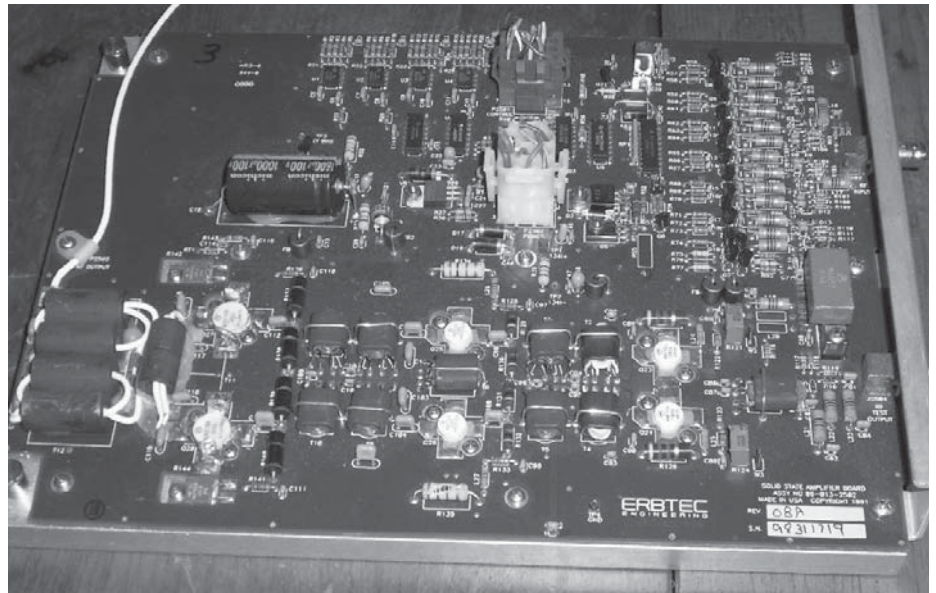


Figure 1 — This photo shows the Erbtec MRI amplifier module, as it was delivered by the eBay vendor.

to a larger heat sink. The first stage runs class A at 24 V while the driver and final need 48 V and a bias source. The LM317 regulator on the bias side of the board was moved to a proto board with 4 trim pots and isolation diodes. There is a thermistor on the board near the finals that was integrated into the LM317 control input, to act as bias temperature compensation. The bias

current only changes a few milliamps over the amplifier temperature operating range. Figure 2 shows a picture of the amplifier board mounted on the new heat sink for use as an HPSDR final amplifier strip.

This amplifier was designed to operate around 63 MHz, so it would take some changes to get it to function down to 160 meters. A number of 0.01 μ F capacitor

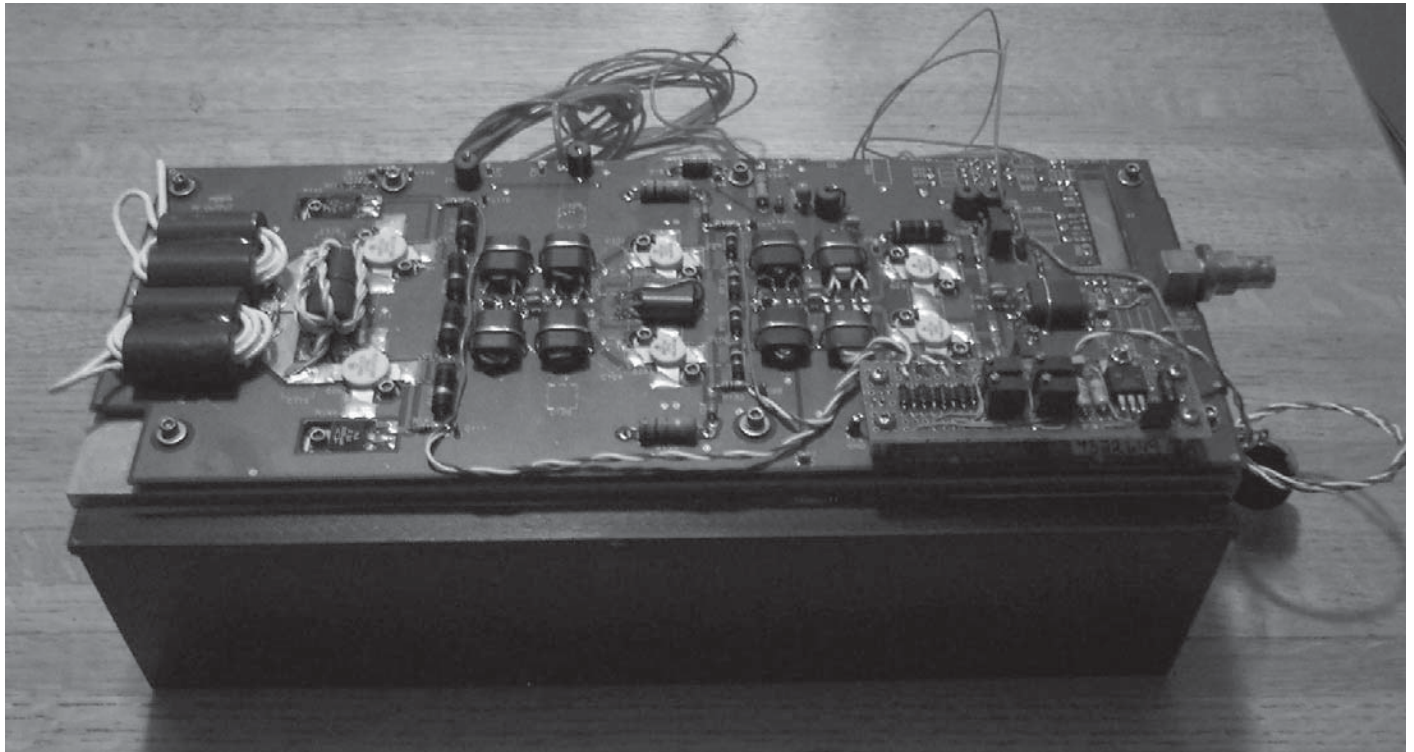


Figure 2 — Here is the modified Erbtec amplifier mounted on a larger heat sink, with the initial transformer modifications.

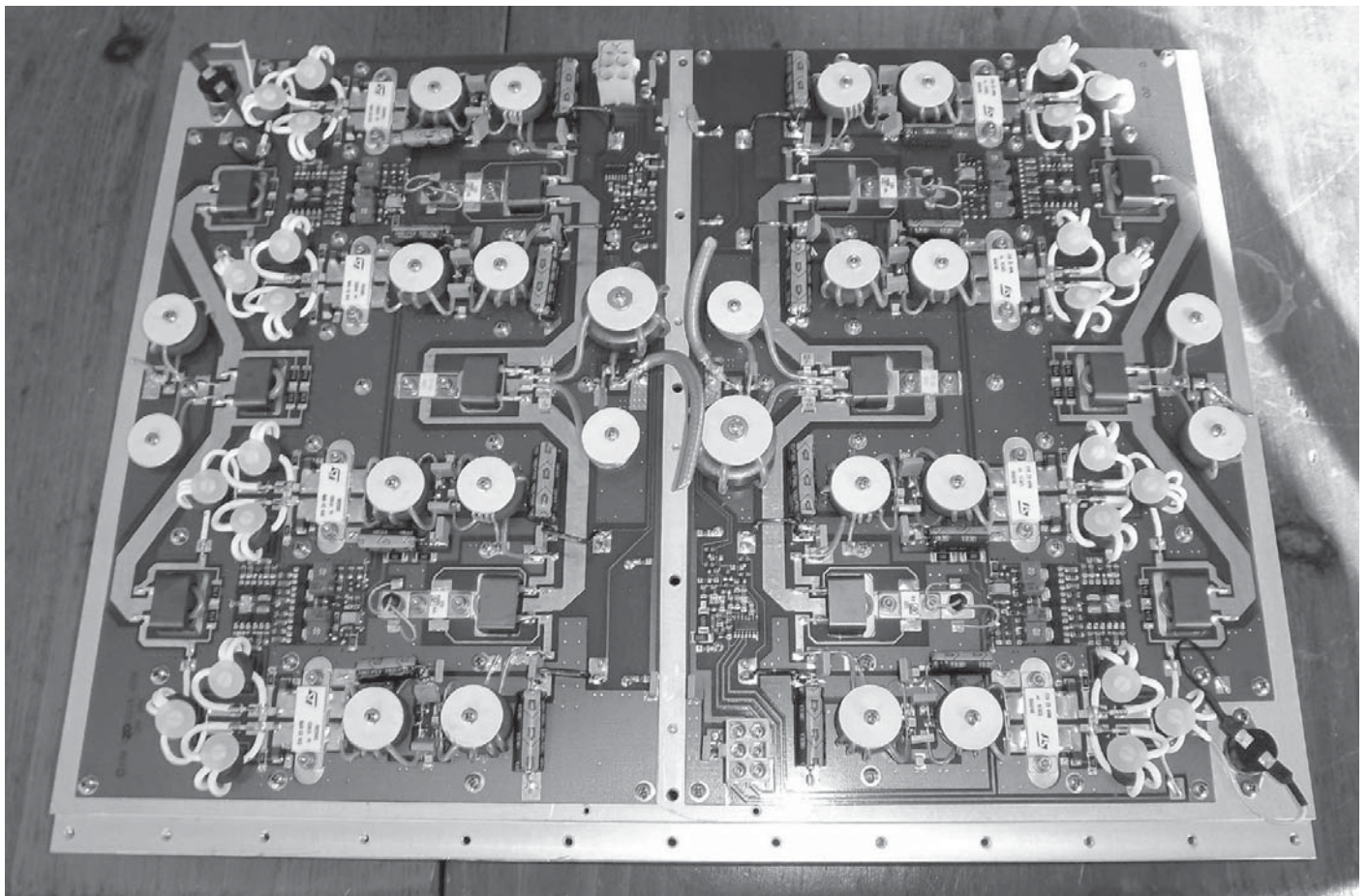


Figure 3 — This photo shows the dual 1200 W MRI amplifier module I purchased next from eBay.

values were increased to 0.1 μF . I set up a couple of power supplies on my test bench to see what the amp would do. Medical grade hardware is very nice to rework without the fear of lifting circuit board traces. The hard part was done and it should be easy to move the operating frequency down. The first step was to power the thing up and sweep it down from 60 MHz to see where the magnetics fell apart. The amplifier worked down to 40 meters and up to around 100 MHz. The Final Drain transformer and DC shunt choke got pretty warm on 40 meters.

I thought that if I doubled the turns on the output transformer and DC shunt choke, I could extend the frequency range to 160 meters. The driver and predriver seemed to work fine down to 160 meters. I added one turn to each output transformer winding and 4 turns of twisted pair on the DC shunt. It all made sense and should work great. I consulted every application note I had and gathered all the advice I could find to verify my modification.

Things now got very frustrating, but interesting. The amplifier would make power throughout the HF band but there was something strange going on. On some bands the efficiency and IMD looked good but on others, like 15 meters, it was quite bad. The second harmonic attenuation was poor, so the performance was clearly not right. I spent

a couple years on and off trying all kinds of transformers and DC shunt chokes with similar results. I had tried every suggestion with the same inconsistent results.

Then Dr. Warren Pratt, NR0V, sent me a copy of his new predistortion software for use with the HPSDR Hermes transceiver board. I built a current transformer pick up and installed it into my set up. The current transformer required some attenuation in line to avoid overdriving the receiver. The system was calibrated using an HP8640B and Boonton 42B digital power meter. This set up proved far more accurate than the Bird 43 wattmeter. The great thing about Warren's software is that you can monitor yourself in real time on the very accurate receiver display. I could check my IMD on all bands in about 15 minutes. When the predistortion software was enabled, all the IMD problems went away so life was almost good, with the third order IMD running in the -45 dBc range.

I ran my system like this for a while and also found a bigger MRI amplifier to get me up to 1200 W PEP output. Figure 3 is a picture of the dual 1200 W MRI amplifier module set up for 80 MHz. Figure 4 is my 1200 W PEP modified MRI Amplifier final. (Yes there are low pass filters.) My HPSDR Hermes transceiver and homebrew linear amplifier worked quite well. The most

expensive part was the copper heat spreaders. The poor efficiency on some bands was not all that bad since I only needed about 25 W of drive. The big amplifier had the same efficiency and IMD problem on 15 and 10 meters as the smaller one had.

The problem with a push pull amplifier is that the output devices do not source current, they only sink it. The transformer design must make up for this. When the output devices are biased in class AB, each device is turned off for over 90° of each cycle. The device sinking current in conjunction with the transformer must make up for this inactivity since there is no resonant tank circuit to provide a flywheel effect, as there is in a single frequency design. I have always felt that shunt fed DC was a band-aid for a poor transformer design but didn't understand why. The transformer should be able to perform the function of a 180° magic T and 1:4 impedance step up in one device. You would never design a push pull audio amplifier with an output transformer configured this way. A Push Pull Class AB audio amplifier has exactly the same problem as a broadband RF amplifier. High-end audio output transformers have interleaved windings as a way to improve coupling and balanced windings.

I tested a number of different DC shunt chokes and found they had a big effect on

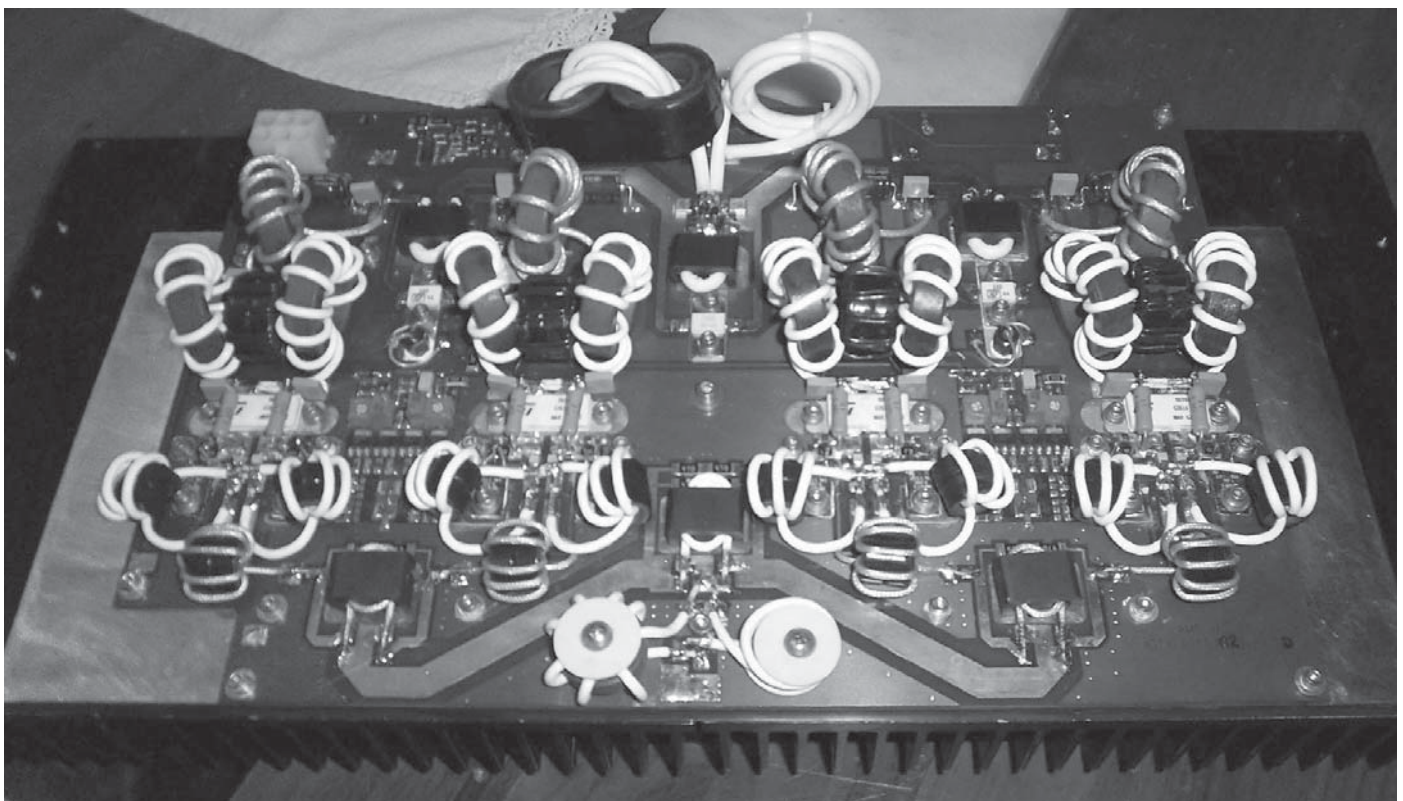


Figure 4 — This photo shows the modified 80 MHz MRI amplifier with typical broadband transformers and current shunt choke design, mounted on a larger heat sink with copper heat spreader.

IMD. When a choke had enough reactance to run at an acceptable temperature on 160 meters, the efficiency and IMD on the higher bands was poor. The Motorola EB104 amplifier has a small DC shunt choke that runs very hot. The two windings in a DC Shunt choke do not produce a balanced magnetic field, as claimed. Many designs, including the EB104, add a third winding as a source for feedback. A perfect balance would yield no feedback. A number of different simulations were tried using *LTspice*, resulting in some common information for a number of configurations. Figure 5 shows the simulated current in a DC shunt choke with about 1 A of DC offset. The two drains of a push pull amplifier must be tightly coupled to each other for good IMD performance. This was true with or without shunt fed power. Any transformer or DC shunt choke must tolerate some DC imbalance, even if wound as a transmission line transformer.

Simulation showed that when the coupling efficiency between drains was reduced below

about 97% the IMD increased. The typical output transformer design does not provide this tight coupling, resulting in distortion. The Erbtec amplifier has a transmission line transformer with no coupling between the primary windings, so the DC shunt fed choke was necessary to couple the drains. The uncoupled transformer performed poorly when DC was fed through the shields in an effort to eliminate the DC shunt choke.

The typical ham transmitter has two ferrite sleeves and brass tube primary with the common center point connected. The only coupling between drains or collectors is the common secondary winding. Adding a DC shunt choke feed helps this coupling. A number of 12 V rigs simply connect the transformer primary center tap to the power supply and rely on the 4 or 5 secondary turns to couple the drains. When transistors were low power devices the output transformer was wound on a toroid that provided tight coupling between the output devices. As power increased to the 100 W level ferrite

sleeves replaced the toroid output transformer. The sleeves provided a convenient layout with transistors at one end with DC power and output leads at the other. At 48 V, with only two secondary turns, this is a problem. This method has been proven to work at the expense of running higher reactance in the windings in an effort to increase the coupling between output devices. This extra primary reactance degrades broadband performance.

Figure 6 shows schematic diagrams of different transformer configurations. The primary connections are shown for simplification. Figure 6A is typically used in 12 V amplifiers where two ferrite sleeves form the transformer with two brass sleeves for the primary winding. The DC power is applied to the center tap. There is no coupling between the two output devices until a secondary winding is added. This was found to be the least desirable configuration with each side of the push pull acting like a pair of single ended amplifiers driving a common secondary. There is considerable waveform

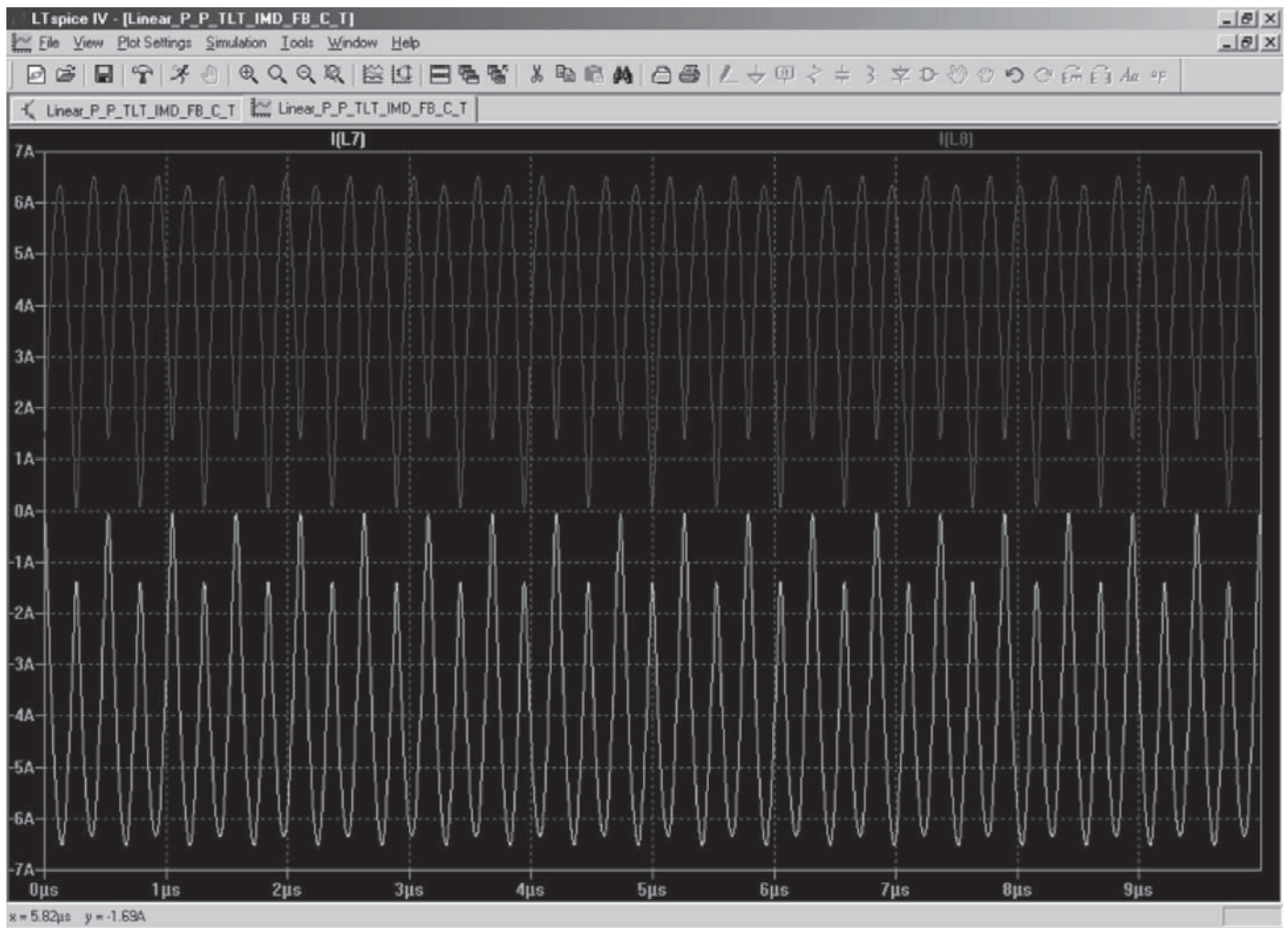
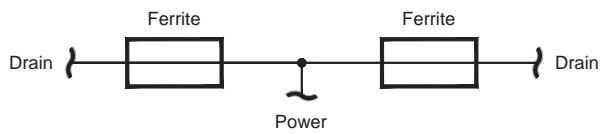
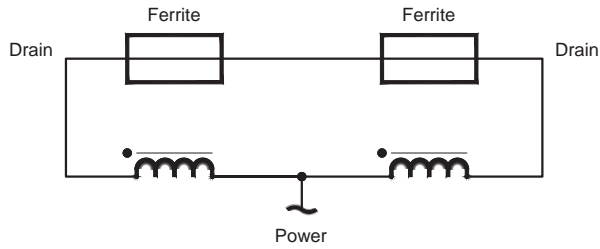


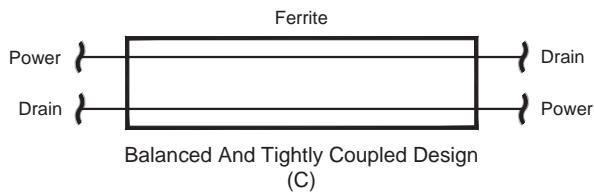
Figure 5 — This graph is the *LTspice* simulated phase currents in a DC shunt feed choke, showing the imbalance between phases that creates the feedback signal.



Transformer With No Coupling Between Output Devices (A)

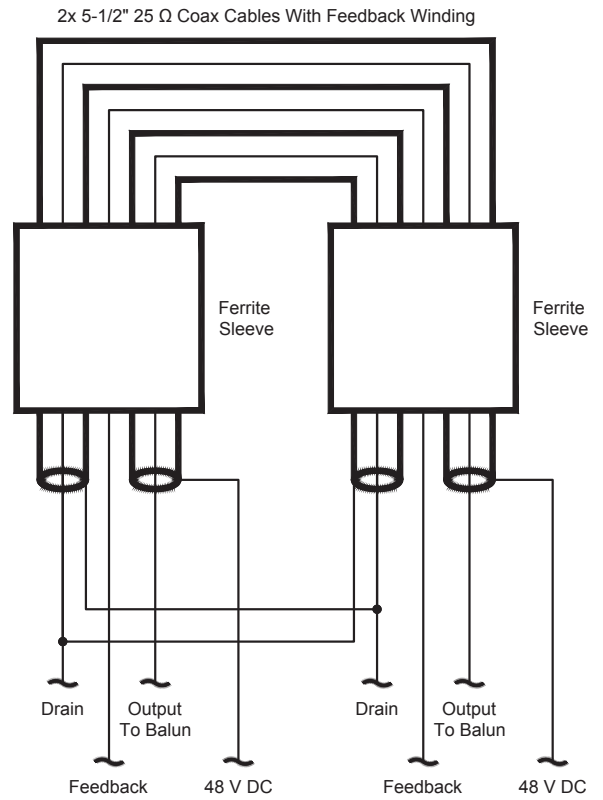


Typical Transformer Design Requiring A DC Shunt Feed Choke For Coupling (B)



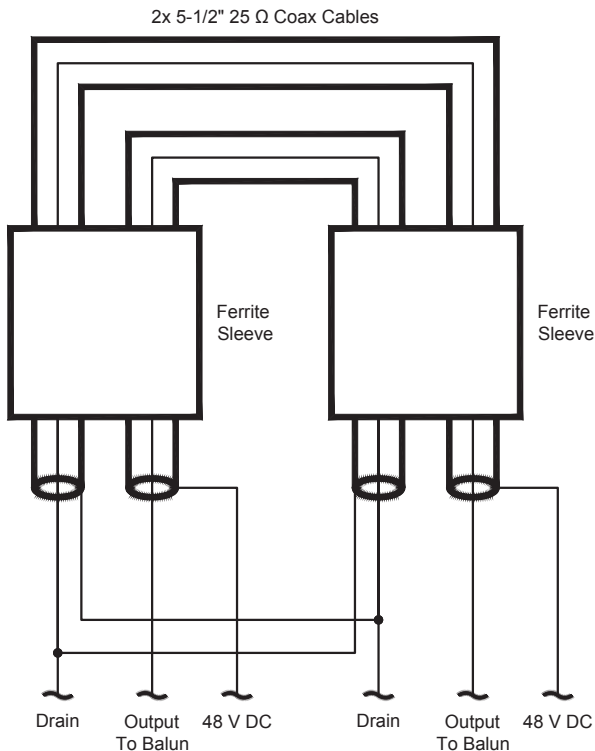
Balanced And Tightly Coupled Design (C)

QX1509-Carcia06a



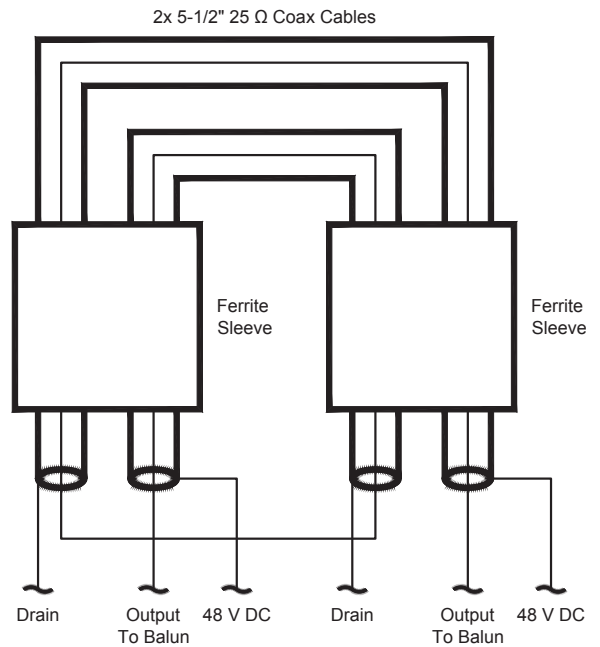
Balanced Transformer Tightly Coupled Design With Feedback Winding (E)

QX1509-Carcia06c



Balanced Transformer Tightly Coupled Design (D)

QX1509-Carcia06b



Balanced Transformer Tightly Coupled Design Wired As 1:1 Turns Ratio (F)

QX1509-Carcia06d

Figure 6 — Part A shows a transformer with no coupling between the output devices. Part B is a typical transformer design, requiring a DC shunt feed choke for coupling. Part C is a balanced and tightly coupled transformer design. Part D is a more detailed diagram of a balanced and tightly coupled transformer design. Part E is a balanced and tightly coupled transformer design that includes a feedback winding. Part F is a balanced and tightly coupled transformer design that is wired with a 1:1 turns ratio.

distortion of the signal near the positive peak. Also the second harmonic output was quite high. When one output device turns off its collector or drain voltage can rise well above twice the power supply voltage. This layout configuration with the devices at one end of the sleeves and power at the other looked nice and efficient but degraded the performance over a single output core.

As time went on I introduced the Figure 6B configuration as a way to take the DC off the transformer. The DC shunt choke provided a method of coupling the two output devices to improve the transformer balance. This reduced some of the strain on the magnetics in the transformer and core heating, at the expense of more complications, but introduced additional leakage reactance in the output circuit.

Along the way I downloaded a Power Point presentation from the Internet, which was written by people working at CERN.¹ They were building basically the same amplifier I was working on, but theirs operated between 0.5 MHz and 6 MHz. They were winding both transformer phases and the DC shunt choke on a common core. I duplicated that transformer with a type 43 core of the same size. A quick test yielded acceptable results, but above 20 meters the efficiency wasn't very good, and the IMD was around -24 dBc IP3. A Harris amplifier board from the junk box used this same transformer design with a 1:1 output turns ratio.

This actually worked quite well, but the additional reactance limited the high frequency performance. Both output drains were tightly coupled to each other with a balanced number of turns, limiting the stress on the ferrite. Figure 6C combines the function of the DC shunt choke and the transmission line transformer into a simple transformer. The tight coupling between phases produced the cleanest waveform of all three configurations. The tight coupling and short lead lengths also reduced the phase shift between the device drains. When a 1:2 transmission line transformer is wound on a common core, fewer turns are required to get minimum reactance when compared to two separate transformer cores. The only trade off is that an output balun is required.

I found that an output balun is a good idea in all configurations to isolate the secondary ground connection from the transformer. When the output transformer is at the low frequency end of the design range, uneven core heating was observed in all transformer configurations. The heating issue was improved with the addition of the balun.

The 1200 W module came with interesting output transformers set up to run at 80 MHz, as shown in Figure 3. This amplifier has four SD2932 amplifiers combined to make 1200 W. They are similar to the Motorola MRF151G, but a newer vintage. My thought was to design a transformer for the MRF150 stage amplifier, and later modify the four SD2932 amplifiers. The SD2932 amplifier

had a dual winding of three turns of semi ridged line and the DC was fed through the center conductor. The core was a 0.87 inch type 61 toroid. The center conductor was tiny, so it would never work as a linear needing to carry over 10 A of DC current. It was fine for low duty cycle MRI pulse service. The module was tested and produced poor performance below 10 meters. This transformer configuration provided tight coupling between drains on a common core.

The CERN, Harris, and SD2932 transformer observations are clearly different than the typical commercial final. The thought was a DC shunt choke is adding excessive leakage reactance to the output circuit and needed to go. Heavier coax could be used and the shield would handle more DC current. The question was finding an approach of creeping up on a workable design that wouldn't blow up the finals.

First, I consulted a very poor quality copy of the "bible" on broad band amplifier transformer design, *ECOM-2989 Broadband Transformer Design for Transistor Power Amplifiers*, by Octavius Pitzalis and Thomas P. Course.² As stated in Motorola application note AN749 and confirmed by Pitzalis and Course, the minimum coax length for a broadband transformer is about 4.5 inches on a type 61 core at 160 meters. As an interesting observation, this is about the same length of coax used in a 2 meter amplifier without ferrite. The output transformer wound on a common core is not a new idea, just not common in the typical amateur transmitter.

A transformer having 40 times the reactance as the one in the SD2932 amplifier at 80MHz would be a safe place to start. The first attempt was a pair of #22 single shielded Teflon wire cables each 36 inches long. This cable has an impedance of just below 25 Ω , and would make a good transmission line. A #24 single shielded Teflon wire has an impedance closer to 25 Ω but the conductors are small, resulting in a lot of temperature rise at 300 W. A #20 single shielded cable is also a good choice, but it has even lower impedance. I used a double stack of six (12 total) 0.87 inch type 61 toroids and threaded two windings into the core stacks. The transformer had two 7 turn windings on two core stacks. Figure 7 illustrates the initial transformer design and the final configuration.

I installed a balun on the output, consisting of 12 turns of RG316 on a single 1.25 inch type 61 toroid. When a Guanella Transmission Line Transformer is wound on a common core, a balun is required to isolate it from an unbalanced load.^{3,4} This was a small price to pay for eliminating the DC shunt choke and getting a tight coupling between drain phases. Testing showed

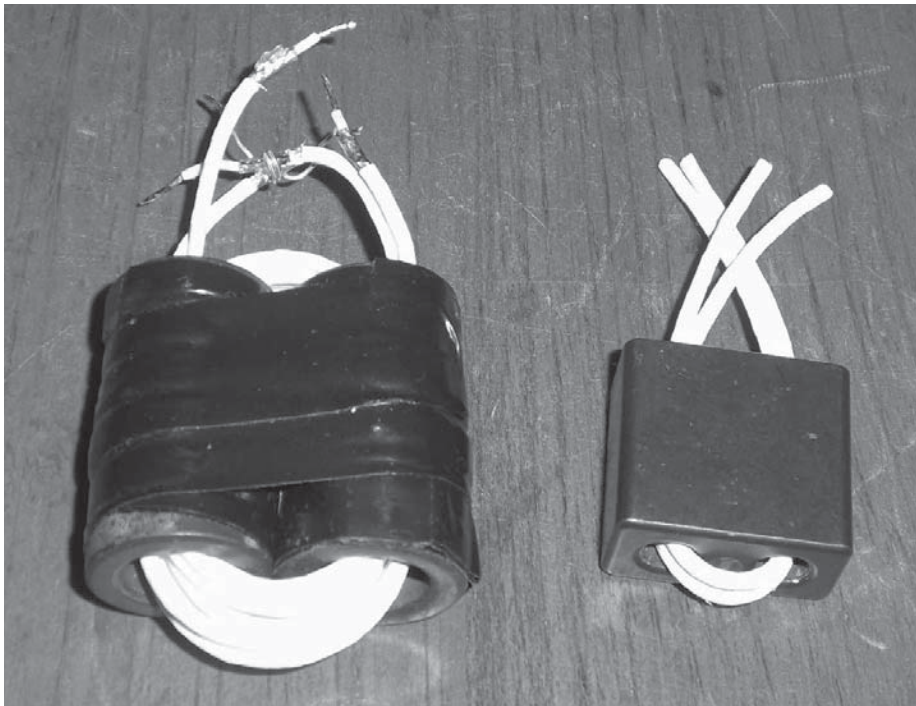


Figure 7 — This photo shows the initial balanced transformer design on the left and the final configuration on the right.

acceptable results, and there was no problem with DC on the transformer. The cores stayed stone cold and the IMD results were fairly good with IP3 on 15, 10 and 6 meters at -25 dBc. The IMD on 160 and 80 meters was quite good, with IP3 = -34 dBc.⁵ The results degraded with frequency, so it was clear the transformer was too big. This configuration was decreased in size until the IMD peak performance was shifted up to the center of the HF band. The IMD on 10 and 6 meters still needed some help so I put my attention on the driver stage. The Driver output fed DC through the uncoupled transformer but there was also a shunt choke across the drains with the center tap bypassed to ground acting as a 180° magic T. Again the transformer was a two core transmission line transformer using a pair of type 61 baluns. The shunt choke and the drain transformers were removed. They were replaced with a pair of type 43 baluns and the transformer was rewound in a different configuration. Each winding was one turn of #24 twisted pair threaded through both cores and soldered into the circuit. Now both drains were coupled to each other in the transformer, eliminating the need for the shunt winding. This last design change produced at least -30 dBc IMD on 160 through 6 meters. The DC power on the transformer eliminated the need for the extra reactance of the DC shunt choke.

The final transformer configuration in the Erbtec amplifier boiled down to three possible combinations. Each used two pieces of #22 single shielded Teflon wire, each $5\frac{1}{2}$ inches long. This pair was passed through the core material with only one turn on each phase, providing good coupling between drains. Figure 6D shows a schematic of the output transformer. It is a 1:4 impedance transmission line transformer with DC passing through the shields to power each FET. The transformer is balanced and the drains are tightly coupled to each other.

The first core configuration was a pair of the sleeves used in the Erbtec amplifier only requiring one turn of the shield for each phase. The core material is type 61, 0.68 inch \times 1.25 inches \times 0.325 inch ID. Two turns, one per phase on two sleeves measured $4.5 \mu\text{H}$, which is sufficient inductance for 160 meters at 12.5Ω drain to drain impedance. This single turn per phase using type 61 material satisfies Equation 2.6 in Jerry Sevick's *Transmission Line Transformers*, Fourth Edition (see Note 4). The $5\frac{1}{2}$ inch cable length is well below the maximum length for 6 meters. Tests show the IMD was very well behaved over the frequency range. Also, the second harmonic energy on all bands was very good, in the -35 dBc to -40 dBc range. At full power — 300 W — the transformer

temperature rise was barely above room ambient temperature.

This transformer uses $\frac{1}{2}$ the core material as the original Erbtec circuit, and did not require a DC shunt choke. An output balun with 12 turns of RG316 coaxial cable on a 1.25 inch type 61 toroid was used to isolate the unbalanced load. The second core material tested was a Fair-Rite 2843009902, two hole balun. Again only one turn through both holes was required for each phase using $5\frac{1}{2}$ inches of #22 single shielded Teflon wire for each phase. A single turn through both holes measured $8 \mu\text{H}$, so two turns would be around $32 \mu\text{H}$. The inductance of the primary was much higher but the test results were the

same. The only difference noted was that there was slightly more core heating. It was warm after running at full power.

The final configuration was to try a type 61 balun of the same size and compare the temperature rise. The type Fair-Rite 2861010002 balun also worked the same as the other two configurations but there was less core heating than the type 43. The primary inductance was measured at $4.7 \mu\text{H}$, slightly higher than the type 61 sleeves. This transformer can also be wound on a toroid with similar results. Two windings of five turns each on a 1.25 inch type 61 toroid was acceptable, but required a couple of more inches of cable on each phase. The toroid was

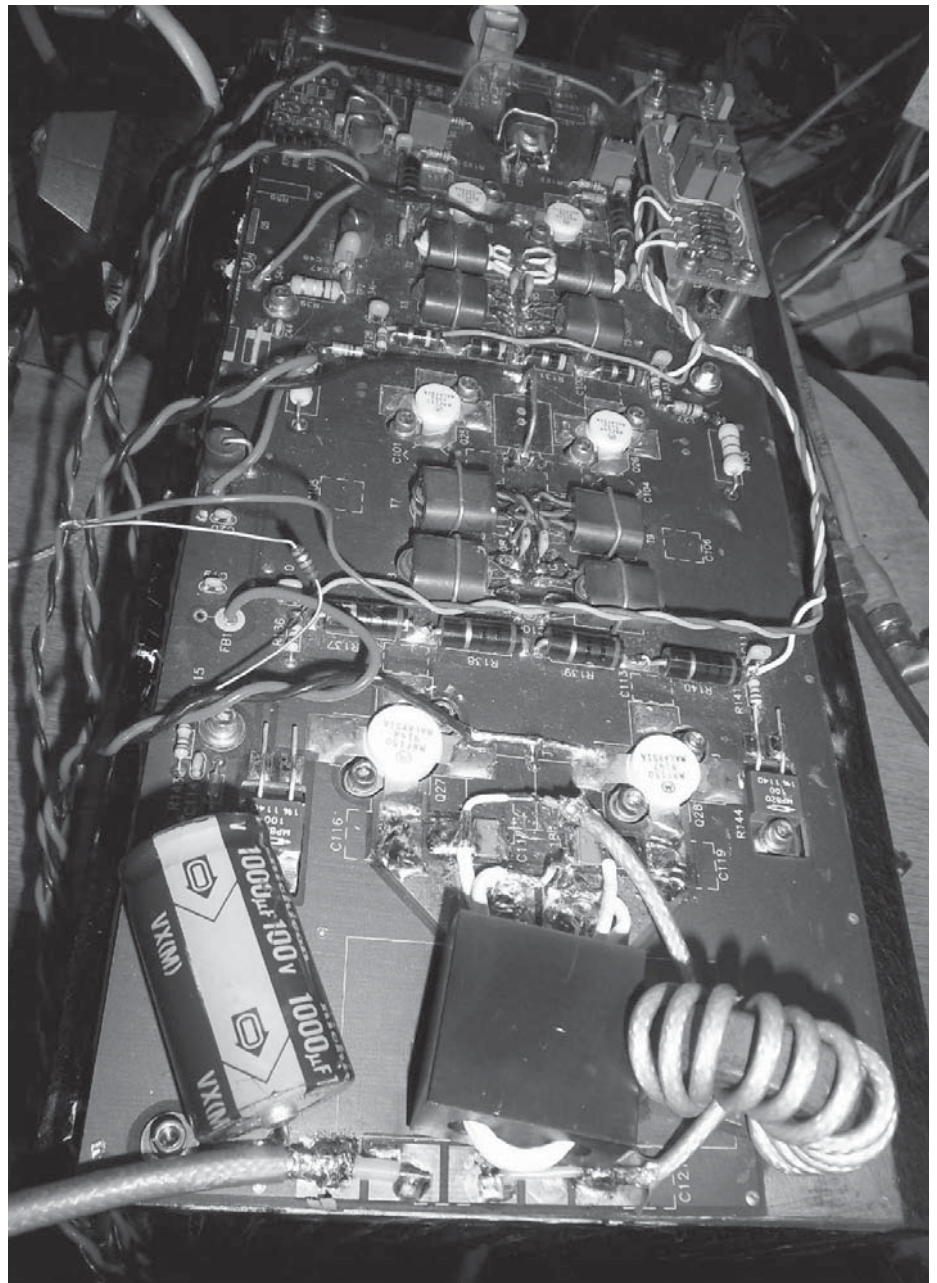


Figure 8 — Here is the final configuration of the Erbtec amplifier with a 1:1 output transformer.

a bit harder to mount with short leads.

The 2843009902 balun core was installed back in the amplifier for additional testing as shown in Figure 8. The type 61 material was slightly better, but my junk box contained enough type 43 baluns to modify the 1200 W module. This was just repeated to verify 43 material as a usable core material. A third one turn winding of #22 Teflon wire was added as a monitor winding and interfaced to an oscilloscope. A schematic of the monitor winding added to the transformer is shown in Figure 6E. The Amplifier was powered up to measure the voltage across the third winding. This voltage was measured at around $80 V_{pk-pk}$, $30 V_{RMS}$. The flux density on 160 meters is $163 \text{ gauss} = 3000 / (4.44 \times 1.8 \text{ MHz} \times 1 \text{ Turn} \times 2.3 \text{ cm}^2)$. Type 43 material has been successfully used in DC shunt chokes, so the DC offset caused by one FET conducting and the other FET turned off did not appear to be a problem.

The IMD performance does not suffer, and efficiency is acceptable, so there is no reason to increase the core size or number of turns. It is surprising that type 43 material can be driven so hard without excessive core heating.

Next, the third winding was configured to source feedback to the gates. The Erbtec amplifier comes with 25Ω feedback

resistors AC coupled between the drain and gate of each output FET. The dissipation is quite high so they were replaced with 100Ω resistors. The new third winding was configured as feedback to the gate load resistors with a pair of 160Ω series resistors. The amplifier IMD performance did not change, but the overall gain dropped slightly. The addition of this feedback was not tested with the gate to drain feedback removed.

FET amplifiers will sometimes oscillate at low levels without some light feedback directly between the drain and gate. This test was just to confirm another possible configuration. The feedback components were removed, since they had no effect on IMD performance with the 160Ω series resistors. Lower resistance values were not tested. The tight coupling between drains in the transformer appeared to be sufficient without additional feedback. There is usually a slight IMD improvement when feedback is added around the DC shunt choke in typical transformer configurations.

This new small transformer duplicated the configuration of the 80 MHz MRI amplifier scaled down to HF and will easily fit in place of the original small core if it is mounted on its end. Figure 9 is a picture of the 1200 W amplifier strip final configuration.

The 1200 W amplifier drive requirements

are well below 300 W, so the Figure 6F transformer configuration was tested in the Erbtec amplifier. The connections of the center conductors were rearranged to form a 1:1 transformer to limit the output power to around 100 W. We would get a better match by using 50Ω cable, but the 25Ω cable produced acceptable results with good IMD because of the short cable lengths. When the predistortion software was enabled, the IP3 sidebands fell into the -55 dBc range, and higher order sidebands went into the noise. At 100 W the Hermes receiver monitor signal was around -25 dBm on the receiver display, with a noise floor set at -120 dBm . At -25 dBm into the receiver, the predistortion software is actually working well below the point of optimum performance, but the signal was still very clean. Again, the IP3 was around -30 dBc (Mil Method) on all bands before the predistortion software was enabled. The 1:1 transformer puts a light load on the FETs, so there is not much gain change near the saturation point compared to the heavier load of running a 1:2 ratio. This transformer configuration also provides DC isolation so there is no need for coupling capacitors on the output to block DC.

The 2843009902 balun core was previously tested in the outputs of the 1200 W amplifier. The windings were not

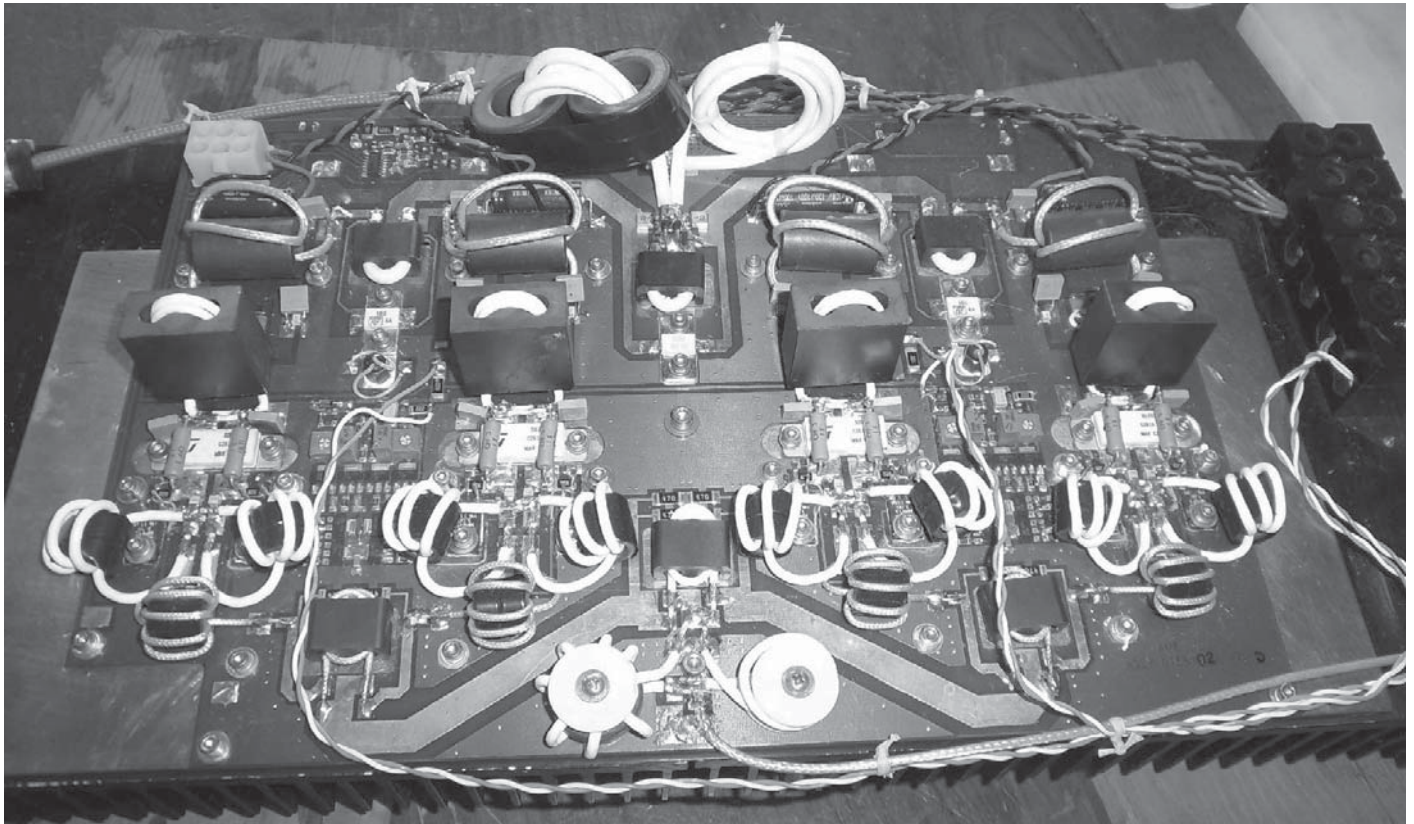


Figure 9 — This photo shows the 1200 W amplifier, with the new balanced transformers on type 43 baluns.

balanced. Each phase was wound with 1½ turns, so there were two turns in one hole and one turn in the other. Both phases wound in the balun core formed three turns in each of the two holes. This put the drains at one end of the balun and the DC power and output at the other. The core ran quite hot when DC power was passed through the shields because of the uneven turns count. The extra ½ turn reduced the flux density but the DC offset was much higher because of the additional ½ turn per phase, and caused winding imbalance. The core temperature was reduced to an acceptable level when a DC shunt choke was installed, removing DC power from the windings. The IMD and efficiency were not acceptable over the whole HF band.

The new transformer configuration was installed in the four stages of the 1200 W amplifier board for testing. The cable length is 5½ inches per phase. The balun core was wound with one turn through both holes per phase to maintain a good balance and tight coupling between drains. This new transformer replaced the DC shunt choke having seven turns of bifilar #20 wire on a 1 inch type 43 toroid and two transmission line transformers each wound with nine turns of #22 single shielded wire on each of the 1.25 inch type 61 cores. These original coax windings measured 16 inches long each.

The SD2932 Amplifier was then tested using the Erbtec amplifier strip as a low power driver with the three stages running in class A. The amplifier produced good power throughout the 160 through 6 meter frequency range, and again the balun core temperature was just warm to the touch after running at 1 kW PEP with a two tone source. The cores do not show as much temperature rise during a typical voice transmission of a couple minutes at over 1 KW PEP. The third order IMD was around 28 dBc (Mil method)

and the second harmonics were down 35 dB. The bias is set low — around 300 mA per FET. The bias current was set higher, to 500 mA per FET, resulting in an IP3 of -30 dBc on all but the 40 m and 10 m bands. At full power above 40 meters the efficiency fell off slightly, putting stress on the 30 A power supply running the two tone test.

The output baluns are three turns of RG316 in type 43 sleeves 0.68 × 1.25 inch size. The output balun cores ran warm compared to the type 61 balun, but the cable lengths were shorter. RG316 runs a bit warm above 200 W, having a small #26 center conductor. The next larger size coax is RG303, with a larger center conductor but a lot harder to work with at almost 0.2 inch outside diameter.

The last output transformer after the combiner is oversized and may be causing some efficiency issues on the higher bands, having 24 inch cable lengths. The DC input current was slightly higher during the two tone test on the higher bands so the baluns and output transformer still need some more work. The extra heat just made the heat sink temperature a bit warmer.

The amplifier has been used on 160 through 6 meters with good reports. Table 1 shows the IMD test results, with the signal levels measured on the receiver display with the coupling factor of the feedback hardware. The power supply capability did not allow two tone tests at 1 kW PEP on the higher bands because of a slight degrading of efficiency. The amplifier and power supply functions at full power under voice conditions. The limited power supply capacity is presently the only protection for the amplifier. The power supply is rated for 30 A_{RMS}, so expecting it to function at 50% overload is really pushing things. It is a constant voltage transformer used as a telephone system battery charger, so at full

power the regulation is poor.

Simulation showed the best IMD performance is when the FETs are biased around 650 mA each, but this would have increased the stress on the power supply. When the amplifier was tested over the air on multiple bands with the predistortion software enabled, the two tone IMD dropped to around -40 dBc measured by local hams. The IMD was around -50 dBc under voice conditions. There is 26 dB of attenuation between the Hermes transceiver and the driver amplifier. This may allow the elimination of one of the four stages of amplification in the future, which should improve the IMD slightly. Typically, IMD is measured by the PEP method in commercial equipment, meaning the IMD performance numbers in Table 1 would be improved by 6 dB.

The Driver performance is included with each output FET biased at 500 mA, and the output transformer configured with a 1:1 ratio. The reason for increased current on 6 meters is suspected to be due to the cable impedance in the output transformer. When configured as a 1:2 transformer, the efficiency was comparable to the other bands. At this low power the extra dissipation is not an issue.

A 1:4 impedance step up output transformer is commonly used in a 300 W 48 V amplifier. When higher ratios are required a second transformer can be cascaded after the drain transformer to achieve the final ratio. This method is used in the Erbtec driver stages, with two 2:1 transmission line transformers cascaded to get a 16:1 step down. Other amateurs have successfully used this method to build higher step up transformation ratios. Roderick Blocksome, KØDAS, published an interesting article on transformer design that illustrates cascaded transformers (see

Table 1
Amplifier Test Results

Band	PEP Output W	PEP Output	Coupler Factor	2 Tone Level	Distortion Level	IP3 Distortion	DC Current
160m	1258	61 dBm	-69 dB	-14 dBm	-44 dBm	30 dBc	23 A _{RMS}
80m	1258	61	-69	-14	-44	30	23
40m	1258	61	-69	-14	-42	28	24
20m	977	59	-69	-16	-46	30	24
15m	977	59	-68	-15	-45	30	25
10m	977	59	-68	-15	-43	28	24
6m	977	59	-68	-15	-47	32	24
<i>Driver Amplifier Strip 1:1 Turns Ratio Transformer, 500 ma Bias Each Output FET</i>							
160m	100	50	-69	-25	-66	41	2.0 A _{RMS}
80m	100	50	-69	-25	-62	37	1.8
40m	100	50	-69	-25	-62	37	2.0
20m	100	50	-69	-25	-62	37	2.2
15m	100	50	-68	-24	-63	39	2.5
10m	100	50	-68	-24	-66	42	2.4
6m	100	50	-68	-24	-63	38	3.7

Note 5). Jerry Sevick, W2FMI, also used cascaded transformers to achieve large transformation ratios (see Note 4). There is no reason the configuration could not be modified to eliminate the DC Shunt choke, and feed DC through the primary, as long as the transformer is wound in a balanced configuration.

In the case of high power, larger cores such as sleeves with larger inside diameters would allow larger cables to support higher current and lower operating impedances. Larger diameter cores with longer magnetic path lengths would also support more DC offset when running higher operating currents with larger FETs. Stacks of toroids could replace the ferrite sleeves as long as the cable coupling to the core is maintained. The cable could also consist of multiple cables in parallel to get to the desired impedance and low resistance for the power required. Type 61 material would be a better choice at high power because it will handle greater DC offsets than type 43, and has lower core losses.

The final cable length in the modified output transformer is 5½ inches per phase, which is the same length used in 2 meter applications. It should be possible to build an amplifier that operates from 160 through 2 meters with a single gain stage if the layout is modified to couple both phases of the transformer. Transformer cables with sufficient ferrite loading would increase the reactance high enough to support 160 meters and have a loss low enough to operate on 2 meters. Imagine a pair of 1200 W FETs with a 1:2 drain transformer followed by a 1:2 or 1:3 transmission line transformer producing the legal limit from 160 through 2 meters. This wide band operation is commonly available in the commercial world, where broadband amplifiers cover even wider frequency ranges. IMD could be improved if the two drain transformer cables in a 2 meter amplifier were coupled to each other rather than floating in two isolated loops of coax cable. This floating loop configuration is typical in many VHF amplifiers. A layout change would allow this drain coupling method. Type 43 losses might be too high for 2 meters, so type 61 or type 67 would be a better choice.

The three stage Erbttec amplifier performance drops off above 80 MHz, so the driver stages would need to be modified to cover 2 meters. The driver stage transformers are wound with twisted pair transmission line and may not be suitable for 2 meter operation. The drive power drops off quickly,

so it is not a final stage efficiency issue. The HPSDR Hermes transceiver operates up to 6 meters, so 2 meters was outside the scope of my requirements. The 1200 W amplifier module should operate down to 600 meters with the type 43 cores in the transformers, but it was not tested because the input transformer would need to be modified.

Additional Configurations Possible

When considering the 1:1 primary turns ratio transformer, it may be possible to use two twisted pair shielded, twisted triple shielded or twisted quad shielded cables as the two conductors, with the shields acting as the coupled primary and the center conductors configured as a 1:2, 1:3 or 1:4 step up secondary. This would increase the length of the secondary and may affect high frequency performance. Also this could be built with multiple single shielded conductors, with the shields in parallel and center conductors in series. Only the single conductor shielded configuration was tested. This method would be usable in a 12 V DC final requiring four secondary turns. The only issue would be that the primary is two turns, so the secondary would need eight turns. This long secondary may be a problem, but maybe smaller cores could be used at this low impedance to offset the additional cable length with two primary turns.

Conclusion

A DC shunt feed choke is not required if the output transformer is a balanced transmission line transformer design. This means both primary phase windings must pass through all sleeves or toroids of an output transformer with an equal number of turns. This provides tight coupling between drains, resulting in improved broadband IMD performance and even harmonic attenuation. Another benefit of winding a transformer on a common core is the reduced length of cables, since less turns are required to achieve minimum reactance low frequency performance, as pointed out by Jerry Sevick, W2FMI (see Note 4). These reduced cable lengths improve high frequency losses due to reduced phase shift between the two drains.

This transformer configuration can also provide a source of feedback by adding a third winding. The offsets between drain phases are just like those present in the DC shunt choke. These offsets would be aggravated by slight differences between output devices. The feedback winding is operating as a flux transformer because it is

operating in the same phase as the primary winding. This transformer configuration uses the shields to perform the function of the DC shunt choke as a coupled pair 1:1 transmission line transformer, while the connection of the center conductors provides the 1:2 turns ratio step up transmission line transformer that carries the RF power. The simulations were run using *LTspice*. It was a challenge to simulate a transmission line transformer with DC current running through it. The transmission line simulation treats DC like a series resistance equal to the impedance. I'm not sure if the simulations of the final design are accurate, but testing proved this configuration to be superior.

This project is a work in progress with a goal of building a bullet proof, low IMD solid state final amplifier. The 1200 W amplifier in the military and commercial world would be rated at 400 W. One of my long term projects is to mount four of these modified MRI boards on a large heat exchanger into a combiner. The bias current would be increased and drain voltage will be reduced to around 40 V for added protection. The third conductor feedback method will also be explored with lower series resistance. My goal is to point out my transformer design observations to anyone who wants to build a broadband amplifier with two or four modern 1200 W FETs.

Frank Carcia, WA1GFZ, has been licensed since 1966. He is an avid home brewer for 50 years, mainly interested in receiver design. Some of his other interests include gardening, woodworking and metal working. Frank has been employed in the electronics industry for 40 years in test, field service and design. He is presently employed as an EMC engineer at United Technologies Aerospace Systems (UTAS).

Notes

¹M. Paoluzzi, High Power, Wideband, Solid-State Amplifiers for Leir and J-Parc RF Systems, 28 March 2008.

²Octavius Pitzalis, Thomas P. Course, *ECOM-2989 Broadband Transformer Design for Transistor Power Amplifiers*, July 1968.

³Philips Application notes ECO6709, ECO7213, AN98032, *Power Amplifier Design*, March 23, 1998.

⁴Jerry Sevick, W2FMI, *Transmission Line Transformers*, Fourth Edition, SciTech Publishing, Dec 2001.

⁵Roderick K. Blocksome, KØDAS, "Practical Wideband RF Power Transformers, Combiners, and Splitters," *Proceedings of RF Expo East*, 1986.

3D Simulation of a Feed Horn for a Parabolic Antenna Using Circular Polarization

The authors present a feed horn design that produces circular far-field radiation from a parabolic dish antenna. The design is a matter of performance trade-offs.

Abstract

We design a feed-horn model for a parabolic antenna, using circular polarization. This source is intended for EME communications in the 23 cm band. The design method, using 3D simulation software is emphasized. The source is decomposed into three separate parts and their interactions analyzed.

Introduction

Moon-bounce communications (Earth-Moon-Earth, or EME) uses very high quality transmit and receive components, in order to compensate for the tremendous attenuation of the signals (about 275 dB).¹ The parabolic antenna, the heart of the system, must be efficiently illuminated by the source, located at the focus, to correctly use the available power when transmitting and receiving. This work is the result of a collaboration with the "Radio-Club de St Quentin en Yvelines," F6KRR, and has been carried out in the frame of a student exercise at the Institut Universitaire de Technologie of Ville d'Avray (University of Paris 10th).² The goal was to design and realize a focal source for EME communications that uses a circular polarization of the waves, at a frequency of 1296 MHz. The parabolic antenna has a f/D ratio of 0.4 (where f = focal length) and a

diameter, $D = 3.05$ m. Our goal was for the following results:

- The coaxial ports of the source (port 1 or Tx, and port 2 or Rx) must be well matched (S_{11} , S_{22} magnitude < -20 dB) in order to optimize the power transfer ratio.
- The isolation magnitude between these two ports: S_{21} and S_{12} must be < -25 dB
- The circularity (ratio of the axes of circular polarization measured in the remote field) must be less than 1 dB (whatever the emission angle).
- The efficiency of the whole source and parabola (the power emitted by the antenna divided by the power entering the Tx port) must be the best possible.

The source is derived from the work of G. Köllner, and has kept its main options.³ Our study has been carried out with the HFSS software from Ansoft. In addition, the software *Feedpatt*, written by Paul Wade, W1GHZ, has been used for the efficiency estimation.⁴

We propose an original conception method, which makes use of the symmetry plane of the source. On the basis of this paper, a source has been built for 2320 MHz, and the measurements results will be published later.

Description of the Source

The focal sources now used for the circular polarization emission, are complex realizations, which embodies three distinct

elements, whose electrical behaviors are partly independent.⁵

- A waveguide and its "septum": a circular waveguide is used, which only allows the HE_{11} mode to be propagated. For the chosen diameter: 164 mm, a HE_{11} mode is possible between 1180 and 1400 MHz. Along its length, in the symmetry plane, it is split by a septum. This conducting plane, constituted of successive steps, converts the linear polarization of the signal applied (via port 1 or Tx) perpendicularly to the septum into a circular polarized signal during emission. The inverse is true when receiving towards port 2 (or Rx). (The moon bounce inverts the circular polarization direction).

- A radiator: a horn or a ring or just the aperture of the cylindrical guide, whose role is to shape the beam emitted from the parabola focus, in order to efficiently "fill" the parabolic antenna area. The "choke-ring," "Kumar choke," or "VE4MA choke," is often used in recent realizations for its better efficiency of the whole: source and antenna.^{6,7}

- Two injection probes (transmit and receive, ports 1 and 2), are located in a symmetric position relative to the septum plane, at the opposite side from the radiator. They make a transition between the feeding coaxial cables and the waveguide body in which the septum is located. In their simplest shape they are cylindrical rods, (acting as antennas) with lengths of about $\frac{1}{4} \lambda$. The

¹Notes appear on page 21

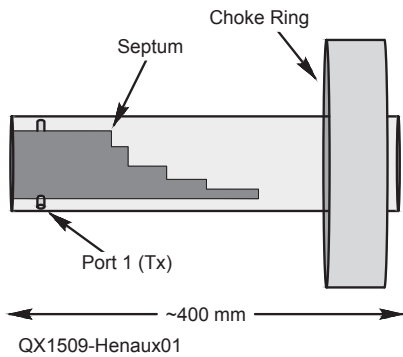


Figure 1 — Circular waveguide focal source using a Kumar choke.

signal introduced into the port 1 (resp. 2) will produce the emission of a left (resp. right) circular wave.

Simulation Method

Our preliminary simulations have shown that the far field circularity as the matching and isolation parameters depend primarily on the septum, whereas the efficiency depends mainly on the radiator size and geometry. The injection probes may be treated afterwards as they only influence the matching properties of the source. Therefore, the three parts of the source have been studied separately. This method already has been suggested by P. Hazdra, R. Galuscak, and M. Mazanek in their presentation, “Optimization of Prime-Focus Circular Waveguide Feed with Septum Polarization Transformer for 1.296 GHz EME Station,” at the European Conference on Antennas and Propagation in 2006.⁸

Stage 1: The Septum Circularity, Isolation, and Match

The recent realizations make use of a scaled-septum, as shown in Figure 1. To our knowledge, there is still no analytic method to calculate the septum shape and size. Therefore, the use of a simulation facility is absolutely necessary. MiCIAN provides a free version of their *μWave Wizard* simulation software.⁹ Ansys *HFSS* software, as well as Computer Simulation Technology (CST) *3D Electromagnetic Simulation Software* provide finite elements, or mode matching simulations.^{10,11} Many actual realizations may be taken as a starting point to a study, however. (See Notes 3 and 5.)

The idea is, given an incoming wave entering perpendicularly to the septum, to generate a wave parallel to it when this incoming wave moves forward towards the guide mouth. R. Behe and P. Brachet wrote about a “Compact Duplexer-Polarizer with Semicircular Waveguide,” in the *IEEE Transactions on Antennas and Propagation*, in August 1991.¹² M. H. Chen and G. N.

Tsandoulas published “A Wide-Band Square-Waveguide Array Polarizer,” in the *IEEE Transactions on Antennas and Propagation*, in May, 1973.¹³ This parallel wave has a slower phase velocity than the perpendicular one, and the two orthogonal waves have no interaction. If the incoming power is equally divided, and the phase difference is 90°, then the wave transmitted out of the guide is circularly polarized. For a given frequency, there is probably no unique solution leading to a particular realization of the septum.

Until now, the actual realizations derive from existing near solutions, (the oldest used a square waveguide), by means of a simulation and optimization. An important property of the septum circular polarizer is the existence of a symmetry plane that allows

us to consider the propagation as the sum of even and odd modes. Chen and Tsandoulas have taken advantage of this property when they designed their square guide polarizer (see Note 13). Unfortunately, they had no opportunity to use 3D simulation, and their method was purely experimental. Z. Samek, OK1DFC, successfully designed other square guide polarizers, as described in “Feed for Parabolic Dish With Circular Polarization,” on a CD-ROM for the 10th International Conference, in 2002 in Prague.¹⁴ Following the work of Chen and Tsandoulas, the case of circular waveguide was extrapolated. (See Notes 3, 7 and 8.)

With the 3D simulation methods, we can apply a similar method, isolating the polarizer (septum) from the injection probes

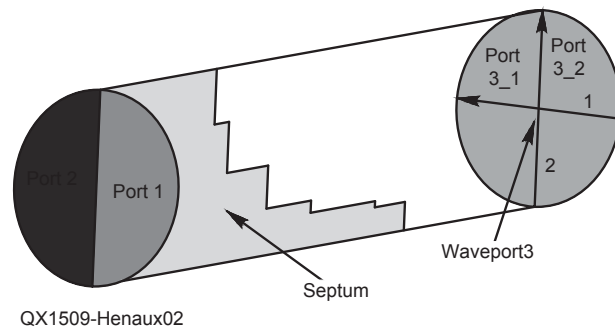


Figure 2 — The polarizer is a four port device, the two ports 3-1 and 3-2 (mouth of the guide) are perpendicular. The 3-2 port is parallel to the septum.

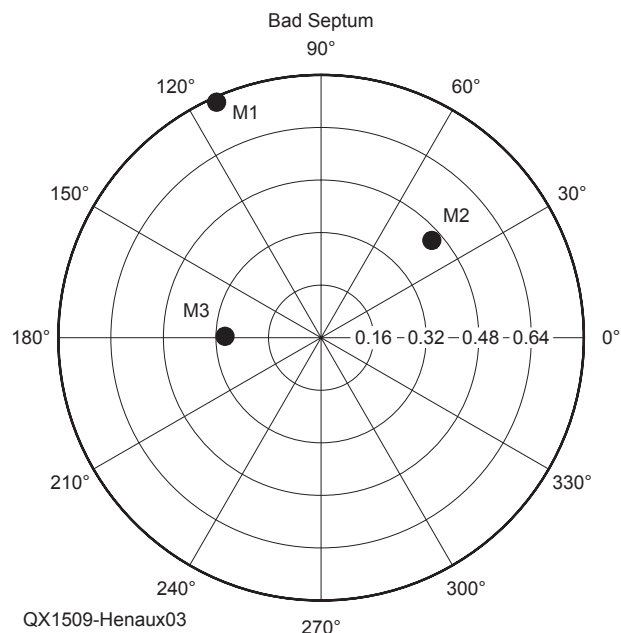


Figure 3 — These septum steps have bad sizes. The m1 and m2 markers represent the transmitted waves to the output ports 3_1 and 3_2. The same m3 marker gives the values of the waves reflected towards the Tx port (port 1) and transmitted to the “isolated” port Rx (port 2). These two waves are not null but are equal.

and from the radiator (horn, ring). In that way, it is possible to get a good circularity out of the mouth of the guide, and a perfect match and isolation of the access ports by optimizing the step dimensions of the septum. For this, in that stage, the polarizer is modeled in Ansys HFSS as a four-port device. See Figure 2. The two ports, 1 (Tx) and 2 (Rx) are supposed to be fed by the same semicircular guides, while port 3 (the mouth of the waveguide) is divided into two sub ports: 3-1, perpendicular to the septum and 3-2, parallel to the septum. There is no radiation, all the ports being matched, and we may define generalized S parameters characterizing the behavior of the polarizer alone. The guide length is chosen longer than the septum, allowing the circularly polarized field to set up before reaching port 3.

The septum is constituted of 5 to 6 steps, and its shape can be seen in Figures 1 and 2. The length and height of the steps have been optimized using Kollner's work as a starting point. (See Note 3.) Kollner used the spreadsheet of Samek (see Note 14), originally built for square guide septums, from the paper of Chen and Tsandoulas (see Note 13).

In our 3D simulation, the analysis of Chen and Tsandoulas has been verified and used as a guideline for the optimization: at the design frequency, 1296 MHz, we first consider the case of a non-optimal septum (bad sizing of the steps), and a wave coming from port 1. See Figure 3. The wave perpendicular to the septum is fully transmitted to the port 3-1. The wave parallel to the septum is partly transmitted to the mouth of the guide into port 3-2, and partly reflected by the septum. The reflected power is divided into two identical waves reaching port 1 and 2. For that reason, we can see that the magnitude of S_{11} (m3 marker) is not zero, and in the same way, the magnitude of S_{21} (under the same m3 marker) has the same complex value. Therefore, the waves transmitted to port 3-1 and 3-2 (m1 and m2 markers) have different magnitudes and their relative phases differ from 90° . As a result, the power not reflected by the septum is transmitted to the parabola with an elliptical polarization.

When the septum is correctly dimensioned, as shown in Figure 4, there is no reflection (m3 marker). The injected power is fully transferred from the aperture of the guide to the parabolic antenna. The two waves (m1 and m2 markers) give rise to a circularly polarized emission.

This result has been obtained by means of a manual optimization of the septum step sizes. The higher steps are the most sensitive.

It is handy to define a "circularity" variable as the complex ratio of the waves into 3-1 and 3-2 ports. This variable is $\pm j$

(with the chosen reference) when the septum has correct dimensions.

The response of the septum depends weakly on frequency, as can be seen in Figure 5, and a 100 MHz frequency band

is capable of being tuned to account for this dependence.

Stage 2: The Radiator, Isolation of the Source, Efficiency

Generally speaking, the diameter, d , of

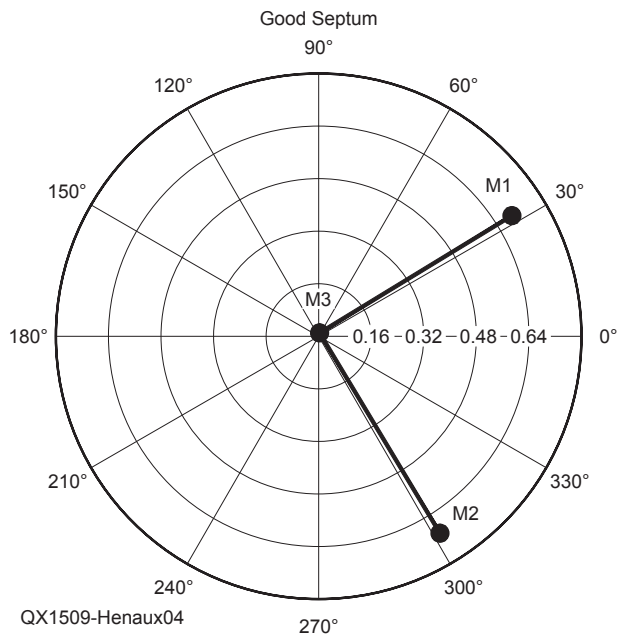


Figure 4 — The steps are correctly sized. The markers m1 and m2 represent, in the complex plane, the waves transmitted to the ports 3-1 and 3-2 (aperture of the circular guide). These waves are equal and their phase difference is 90° . The same marker, m3, gives the value of the reflected wave to the input port 1 (Tx) and the value of the transmitted wave towards the "isolated" port 2, (Rx). These two waves have a null amplitude.

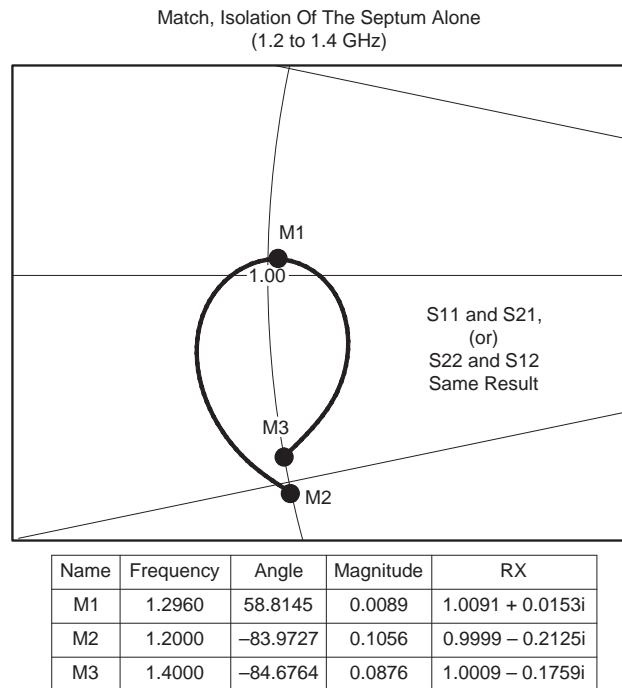


Figure 5 — The septum is studied alone, around the design frequency, 1296 MHz. After a correct choice of the step sizes, the reflection and isolation are less than 0.01 (-40 dB) at 1296 MHz, and remain near -20 dB from 1200 to 1400 MHz.

the mouth's source must be sized, taking into account the frequency to diameter (f/D) ratio (the "aperture") of the parabola to be used.¹⁵ The wider "open" the parabola is (low f/D), the wider the beamwidth must be. This beamwidth, α , is calculated for a -6.5 dB attenuation on the edge of the parabola. (It is commonly assumed that the edge of the parabola is efficiently illuminated when it receives a -10 dB power under the axial illumination, a $+3.5$ dB correction is applied for the nonspherical shape of the antenna.¹⁶

For a $f/D = 0.4$, the edge of the parabola is seen from the focus under a total angle $\alpha = 2 \times 66^\circ$. On the other side, applying the rule for radiating surfaces, the emitted beamwidth grows with λ / d .^{17,18} (λ is the free wavelength, d is the dimension of the radiating aperture, the wave is supposed to be plane.) Therefore, the diameter, d , plays a major role in the determination of the efficiency, η , for the whole antenna (source plus parabola). Furthermore, for any radiator chosen for the source, it gives rise to a non-null reflection coefficient, ρ , seen by the guide. This reflection has two drawbacks: it is the cause of power loss, and a wave is

returned to the port 2. This wave goes to port 2 only because the direction of the circular polarization is inverted in that reflection. This power, observed in port 2 (S_{21}) is interpreted as an isolation defect between port 1 (Tx) and 2 (Rx).

The determination of the efficiency, η , for the whole transmission, involving both source and parabola, makes use of the program *Feedpatt* by Paul Wade, W1GHZ (see Note 4). This program integrates on the parabola area, the source power calculated by *HFSS* (the far field condition is fulfilled for these conditions — see Notes 17 and 18). The total emitted power is taken into account whatever the circularity defects are (this assertion is justified for the radiation part received by the parabola).¹⁹

Feedpatt draws the radiation diagram of the source and calculates the efficiency of the whole antenna (power received by the parabola divided by the total power emitted by the source). It takes into account the illumination losses: bad filling (illumination), spillover (power not used by the parabola) and feed blockage (the shadow of the source). The program gives the theoretical

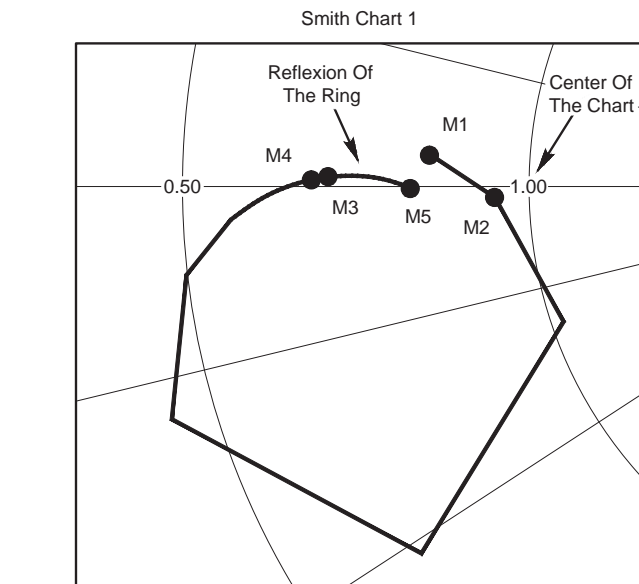
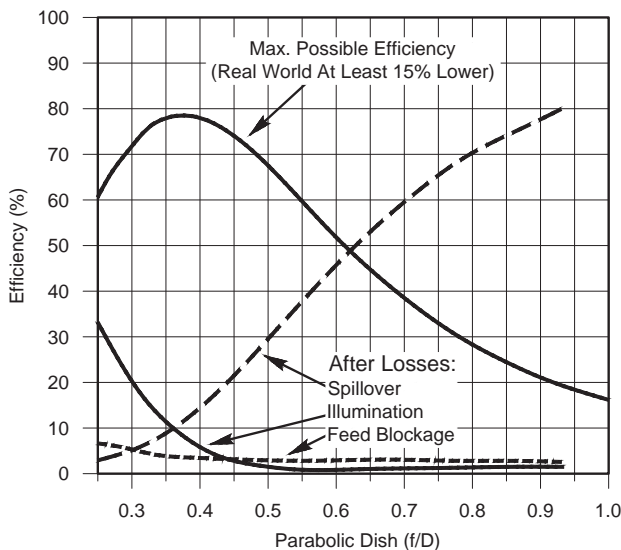
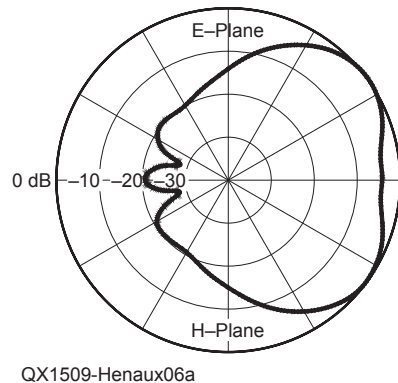
efficiency of the power transfer between the source and the parabola (without including Joule losses, geometric defects, circularity defects, reflection between the source and the parabola, position of the phase center relative to the focus and other factors). Figure 6 shows the results of the *Feedpatt* calculation.

Several kinds of radiator may be used:

- The simplest option is to leave the cylindrical waveguide itself radiate the power right out of the mouth. The waveguide diameter is 164 mm, and the simulation shows that the radiation pattern is a bit too wide. The global efficiency is 68%. (The relatively small aperture makes little "shadow" on the parabola, and therefore little feed blockage losses). The major drawback is the reflection coefficient, ρ , of the opening (magnitude = 0.18 or -15 dB), leading to an isolation measurement of the same value. This unacceptable value cannot be improved without a modification of the septum.

- Another possibility is to use a conical horn as a radiator. This solution preserves the good isolation obtained from the septum optimization: the conical antenna makes a smooth transition to the plane wave, and its

Figure 6 — Result of the *Feedpatt* program. The radiator is a "Kumar choke or choke-ring," whose outer diameter is 444 mm. The frequency is 1296 MHz, λ is 23 cm.



Name	Frequency	Angle	Magnitude	RX
M1	1.2000	162.8878	0.0996	0.8248 + 0.0488i
M2	1.2100	-161.8195	0.0362	0.9333 - 0.0211i
M3	1.3000	177.2675	0.1921	0.6779 + 0.0129i
M4	1.2900	178.1659	0.2076	0.6563 + 0.0091i
M5	1.4000	-179.1409	0.1140	0.7954 - 0.0028i

Figure 7 — Reflection coefficient of the ring alone, measured in the output aperture plane, in the frequency band 1.2 to 1.4 GHz. Here, the ring diameter is 444 mm.

own reflection coefficient is low. With a cone length of 300 mm and an opening diameter of 200 mm, a 72% efficiency is expected, and the other goals are met. A solution using a cone followed by a length of cylindrical guide has also been used by M. J. Franco.²⁰

- The third possibility is to use a choking, or Kumar choke (as shown in Figure 1), to give a better efficiency. The ring is defined by three dimensions: diameter, height, position (relative to the waveguide mouth). These dimensions influence the radiation diagram, and therefore the efficiency (see Figure 1 and Figure 13, which gives the dimensions for 1296 MHz).

Study of the Choke-Ring Alone

The Kumar choke has not given rise to analytic studies of its working, however several antenna types come close: the “short backfire antenna” described by Matjaz Vidmar on the S53MV website, and the “box-horn” described by L. Eyraud in *Theorie et Technique des Antennes*.^{18, 21} These have an optimal ratio between the external dimension and that of the feeding guide. One may guess that third-order modes in the large area plays an important role (see Note 18). Many trials have shown that the maximum efficiency is obtained when the outer diameter is about two times the wavelength. Paul Wade, W1GHZ, described this in “VE4MA and Chaparral Feeds with Septum Polarizers.”²² The radiation diagram exhibits a “heart” shape, which is typical of this ring, as shown in Part A of Figure 6.

It is possible to simulate the choke ring isolated from the septum and access probes Tx and Rx. For that purpose, we cut the source beyond the septum, and we launch a linearly polarized wave into the cylindrical guide. The HFSS program gives the reflection coefficient and the far field radiation pattern emitted by the ring. Many simulations have been carried out with varying ring dimensions. We can observe that the most critical parameter is the external diameter of the ring. The height of the ring is 100 mm and the position is 30 mm from the aperture. These two dimensions have been proposed by Paul Wade, W1GHZ, (see Note 22) as giving the best efficiency, and have been kept. When the diameter varies, two types of curves may be plotted: one may first plot the reflection coefficient calculated by HFSS versus frequency, as shown in Figure 7. We can observe a strong frequency dependence, which suggest the existence of a resonance phenomenon, then plot the reflection coefficient of the ring alone (versus diameter) for the design frequency of 1296 MHz as shown in Figure 8.

Figure 9 is plotted from Paul Wade’s *Feedpatt* program (also see Figure 6) for various diameters gives the maximum

expected efficiency. On the graphs of Figures 8 and 9, two points have a special importance: for point A, we observe the better match of the source, the reflection coefficient is 0.05, or about -25 dB (and will give the best isolation of the whole source, as will be seen in the next section) but the efficiency is

poor: 60%. Point B (diameter 444 mm) gives the best efficiency: 78%, with an important mismatch of the ring (reflection coefficient 0.2, or -14 dB), which will strongly lower the isolation of the access ports.

It is worth noting that between these two options, the difference in efficiency is 1.2 dB.

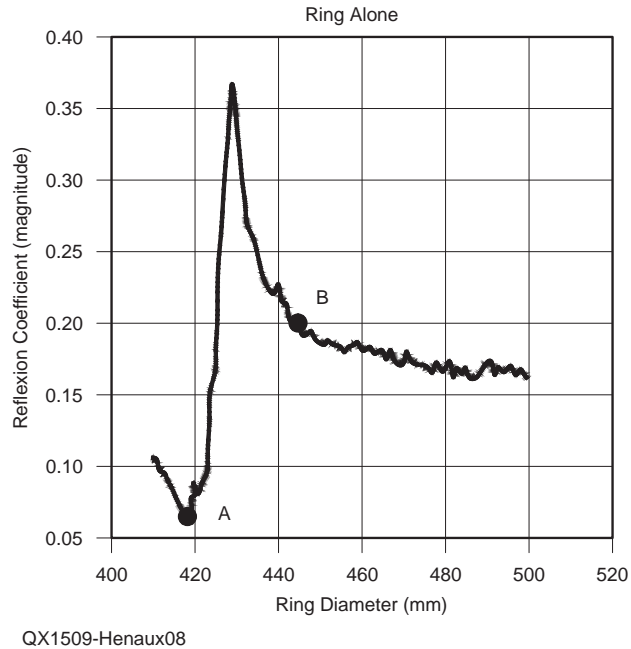


Figure 8 — Magnitude of the reflection coefficient of the ring alone versus the external diameter for 1296 MHz. The height of the ring is 100 mm and the position 30 mm. (see Figure 13). The reflection coefficient is the lowest for 420 mm (point A).

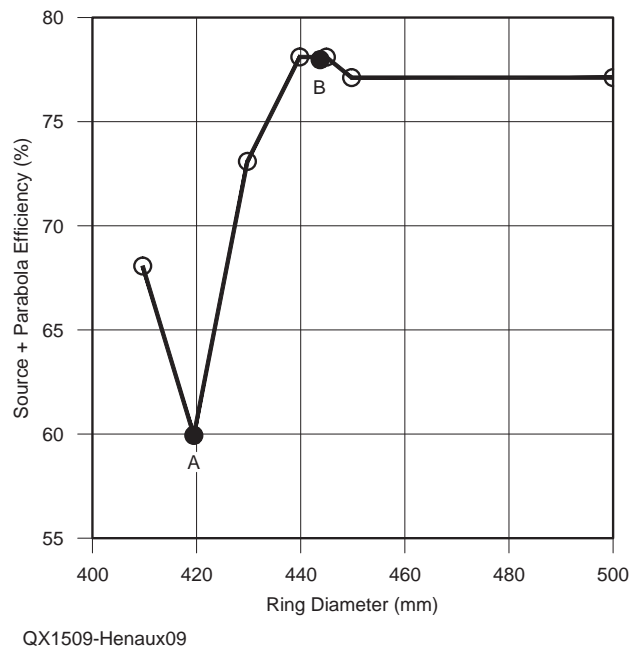


Figure 9 — Efficiency of the whole source and parabola versus ring diameter, with the same height and position as shown in Figure 8. The efficiency is the best: 78%, for 444 mm, point B.

Moreover, the experience shows an actual efficiency 12 to 15% lower than calculated. Paul Wade, W1GHZ shows this in his article, High-Efficiency Feed Horns for Prime-Focus Dishes.”²³

The Choice: Efficiency or Isolation?

If we choose the diameter corresponding to point A, it is possible to favor the isolation of the source, without having to modify the dimensions of the septum, whose working is satisfactory, with regard to matching and circularity. This option is not convenient for EME communications, however, where

efficiency is crucial. In that case, a trade-off must be found between efficiency and isolation.

In stage 1, the septum was optimized alone, (the port 3 was matched) and we saw that the magnitude of S_{21} was very low (Figure 4). We suppose now that the ring giving the best efficiency (point B is chosen), is placed at the aperture of the guide, and that the septum is correctly designed. We simulate these elements together, leaving apart the injection probes. We still suppose that the power is sent into the semicircular port 1, Tx (a waveguide port as in Figure

2), as a linear polarization, perpendicular to the septum. The left circular wave produced by the septum will be reflected by the ring, onto the reflection coefficient magnitude, $\rho = 0.2$, giving rise to a right circular wave. Therefore, we will observe from port 2 (and from port 2 only), a wave proportional to ρ , whose phase depends on the guide length (point m2 on Figure 10) and Figure 11A.

This isolation defect can only be canceled by a slight change in the dimensions of the steps of the septum, so that it gives rise to a reflection coefficient, ρ' , having the same magnitude and opposite phase. (If necessary, the length of the guide may be changed to accommodate the phase of ρ .) This can be seen in a schematic way in Figure 11, parts B and C.

In Figure 12, the septum and the guide length have been modified for that purpose. The isolation is now acceptable (-30 dB, point m3). As you can see, the reflection coefficient S_{11} (S_{22}) of the source is now 0.17

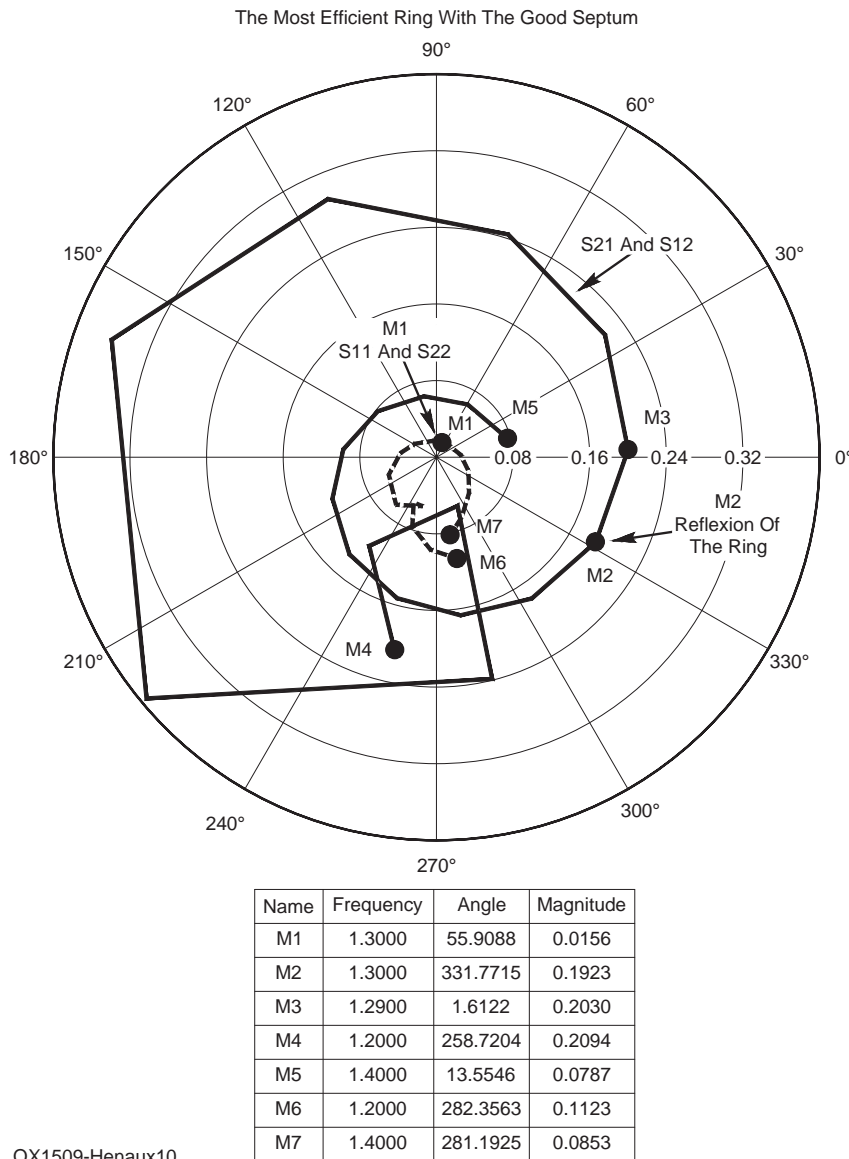


Figure 10 — The frequency varies from 1.2 to 1.4 GHz and the isolation, S_{21} , is measured. The reflection coefficient, ρ , of the ring placed at the aperture of the guide is seen from port 2 (Rx), as a poor isolation (point m2, near 1296 MHz). The reflection, S_{11} , remains very low (point m1, near 1296 MHz).

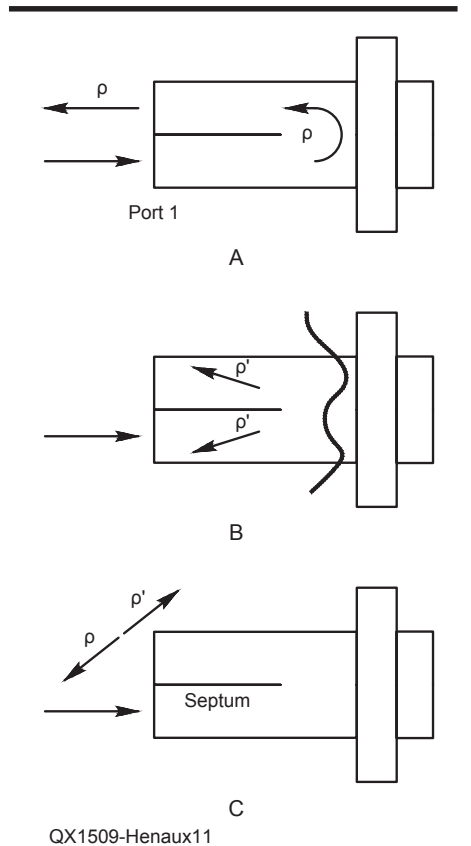


Figure 11 — Part A shows the reflection, ρ , on the choke, which inverts the direction of the circular polarization, and is transmitted to port 2 only. Part B shows the reflection, ρ' , from the septum alone is null if the septum is correctly designed. If this is not the case, the magnitude of S_{21} and S_{11} , are not zero. Part C shows the reflection, ρ' , from the septum is used to nullify the reflection, ρ , from the choke.

(-15 dB, point m1). We have compensated the isolation, but the reflection coefficient of the septum, which was necessary for that compensation, reappears now as a match defect. Fortunately, this can be easily corrected when choosing the position and length of the injection probes, and a good match can be obtained.

What is the price to pay for that trade-off? The circularity will likely be lowered: the two orthogonal waves coming out of the guide towards the parabola will not have the same magnitude because the septum has been slightly modified. We observed, however, that this lack of circularity remains moderate, as shown in Figure 15.

Stage 3: The Injection Probes (Coaxial to Circular Guide Transition)

The two semicircular waveguide ports used in stage 1 and 2 are now replaced in the simulation by two 7 mm coaxial connectors. In their simplest shape, the probes are an extension of the 3.05 mm inner part of the connector. The length is about one quarter of the free wavelength, as described by Peter Delmotte, ON4CDQ, at the 2001 Belgian Microwave Roundtable.²⁴ The signal introduced into the port 1 (resp. 2) will produce the emission of a left circular wave (resp. right) at the output of the source. The length and position of the probes are quite sensitive but their optimization is easy: it is enough to get the parameters S_{11} and S_{22} as low as possible. Though the optimization of the probes is not able to improve or lower the isolation, S_{21} , due to the sensitivity of the position and length of the probes, a careful adjustment of the connectors and probes is of great importance for a good match. Following this approach, a solution is proposed, which fulfills the requirements, and a 78% maximum efficiency is expected.

Simulation Results of the Source

Reflection and Transmission

When the probes have been optimized, in the vicinity of the design frequency, 1296 MHz, the matching S_{11} is expected to be better than -28 dB (point m4, Figure 14), and isolation S_{21} is -32 dB, (point m2), which is within the specification.

Circularity

The circularity is plotted in Figure 15 for several angles, θ , of the emission cone: from 0° (emission axis) up to 60° (parabola edge), taken from the propagation axis (See Figure 16 for the definition of the angles and axis). The ϕ angles are reported at the periphery of the diagram. For each θ and ϕ pair of a point on the curves, the radius represents the value of the circularity calculated by $HFSS$ (ratio of the polarization axis, in dB).

When a wave enters the Tx port (port 1) the source emits a Left Hand Circular Polarization (LHCP) wave. As you can see from this simulation, the circularity becomes poor when the observation is made in a large cone ϕ . The value 2.8 dB is reached for $\theta = 60^\circ$ (near the edge of the parabola).

We have simulated the emission of the source when the power is applied to the Tx port. See Figure 17. Two curves are plotted: one represents the radiation of the LHCP wave alone, and the other takes both polarizations into account (LHCP plus Right Hand Circular Polarization — RHCP). These curves show that the losses due to the existence of RHCP in the front radiation may be neglected. This is not the case for the rear radiation producing the “spillover” in efficiency (see Note 19). This low power radiation (-20 dB, point m3) is mainly RHCP. The special shape of the radiation pattern (Figures 16 and 17) is typical of the choke ring effect. In our case, a maximum

of the emitted power is observed for $\theta = 35^\circ$ and the gain of the source is 7 dB (Figure 16).

Efficiency

The theoretical efficiency of this source predicted by the *Feedpatt* program is 78%. This result takes into account the total emitted power (both polarizations). We can see on Figure 6 that the “shadow” of the ring causes a 5% loss in efficiency because the ring diameter is not small enough with respect to the parabola dimension. Another option, such as replacing the ring with a simple conical horn should reduce these losses. As a matter of fact, the realization of a septum giving good circularity, match and isolation is quite easy if we have a 3D simulator at our disposal. The usable bandwidth of such a septum, considered alone, is quite large: about 100 MHz. See Figure 5. A well-designed conical horn has low reflection, and when placed beyond the septum it does not modify these properties.

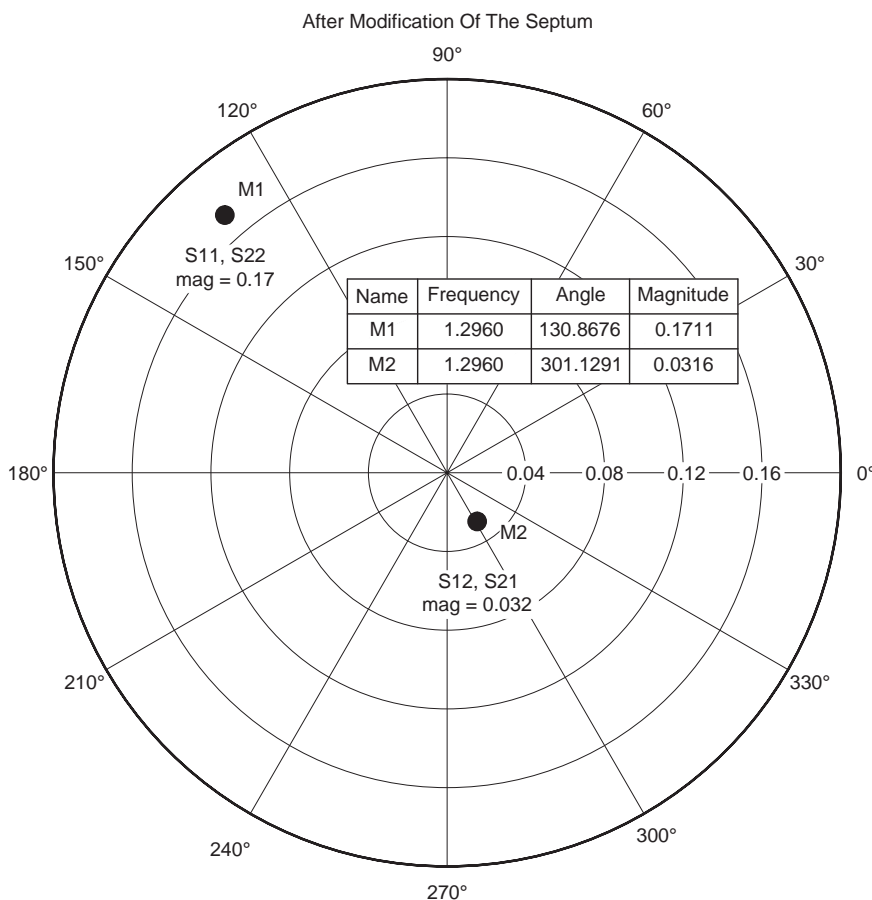


Figure 12 — The steps of the septum and the guide length have been modified. The isolation is now satisfactory (0.032, or -30 dB, point m2). These modifications give rise to a source mismatch (point m1) whose magnitude (0.17) is very close to that of the choke (0.19).

Moreover, the injection probes also may have a wide bandwidth if the rods are replaced by solid shapes such as cone, mushroom or cylinder steps. In this way, we can get a circularly polarized source working in about several tens of MHz.

The simulations of the source at 1296 MHz show that making use of the Kumar choke leads to more difficulties than the use of a conical horn. The reflection coefficient is about 0.2 if high efficiency is desired (point B, Figure 9). The result, after modification of the septum (Figure 14) will have a lower bandwidth, typically ≤ 10 MHz, and this result will not be improved by the use of sophisticated probes.

Sensitivity to the Dimensions

Such a source is difficult to build, and dimensional errors are unavoidable. It is

worth trying to estimate what accuracy is necessary. We have first modified the diameter of the choke by ± 1 mm, and looked at the match and isolation (Figure 18). The frequency is 1296 MHz, except for the solid line where the frequency changes in the band 1292 to 1300 MHz. It seems that the isolation (the right side of Figure 18) is the most sensitive, and the realization must be very aware of that. If we remember the strong coupling between the isolation and reflection of the ring, this is not a surprising result. On the other side, the resonant character of the ring is reflected by a rapid variation of S_{21} when the frequency varies. The reflection S_{11} is less sensitive.

In Figure 19, we have plotted the sensitivity to a change in the height of the first step, which supports the strongest field when the incoming wave is converted into

circular polarization. Obviously, a ± 1 mm inaccuracy is acceptable regarding this dimension.

Conclusion

The isolation between the two ports, Tx and Rx (port 1 and 2), is strongly dependent on the radiating element being placed at the aperture of the circular waveguide. Using a choke ring to improve the calculated efficiency of the source (up to 78%) implies a trade-off. The isolation may be preserved at the design frequency, but the behavior of the circularity is not predictable and must be verified by a simulation. In any case, the circularity reduces as the illumination angle, θ , increases, and a goal of 1 dB whatever the angle, θ , is difficult to reach. On the other side, the reflection of the access ports,

23 cm Source $f = 1296$ MHz
 IUT Ville d'Avray, UPX
 Radio-Club F6KRR

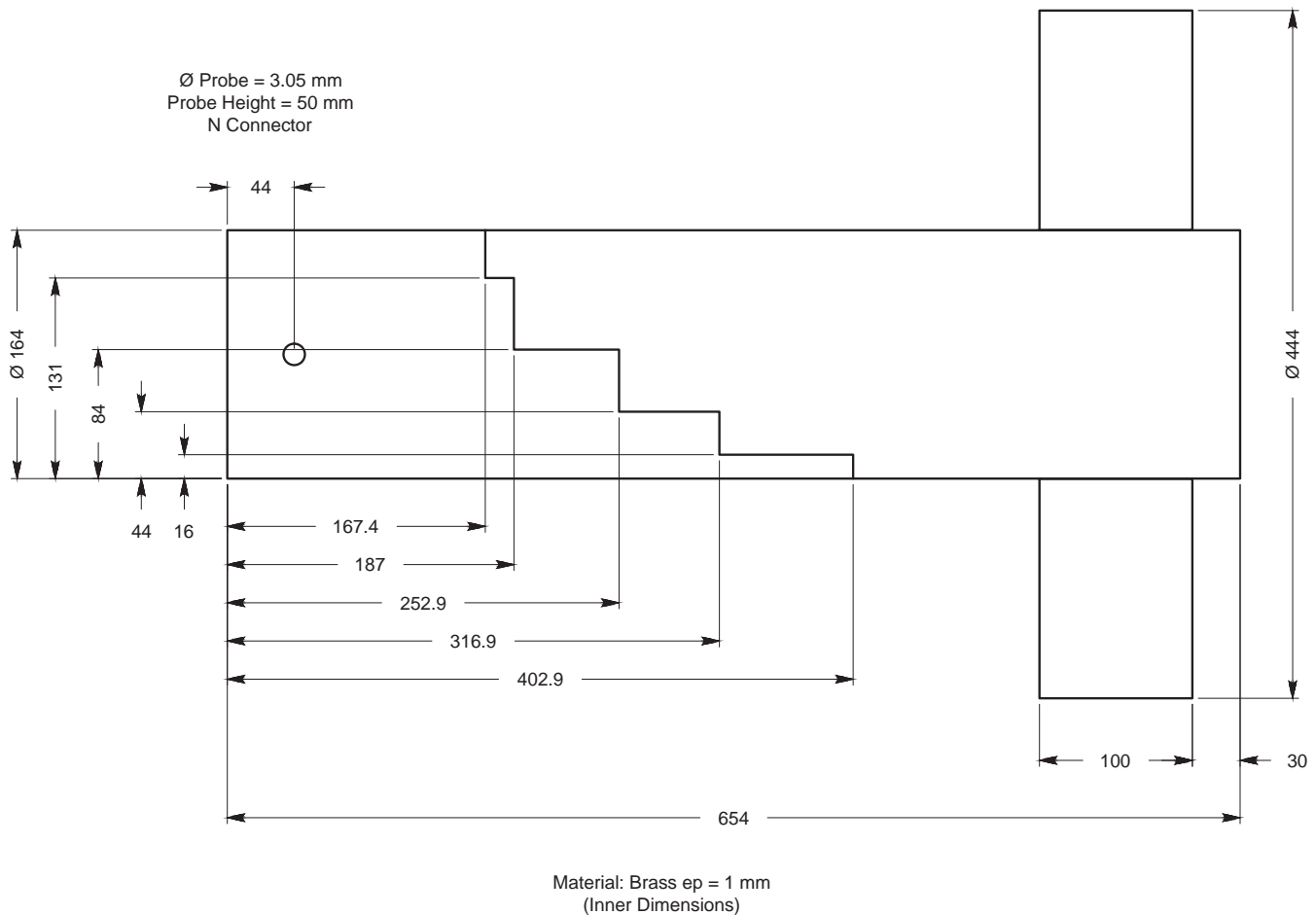


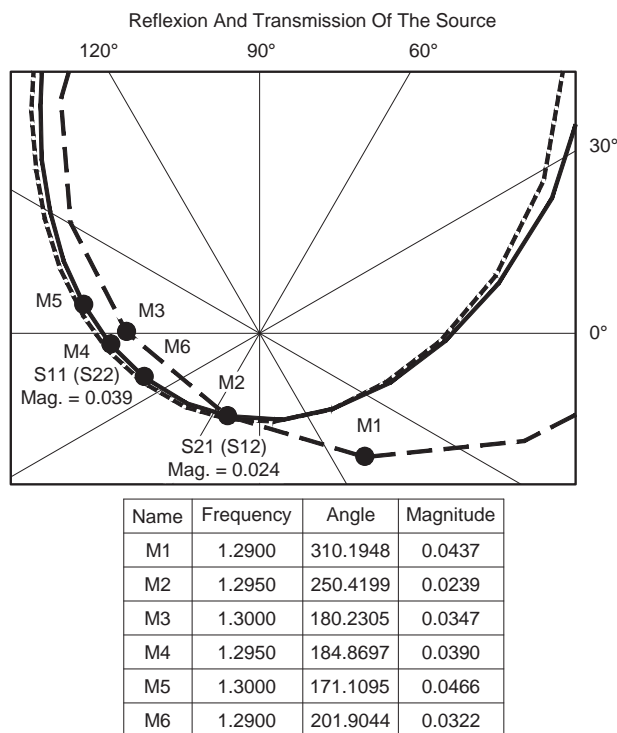
Figure 13 — Dimensioned sketch of the proposed source for EME communication in the 23 cm band.

Tx and Rx (port 1 and 2), may be easily maintained under the goal -20 dB. Another problem has not been taken into account: the reflections on the parabola have an effect similar to that of the choke. In the same way, they result in a reduced isolation and can be observed experimentally, but are difficult to model. R. Galuscak, OM6AA, described this in "A Septum Feed Revisited," *DUBUS*, April, 2004.²⁵

It clearly appears that the higher efficiency of the Kumar choke has a counterpart in a narrower bandwidth. This should not be a drawback for the EME link. If a wider bandwidth is needed, a conical horn would be more suited, provided it would correctly illuminate the parabola (this is possible for $f/D = 0.4$). With the tools used in this study, we can't easily compare the influence of the thermal noise due to the rear radiation of the horn versus the choke, when placed at the focus of the parabola. A field experiment will be essential for that purpose.

Finally, the results suggest that the realization accuracy should be better than ± 1 mm. This is particularly true for the ring, and this is a difficult requirement to meet.

We wish to thank Matthieu Cabellic, F4BUC, Laurent Reinhard, F4GEV, and Jean-Pierre Maillot, F6BPS, for their involvement in this project.

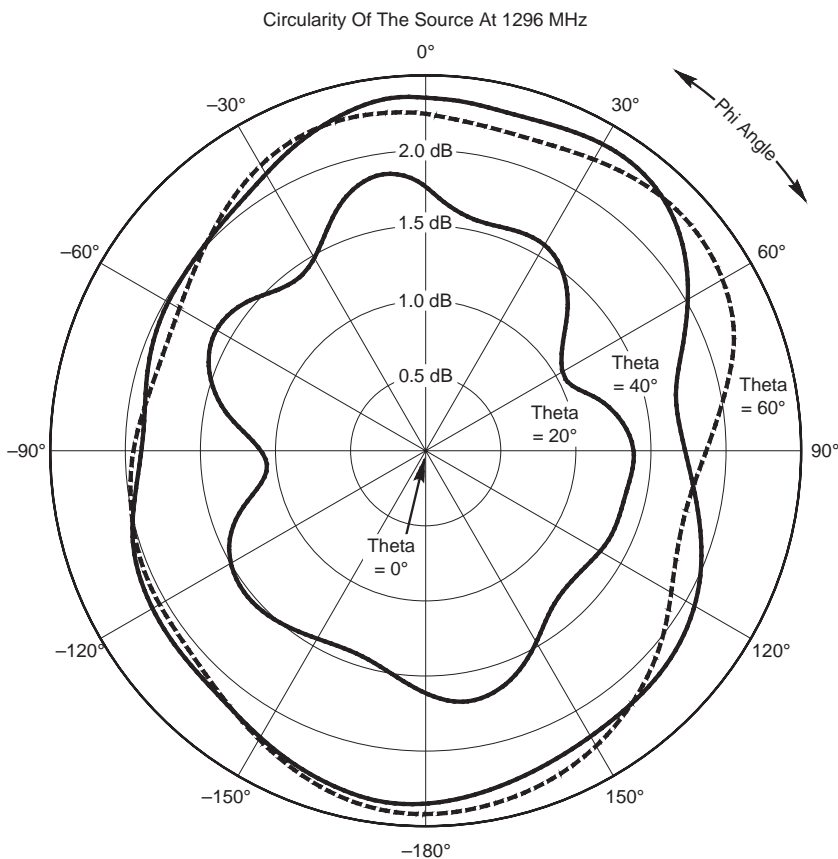


QX1509-Henaux14

Figure 14 — Match and isolation of the source (23 cm, HFSS simulation).

Notes

- ¹H. Ward Silver, NØAX, *Ed, 2011 ARRL Handbook*, Chapter 30, EME Communications, 2010, ARRL.
- ²There is more information about work done by the Radio Club de St Quentin en Yvelines at the club web site: <http://f6krk.org/Site/fr/menu/presentation-f6krk>.
- ³G. Kollner, DL4MEA, "Designing a Super-VE4MA Feed Horn for 23 cm and 13 cm," *DUBUS*, Jan 2007, p 33.
- ⁴For information about Paul Wade's *Feedpatt* software, and to download the software, go to Paul's website, and scroll down to find *Feedpatt*. www.W1GHZ.org/10g/software.htm.
- ⁵SM6FHZ and SM6PGP, Swedish EME Meeting, May 2013.
- ⁶A. Kumar, "Reduce Cross-Polarization in Reflector-Type Antennas," *Microwaves*, March 1978, pp 48 – 51.
- ⁷B.W. Malowanchuk, VE4MA, "VE4MA 3456 MHz Circular Polarization Feed Horn," *North Texas Microwave Society Feedpoint*, Nov/Dec 1991.
- ⁸P. Hazdra, R. Galuscak, M. Mazanek, "Optimization of Prime-Focus Circular Waveguide Feed with Septum Polarization Transformer for 1.296 GHz EME Station," 2006 European Conference on Antennas and Propagation (EuCAP).
- ⁹The free version of MiCIAN μ Wave Wizard simulation software is available on their web site: <http://MiCIAN.com>.
- ¹⁰For more information about Ansys and their HFSS software, go to: www.ansys.com/Products/Simulation+Technology/Electronics/Signal+Integrity/ANSYS+HFSS.



QX1509-Henaux15

Figure 15 — Circularity of the source at 1296 MHz (simulation) (scale in dB).

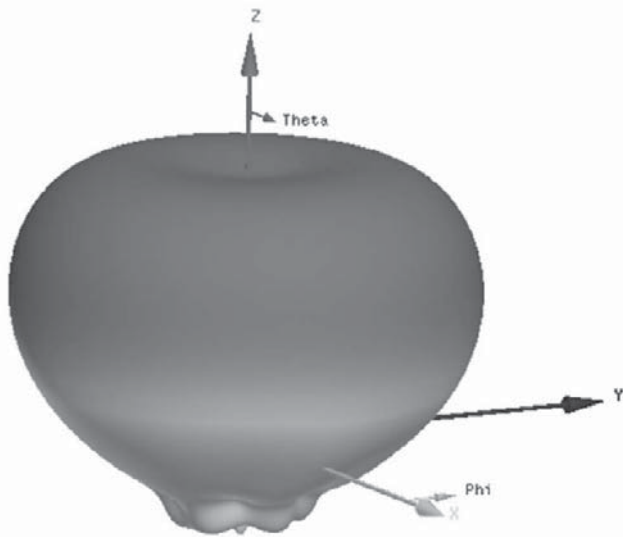
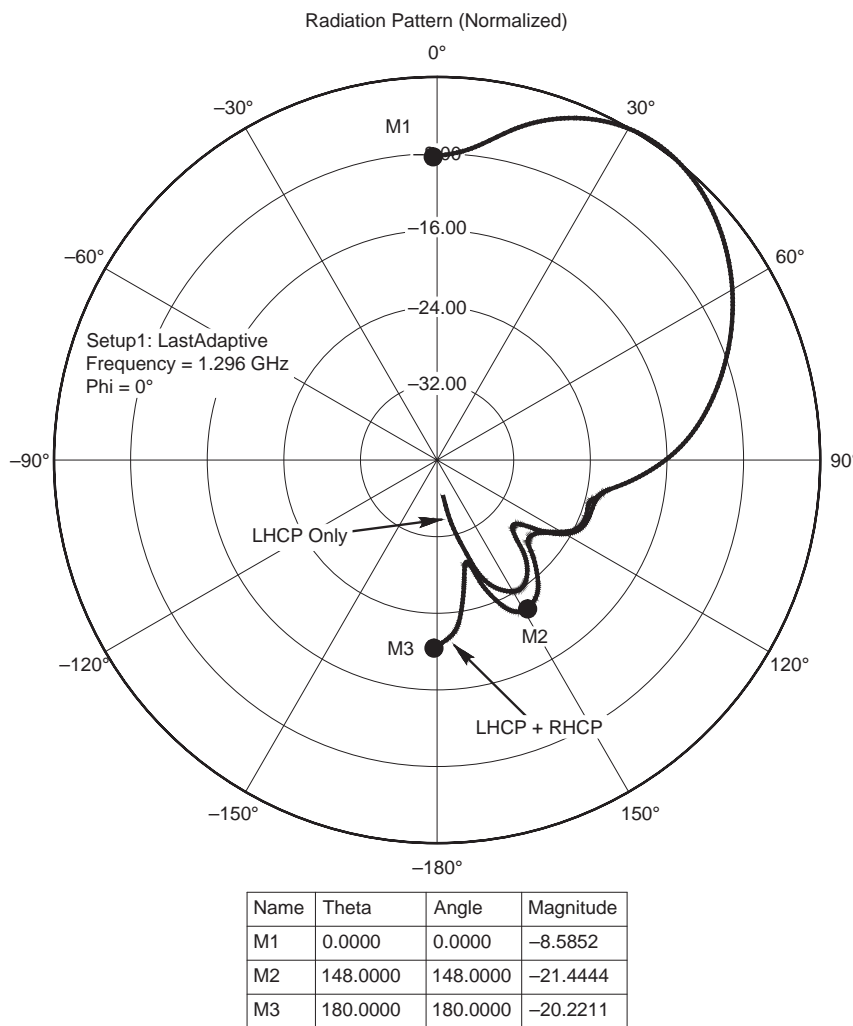


Figure 16 — The 3D radiation pattern of the source.



QX1509-Henaux17

Figure 17 — Radiation diagram of the source plotted for 1296 MHz (dB scale).

¹¹For additional information about Computer Simulation Technology (CST) and their 3D Electromagnetic Simulation Software, go to: <https://www.cst.com>.

¹²R. Behe and P. Brachat, "Compact Duplexer-Polarizer with Semicircular Waveguide," *IEEE Transactions on Antennas and Propagation*, August 1991 Vol, 39, pp 1222 – 1224.

¹³M. H. Chen, G. N. Tsandoulas, "A Wide-Band Square-Waveguide Array Polarizer," *IEEE Transactions on Antennas and Propagation*, May 1973, Vol 21, pp 389 – 391.

¹⁴Zdeno Samek, OK1DFC, "Feed For Parabolic Dish With Circular Polarization," CD-ROM for 10th International Conference 2002 in Prague. There is a lot of information on Zdeno's web site, especially under the "EME Page" tab: <http://OK1DFC.com>.

¹⁵Paul Wade, W1GHZ, website: www.w1ghz.org/antbook/preface.htm.

¹⁶Paul Wade, W1GHZ: www.w1ghz.org.

¹⁷H. Jasik, R.C. Johnson, Eds, *Antenna Engineering Handbook*, 3rd Edition, ISBN 0-07-032381-X.

¹⁸L. Eyraud, G. Grange, H. Ohanessian, *Théorie et Technique des Antennes*, Paris Vuibert (1973), p 209.

¹⁹R. Galuscak, P. Hazdra, "Circular Polarization and Polarization Losses," *DUBUS*, April 2006, ISSN 1438-3705.

²⁰M.J. Franco, "A High-Performance Dual-Mode Feed Horn for Parabolic Reflectors with a Stepped Septum Polarizer in a Circular Waveguide," *IEEE Transactions on Antennas and Propagation*, June 2011, Vol 53, No. 3.

²¹Matjaz Vidmar, S53MV, website: lea.hamradio.si/~s53mv/wumca/sbfa.html.

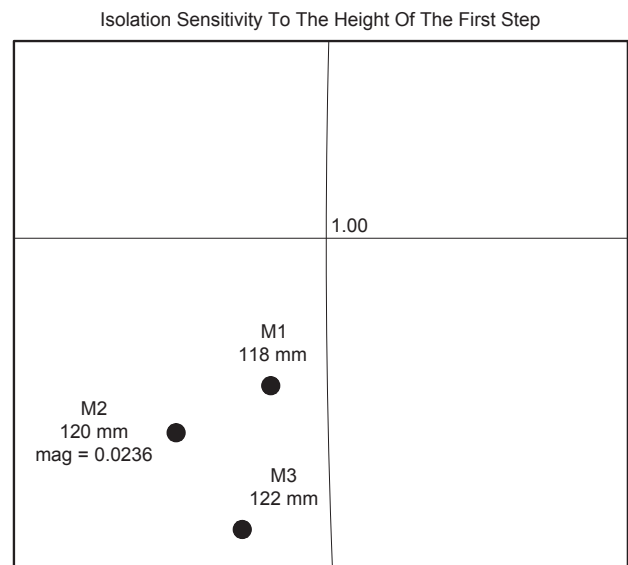
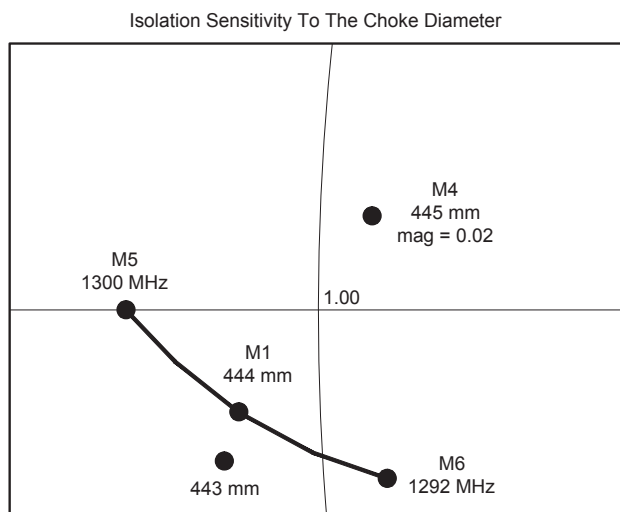
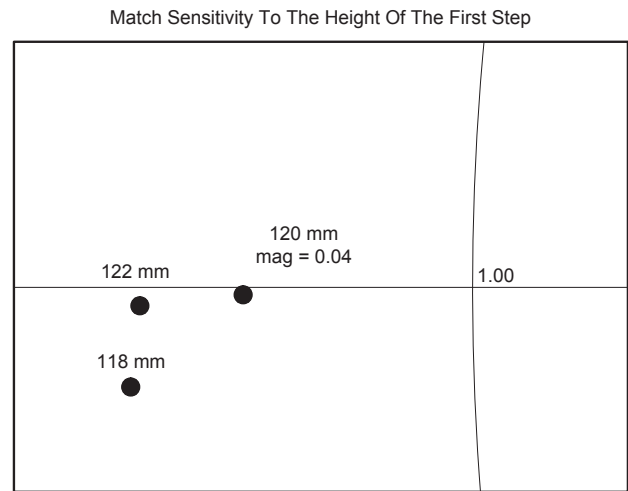
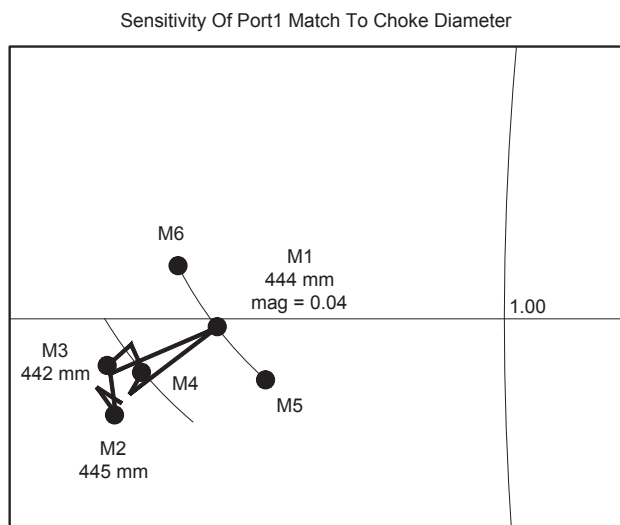
²²Paul Wade, W1GHZ, with measurements by Tommy Henderson, WD5AGO, "VE4MA and Chaparral feeds with Septum Polarizers," 2006. This paper was presented at the 2006 Eastern VHF/UHF Conference. The paper is available for download from Paul Wade's web site: www.w1ghz.org/antbook/conf/VE4MA_Chaparral_septum_feeds.pdf.

²³Paul Wade, W1GHZ, with measurements by Tommy Henderson, WD5AGO, "High-Efficiency Feed horns for Prime-Focus Dishes; VE4MA and Chaparral feeds with Septum Polarizers," 2006. This paper was presented at the 2006 EME Conference and the 2006 Microwave Update. It is very similar to the paper referenced in Note 21. The paper is available for download from Paul Wade's web site: www.w1ghz.org/antbook/conf/high_efficiency_prime_feeds.pdf.

²⁴Peter Delmotte, ON4CDQ, "Waveguide-Coaxial Line Transitions," Belgian Microwave Round-table, 2001.

²⁵R. Galuscak, OM6AA, "Septum Feed Revisited," *DUBUS*, April, 2004.

Additional References
 Paul Wade, W1GHZ, "Understanding Circular Waveguide — Experimentally: Old-Fashioned Microwave Engineering, Jan/Feb 2001 QEX, pp 37 – 48.
 Web site: www.cva.u-paris10.fr/lpmhr.



QX1509-Henaux18

QX1509-Henaux19

Figure 18 — Sensitivity to the choke diameter, plotted for 1296 MHz. The upper part shows the port 1 match, and the lower part shows the isolation.

Figure 19 — Sensitivity to the height of the first step of the septum, plotted for 1296 MHz. The upper part shows the port 1 match, and the lower part shows the isolation.

Jean-Claude Henaux worked on Josephson effects in superconductive junctions and received his PhD in 1983 from the Paris Sud-Orsay University. As a professor at Paris Sud-Orsay University and Paris-Ouest Nanterre, he was involved in design and measurements on microwave GaAs ICs and taught electronics, and particularly microwave electronics. He is now retired and helps (for pleasure) with student microwave projects at the Ville d’Avray Institute of Technology.

des Technologies de l’Information et de l’Energie, ENS Cachan, France) on RADAR systems.

Frank Daout received his MS and PhD degrees in electronics from the University of Nantes (France) in 1996. From 1997 to 1999 he was a Research Engineer at the French Naval Academy, at Brest, France, Groupe de Traitement du Signal Laboratory in the SONAR team. In 1999, he became an Assistant Professor at the University of Paris-Ouest Nanterre la Defense. His research and teaching courses are in the fields of electromagnetic wave propagation, microwave and signal processing. Currently, he works at the SATIE Laboratory (Systemes et Applications

Patricia Grassin received her PhD from the University of Pierre and Marie Curie (Paris IV — UPMC), France, in 1992. Her main areas of expertise are in antennas, RF/microwave/millimeter wave circuits and electromagnetic modeling. She was appointed a full time academic position in 1993 at the Ville d’Avray Institute of Technology.

Gilles Holtzmer works as a technician in the Electrical Engineering and Industrial Computing (EEIC) Department. His skill in mechanics and electronics was essential to the realization of a prototype of the source.

Laurent Paupert, Mathieu Phelipon, Aurelien Janon have received their “Diplome Universitaire de Technologie” in 2014 and are now working towards higher degrees in Microwaves and Electronics.

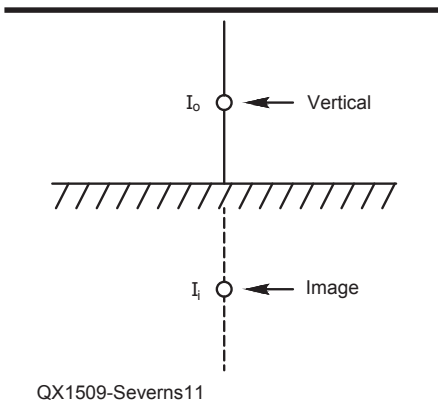
Radiation and Ground Loss Resistances In LF, MF and HF Verticals; Part 2

With the impending FCC announcement about the release of a new LF and a new MF band, hams will be interested in practical antennas and learning how to calculate EIRP to legally operate on those bands.

Soil-Antenna Interaction

As illustrated in Figure 11, one way to analyze a vertical antenna over ground is to use a hypothetical image. If the ground is perfect then the image antenna will be a duplicate of the actual antenna with the same current amplitude and phase. For a dipole a short distance above ground, the image is another dipole the same distance below ground. We now have a system of two coupled dipoles and it's no surprise that R_i of the upper dipole is no longer $\approx 72 \Omega$, but in these examples $R_i \approx 94 - 100 \Omega$. What's happening is that the upper vertical (the real one) has a self resistance of $\approx 72 \Omega$, but added to that is a mutual resistance (R_m) coupled from the image antenna.

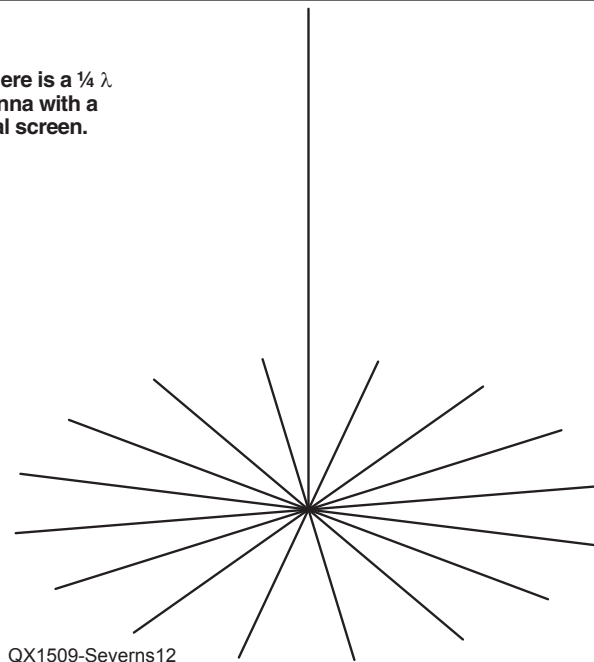
If the ground is not perfect, however,



QX1509-Severns11

Figure 11 — This is an example of an antenna and its image.

Figure 12 — Here is a $\frac{1}{4} \lambda$ vertical antenna with a buried radial screen.



QX1509-Severns12

then the image antenna will not be an exact replica of the real antenna. The current amplitude and phase on the image will be different, so we should not be surprised if R_i does not have the same value as either the free space or perfect ground cases. Viewing R_i as a combination of the free space value and some mutual $\pm R_m$, because of the soil is perfectly valid, and this was Wait's approach in *Antenna Theory*.⁸ He calculated the $\pm \Delta R_i$,

⁸Notes appear on page 28

as the soil and/or radial fan is changed. This $\pm \Delta R_i$ was a combination of changes in R_r and R_g , however, and not R_g alone.

R_r and R_g for a $\frac{1}{4} \lambda$ Vertical Antenna at 7.2 MHz

The $\frac{1}{4} \lambda$ vertical antenna with a buried radial screen shown in Figure 12 is more representative of typical amateur antennas for 40 m than a full-height $\frac{1}{2} \lambda$ vertical dipole. Amateurs are not likely to use a full

$\frac{1}{4} \lambda$ vertical antenna on 630 m, however. Such an antenna would be ≈ 500 feet high! We'll look at a more typical 630 m antenna in a later section.

I calculated data points for 16, 32, and 64 radials, with lengths of 2, 5, 10, and 16 m over poor (0.001/5), average (0.005/13) and very good (0.03/20) soils. Figure 13 is a graph showing the behavior of R_i , R_r , and R_g as a function of radial length when 64 radials are employed over average ground at 7.2 MHz.

On the graph there is a dashed line labeled "36 Ω " corresponding to the value of R_r for a resonant $\frac{1}{4} \lambda$ vertical antenna over infinite perfect ground.

The fact that R_i does not decrease or even flatten out for radial lengths $> \frac{1}{4} \lambda$ but instead starts to increase has been predicted analytically (for example in Wait — see note 8), my earlier NEC modeling (see Appendix D) and as seen in practice. (Note: Appendices A, B, C, and D are available for download from the ARRL QEX files website.⁹) What's

interesting is that $R_r \neq 36 \Omega$! R_r starts out well below the value for an infinite perfect ground plane, but as the radial length is extended it approaches 36 Ω . Increasing the radial number and/or extending radial

length also moves R_r closer to 36 Ω . Figure 13 represents only one case: 64 radials over average ground.

Figure 14 gives a broader view of the behavior of R_r for different soils and radial

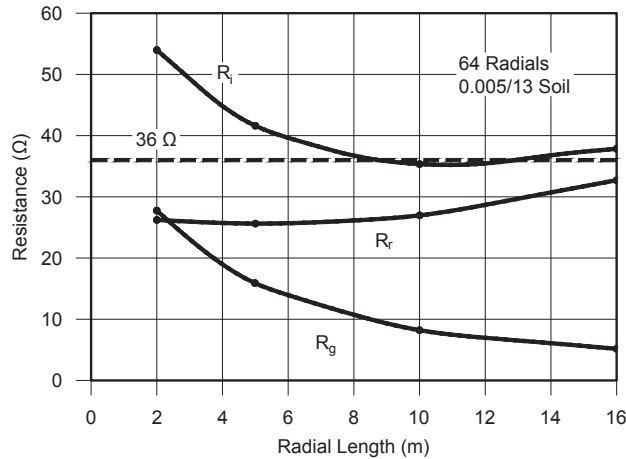
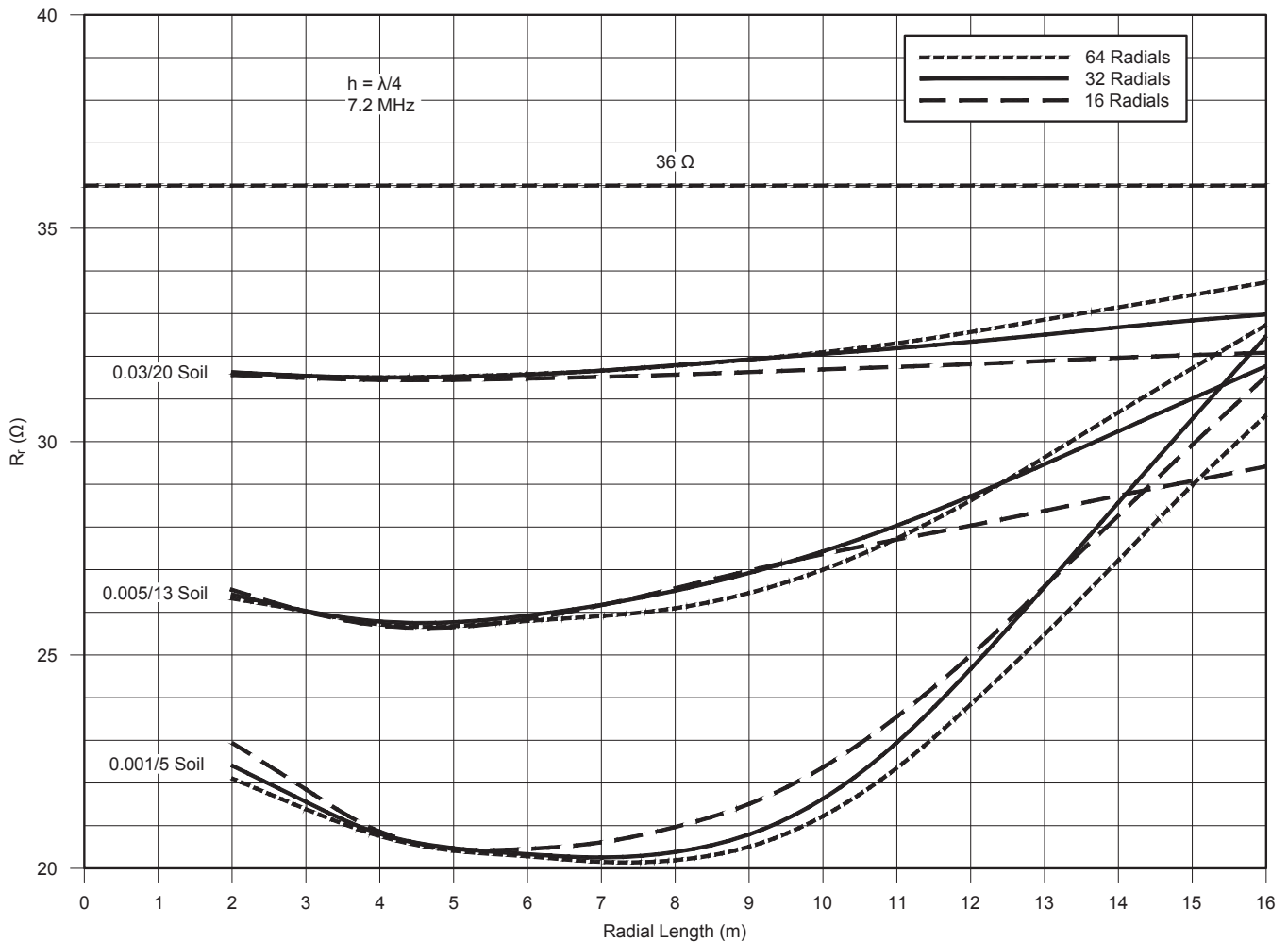


Figure 13 — This graph shows R_i , R_r , and R_g as a function of radial length for a 40 m $\frac{1}{4} \lambda$ vertical antenna.

QX1507-Severns13



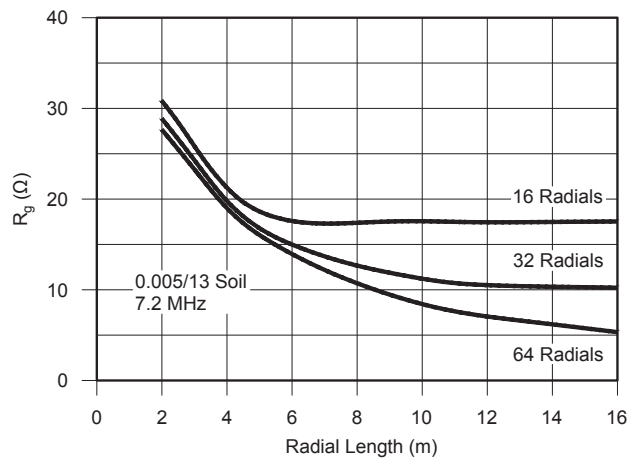
QX1507-Severns14

Figure 14 — Here is a graph that plots R_r as a function of soil, radial number, and radial length.

numbers as radial length is varied.

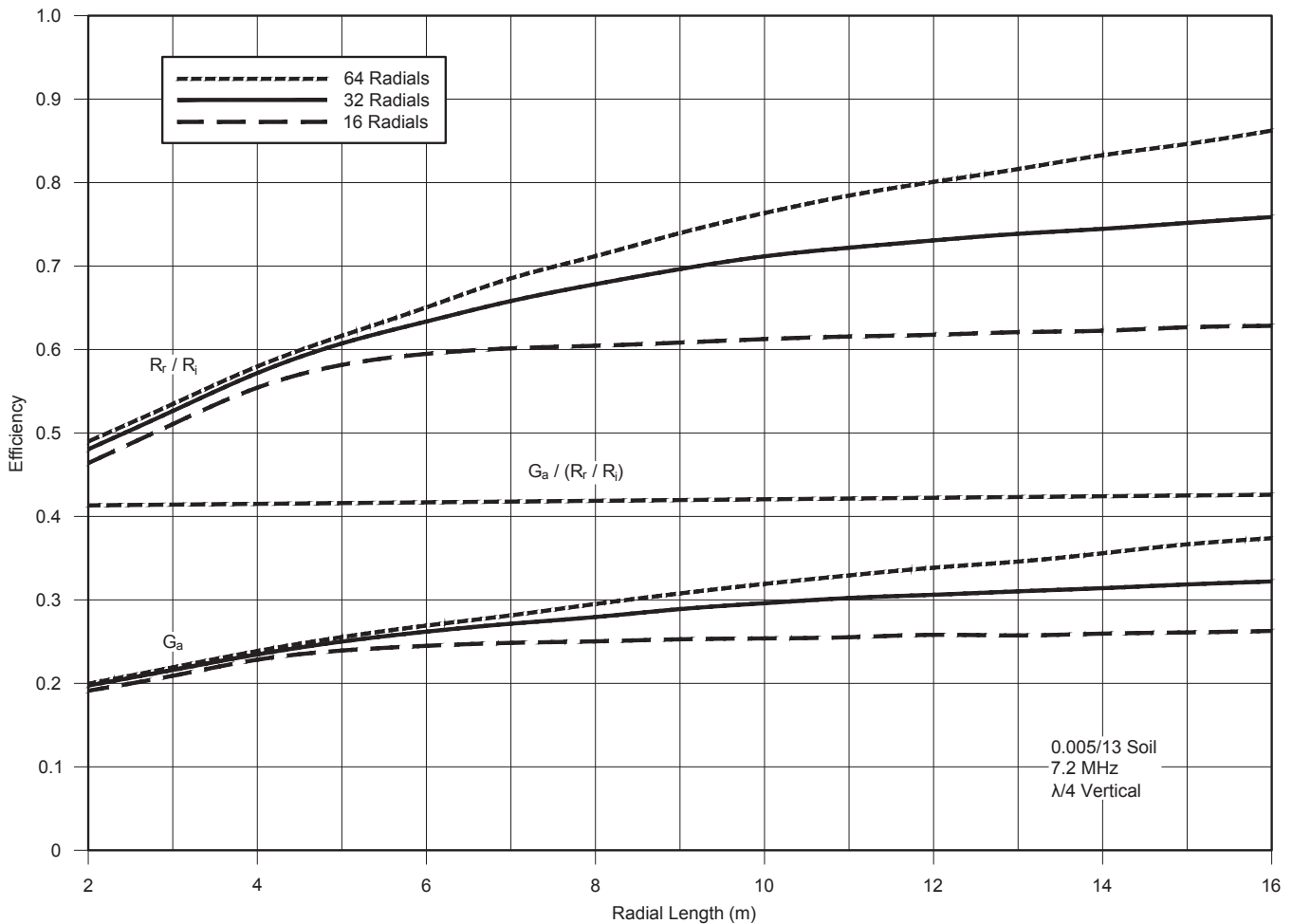
It's abundantly clear that $R_r \neq 36 \Omega$ but as we improve the soil conductivity and/or increase the number and/or length of the radials R_r converges on 36Ω . We can also graph the values for R_g as shown in Figure 15, which nicely illustrates how more numerous and longer radials reduce ground losses.

For a given model, NEC will give us R_i , G_a , and the field data from which we can determine R_r using the Poynting vector and a spreadsheet. With this information we can have some fun! R_r / R_i is the radiation efficiency, including only the ground losses within the radius of integration, which in this case is $\approx 1/2 \lambda$. G_a is the radiation efficiency including all the losses, near and far field. The ratio $G_a / (R_r / R_i)$ gives us the loss in the far field, separate from the near field losses. Figure 16 graphs all three, G_a , R_r / R_i , and $G_a / (R_r / R_i)$ with various numbers of radials over average ground. Note that the far field loss is almost independent of the radial



QX1507-Severns15

Figure 15 — This graph plots R_g as a function of radial length and number.



QX1507-Severns16

Figure 16 — Here is a graph of antenna efficiency as a function of radial length and number.

number or radial lengths, which is what you would expect because we haven't changed anything in the far field as we modified the radials. In fact any bumps or anomalies in that graph would indicate a screw-up in the calculations! It serves as a much needed cross check on the calculations.

After seeing Figure 16, Steve Stearns, K6OIK, suggested adding a graph of $(R_i / R_g) - G_a$, which is the ground wave radiation efficiency. This is shown in Figure 17.

By repeating the calculations for a $\frac{1}{4} \lambda$

vertical at 1.8 MHz, we can compare the results to expose the effect of frequency on R_i , R_r , and R_g for the same type of antenna. An example is given in Figure 18. The solid lines are for 1.8 MHz and the dashed lines are for 7.2 MHz.

What we see is that even though both antennas are $\frac{1}{4} \lambda$, with the same length radials (in λ) and the same soil characteristic, the values for R_i , R_r , and R_g are substantially different. At 1.8 MHz, R_r is much closer to 36Ω . Using $\frac{1}{4} \lambda$ radials at 7.2 MHz and

integrating the radiated power, $R_g \approx 8 \Omega$. If you subtracted the R_i value given by NEC from 36Ω , however, you would think R_g was essentially zero! At 1.8 MHz, $R_g = 36 - R_i \approx 2 \Omega$, which seems reasonable. The power integration for the 1.8 MHz vertical gives $R_g \approx 6 \Omega$, however, which means the efficiency is lower than we thought. As the soil conductivity (σ) increases, the values for R_i move closer to 36Ω . If we lower the frequency to the lower AM broadcast band (say 600 kHz) using a $\frac{1}{4} \lambda$ vertical with 120 0.4λ radials, R_r will be very close to 36Ω . This is a frequency range where a great deal of profession work has been done, which might explain why the discrepancy between estimated and actual R_g and R_r went unnoticed. The difference would be very small, easily within the range of experimental error!

A Small 630 Meter Vertical Antenna

On 630 m (472 to 479 kHz), where $1 \lambda \approx 2000$ feet, any practical antenna is very likely to be small in terms of wavelength. Figure 19 shows an example of a short top-loaded vertical for 630 m. The vertical is 15.24 m high (50 feet, 0.024λ) with 7.62 m (25 feet, 0.012λ) radial arms in the hat. The usual practice for very short verticals is to have a dense ground system that extends some distance beyond the edge of the top-hat and/or a bit longer than the height of the vertical. Two cases were modeled: 64 and 128 radials, all 18 m long.

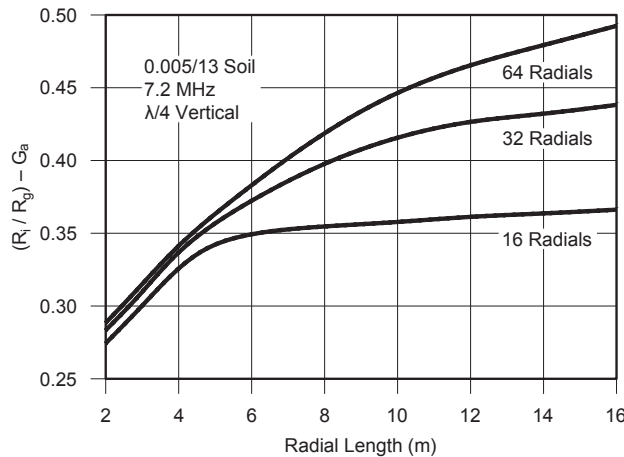
The results calculated from the NEC field data are given in Table 1. Over perfect ground $R_r = 0.7 \Omega$

For this antenna with real soils, R_r is somewhat higher than the perfect ground case and converges on the perfect ground case as the soil conductivity improves. In this example using the perfect ground value for R_r yields an efficiency somewhat lower than real soil, as shown in the $0.7 / R_i$ column, but the difference is not very large. We should also keep in mind, as shown in Appendix C, that the computed values for R_r depend on the integration radius, which is somewhat arbitrary. If I had used a slightly larger radius, the R_r values would have been a bit lower, or closer to the ideal ground value.

Summary

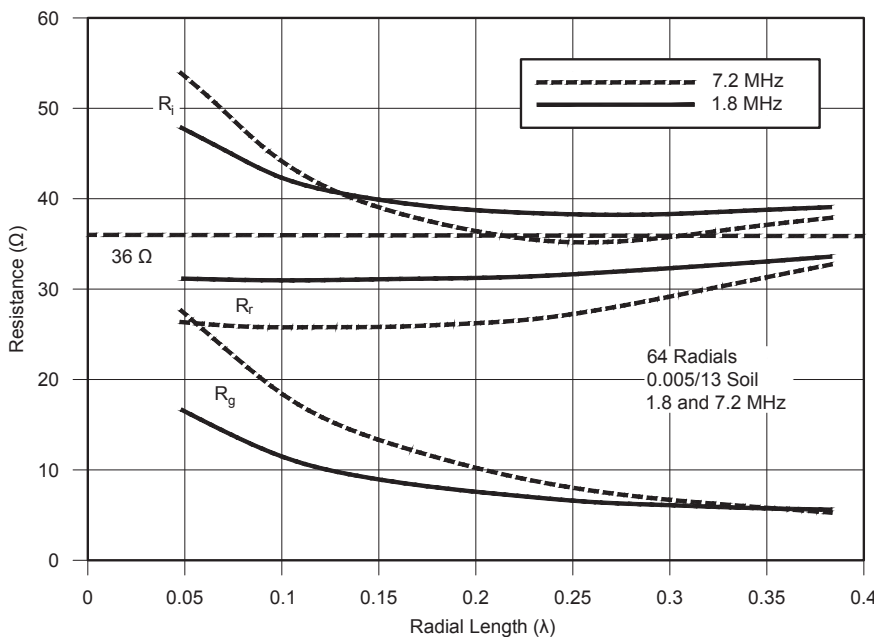
For a lossless antenna in a lossless environment, the calculation of radiation resistance is very straight forward: integrate the power density over a hypothetical surface enclosing the antenna. The net power outflow divided by the square of the rms current at the feed point gives R_r . We can extend this technique to antennas in a lossy environment by using the field values obtained from NEC modeling and a spreadsheet.

At HF, values for R_r over real soils appear



QX1507-Severns17

Figure 17 — This graph plots ground wave radiation efficiency; $(R_i / R_g) - G_a$.



QX1507-Severns18

Figure 18 — Here is a graph showing R_i , R_r , and R_g for a $\frac{1}{4} \lambda$ vertical antenna with 64 radials at 1.8 and 7.2 MHz.

to be significantly lower than the values for the same antennas over perfect ground, at least in the case of $\frac{1}{4} \lambda$ and $\frac{1}{2} \lambda$ vertical antennas! For short verticals at LF and MF, however, the real-ground R_r appears to be close to the ideal-ground value depending on the details of the soil and the ground system. It is my opinion that calculating P_r and efficiency using the perfect ground value for R_r is a reasonable approximation for the vertical antennas likely to be used by Amateur Radio operators at 630 m and 2200 m.

Measuring E-field intensities accurately many km from the antenna at low power levels and also figuring out the ground wave attenuation factors from soil measurements isn't practical for most hams. At LF and MF, forget the E-field measurements; just do some simple modeling to determine R_r over perfect ground and measure your base current: $P_r = I_o^2 R_r!$

Acknowledgements

I want to express my appreciation to Steve Stearns, K6OIK, for his very helpful review of this article. He put in a lot of effort and I've incorporated many of his suggestions in the main article and in the Appendices. I also appreciate the comments from Dean Straw, N6BV, and Al Christman, K3LC. All of the modeling employed a prototype version of Roy Lewallen's *EZNEC Pro/4* that implements *NEC 4.2* and Dan McGuire's (AC6LA) *AutoEZ* which is an *EXCEL* spreadsheet that interacts with *EZNEC* to greatly expand the modeling options.^{10, 11} Without these wonderful tools this study would not have been practical and I strongly recommend both programs.

Rudy Severns, N6LF, was first licensed as WN7WAG in 1954 and has held an Amateur Extra class license since 1959. He is a consultant in the design of power electronics, magnetic components and power conversion equipment. Rudy holds a BSE degree from the University of California at Los Angeles. He is the author of three books, more than 90 technical papers and a past editor of QEX. Rudy is an ARRL Life Member and an IEEE Life Fellow.

Notes

- ⁸J. Wait, R. Collin and F. Zucker, *Antenna Theory*, Chap 23, Inter-University Electronics Series (New York: McGraw-Hill, 1969), Vol 7, pp 414 – 424.
- ⁹The Appendices and other files associated with this article are available for downloading from the ARRL *QEX* files web page. Go to www.arrl.org/qexfiles and look for the file **7x15_Severns.zip**.
- ¹⁰Roy Lewallen, W7EL, *EZNEC pro/4*, www.eznec.com.
- ¹¹Dan McGuire, AC6LA, *AutoEZ*, www.ac6la.com/autoez.html.

Table 1A

630 m Vertical 64 Radials, Integration Radius = 100 m.

Soil	R_i [Ω]	R_r [Ω]	R_g [Ω]	R_r / R_i	$0.7 / R_i$	G_a
0.001/5	5.50	1.01	4.49	0.18	0.13	0.060
0.005/13	2.01	0.844	1.17	0.42	0.34	0.232
0.03/20	1.09	0.76	0.32	0.70	0.63	0.533
Perfect	0.69	0.69	0	1.00	1.00	1

Table 1B

630 m Vertical 128 Radials, Integration Radius = 100 m.

Soil	R_i [W]	R_r [W]	R_g [W]	R_r / R_i	$0.7 / R_i$	G_a
0.001/5	4.90	1.009	3.895	0.21	0.14	0.067
0.005/13	1.883	0.843	1.04	0.45	0.37	0.247
0.03/20	1.033	0.78	0.253	0.76	0.67	0.561
Perfect	0.69	0.69	0	1.00	1.00	1.00

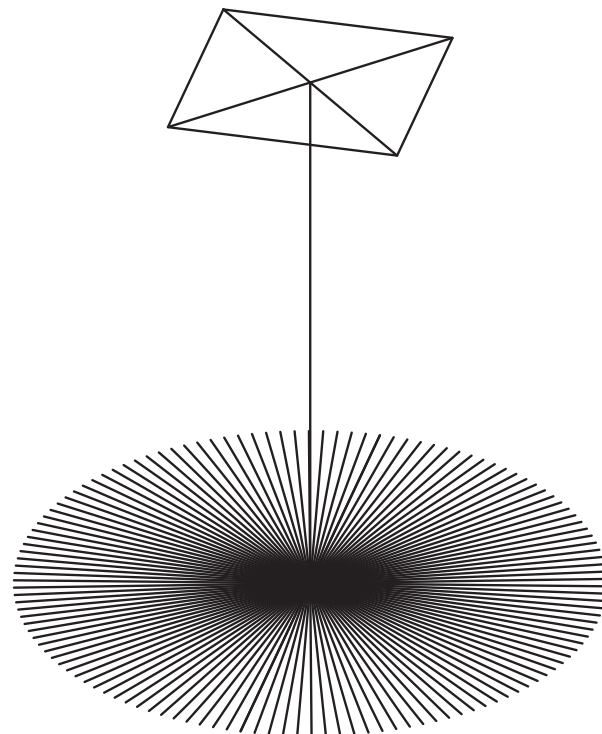


Figure 19 — This model shows a 630 m antenna example.

There was an error in the way Equation SB2 was printed in Part 1 of this article. That equation, in the **EIRP and Radiated Power, P_r , From Verticals** sidebar on page 29 of the July/August 2015 issue of *QEX*, was printed without the subscripts, superscripts and equals sign. There was also an error in the denominator of the equation. The correct equation is reproduced here. We apologize for this error, and offer our thanks to Andy Talbot, G4JNT, for being the first to point out the problem with this equation. — Ed.

$$EIRP = \frac{r^2 |E_z|^2}{30} [W] \quad [Eq SB2]$$

Quality Factor, Bandwidth, and Harmonic Attenuation of Pi Networks

The author looks at several definitions of Q , and makes some interesting discoveries about what these calculations can tell us about the design of pi networks..

I recently became interested in pi networks, a type of impedance-matching resonant network that provides harmonic attenuation and is often used in tube-type Amateur Radio transmitters. I was particularly interested in the relationship between the quality factor, Q , and the bandwidth of these networks. In various editions of *The ARRL Handbook for Radio Communications*, I found three definitions of Q , all different. None of the three were very good predictors of the bandwidths of pi networks for most values of the load and source impedances. During these explorations, however, I discovered that a modification of one of the three provided a much better predictor of bandwidth. Subsequently, I was able to derive this modified form of Q theoretically.

While the bandwidth of pi networks is interesting, a perhaps more important characteristic of these networks is their ability to attenuate harmonics present in the signals passing through them. This paper presents data on the harmonic attenuation of these networks as a function of their quality factors.

Finally, I investigated whether the methods used in this paper could be extended to more complex networks. For pi-L networks, they yield a value for Q that fairly accurately predicts bandwidth but not harmonic attenuation. They also yield quality factors for more complicated networks, but these values do not seem to have much relationship with bandwidth.

Quality Factor of Impedance-Matching Networks

Impedance-matching networks are characterized by, among other things, their design frequency (the frequency at which the input and output impedances are matched) and by the quality factor, Q . Quality factor is defined in two different ways. The first, and perhaps most common way, to define Q is given by Equation 1.

$$Q = 2\pi \times f_0 \times \frac{\text{Average energy stored in reactive elements}}{\text{Power dissipated by lossy elements}}$$

[Eq 1]

where f_0 is the design frequency (in which the output and input impedances are matched), and dissipated power is the electrical energy dissipated per second, that is, converted into some other form of energy, such as thermal or radiation. (Dissipated power divided by frequency is the energy dissipated per cycle.)

Equation 2 gives a second definition of Q .

$$Q = \frac{f_0}{BW} \quad \text{[Eq 2]}$$

where BW is the 3 dB bandwidth, which is the width between the upper and lower frequencies at which the response of the circuit is down 3 dB from its response at f_0 .

Circuit-analysis textbooks show that these two definitions are exactly equivalent for simple series and parallel RLC circuits. For circuits using more than two reactive components, such as the pi network, it is unclear (to me at least) that the definitions given by Equations 1 and 2 are even approximately equivalent. This is important because the Q of a more-complicated matching network is most easily calculated using Equation 1, because this calculation can only be performed at one frequency, whereas the bandwidth and the network's ability to attenuate harmonics of the design frequency are usually the more important parameters in the design process. That is, it seems to me that Q is useful for practical design work in so much as it provides information about the bandwidth and/or harmonic attenuation of a circuit.

Wes Hayward, W7ZOI, in his ARRL book *Introduction to Radio Frequency Design* has the following discussion of Q .¹

" Q is not well defined for networks with three or more reactive components. Still, Q is a frequently used parameter in the design equations for more complex networks. The meaning of Q is different when applied to such networks. It is the ratio of a

¹Notes appear on page 35

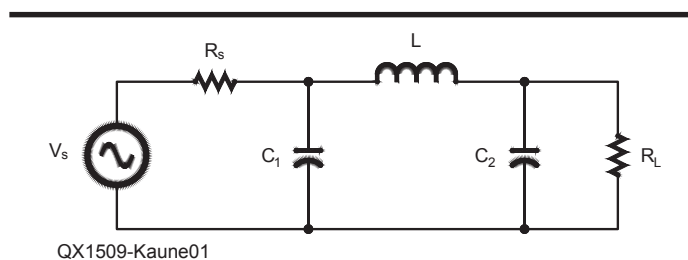
resistance to a reactance when looking into one end of the network at one frequency. Network reduction methods are always used. The user should not deduce the bandwidth of the network by the Q used for design.”

After puzzling about this for some time, I decided to look into the relationship between Q and bandwidth for a specific matching circuit, the pi network (which includes three reactive components).

Quality Factor and Bandwidth of Pi Networks

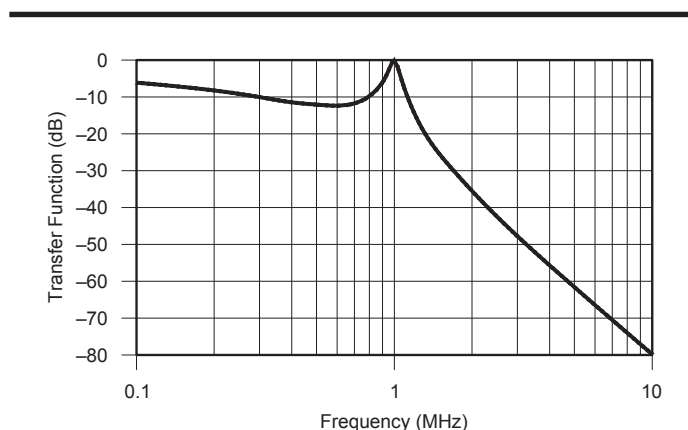
Figure 1 shows a pi-network circuit configuration often used to match a load impedance, R_L , to a source impedance, R_S . A common application of pi networks is in the output circuits of tube-type power amplifiers, where relatively large source impedances have to be matched to relatively low antenna impedances. The configuration shown in Figure 1 forms a low-pass filter and provides substantial attenuation of harmonics of the design frequency. There is also a high-pass form of the pi network, but this configuration is not often used in Amateur Radio equipment, so I will concentrate solely on the low-pass form.

The transfer function of a pi network is defined as V_L / V_S , where V_L is the voltage across the load resistor and V_S is the source voltage. Figure 2 is a typical transfer function for a pi network, as a function of frequency. In this example, the design frequency was 1 MHz, the source and load resistances were 500 and 50 Ω , respectively, the 3 dB bandwidth was 100 kHz, and the transfer function was normalized to 0 dB at the design frequency. Notice the peak that occurs in the transfer function at the design frequency: It is the 3 dB width of this peak that defines bandwidth.



QX1509-Kaune01

Figure 1 — This schematic diagram shows a low-pass pi network.



QX1509-Kaune02

Figure 2 — Here is a plot of the transfer function (T) of a pi network. The design frequency for this example was 1 MHz. T is normalized to 0 dB at the design frequency.

I first looked into the Amateur Radio literature to see what others had learned about Q and bandwidth for pi networks. I discovered a 1983 paper by Elmer Wingfield, W5FD, titled “New and Improved Formulas for the Design of Pi and Pi-L Networks,” published in *QST*.² In this paper, the author notes that earlier ARRL publications had defined the pi network quality factor as the expression given in Equation 3.³

$$Q_I = \frac{R_S}{|X_{C1}|} \quad [\text{Eq 3}]$$

where R_S and $|X_{C1}|$ are the source resistance and the magnitude of the reactance of the input capacitance. (Note that capacitive reactances are negative so, in this case, $X_{C1} = -|X_{C1}|$.) Since this definition of Q refers only to the input section of the pi network, I will refer to it as Q_I in the remainder of this paper. Wingfield argued in his paper that a better value for Q would be one that accounts for both the source and load resistances, and proposed that Q be defined by Equation 4.

$$Q_W = \frac{R_S}{|X_{C1}|} + \frac{R_L}{|X_{C2}|} \quad [\text{Eq 4}]$$

This expression, which I will refer to as Q_W , includes both input and output resistances and reactances.

The next documents I looked at were the 2003 and 2007 editions of *The ARRL Handbook for Radio Communications*, where the results reported by Wingfield were essentially reproduced.^{4,5} I then looked at the 2013 and 2015 editions of the *Handbook*, where I found a new, and slightly more complicated, definition for Q , given in Equation 5.^{6,7}

$$Q_M = \begin{cases} \frac{R_S}{|X_{C1}|} & \text{if } R_S > R_L \\ \frac{R_L}{|X_{C2}|} & \text{if } R_S \leq R_L \end{cases} \quad [\text{Eq 5}]$$

I will call this definition Q_M because it refers to the latest, most modern definition of Q that appears in *The ARRL Handbook*.

Finally, I am going to define a fourth expression, Q_{BW} , based on the actual bandwidth of the circuit, as calculated using Equation 2. As discussed earlier, the Amateur Radio literature uses at least three different definitions for the quality factor of a pi network. Are these definitions equivalent, and if not, which is the best predictor of the actual bandwidth of the circuit, that is, Q_{BW} ?

To answer this question, I wrote a computer program (using *Visual Basic 6.0*) that, for a given pi-network design, calculates Q_I , Q_W , and Q_M , and also the transfer function from which the bandwidth and Q_{BW} can be determined. I then used this program to consider four cases, in which $R_S = 5, 50, 500$, and 5000 Ω , while $R_L = 50 \Omega$. In each case, I selected values for X_{C1} , X_L , and X_{C2} so that the bandwidth of the resulting circuit was exactly 1/10 of the design frequency, that is, with $Q_{BW} = 10$. Table 1 shows my results. This table shows very clearly that the four definitions of Q are in substantial disagreement. For example, Q_I varies between 4.8 and 19.0 as the source resistance is varied from 5 to 5000 Ω , even though the bandwidth is held constant. Q_M , on the other hand, consistently indicates a smaller bandwidth than the actual value; when $R_L = 5000 \Omega$, the indicated bandwidth is 53% of the actual value. Obviously, these two definitions of Q would be poor predictors of bandwidth (except when $R_S \approx R_L$).

The Wingfield value for Q remains consistently in the range 20.4 to 20.6 as the source resistance is varied. If we were to divide this value by 2, we would obtain values nearly equal to Q defined by bandwidth. This suggests that the definition for Q given by Equation 6 might be more useful for predicting the bandwidth of a pi network.

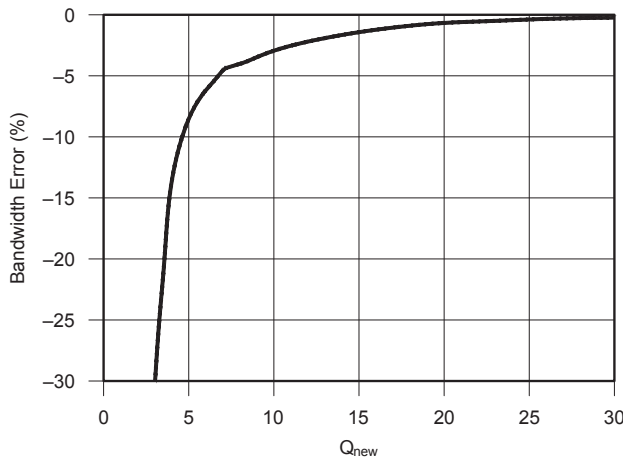
Table 1

Calculated Q Values and Harmonic Attenuations for Selected Source and Load Resistances, With Constant Bandwidth. $Q_T = R_S / |X_{C1}|$, $Q_W = R_S / |X_{C1}| + R_L / |X_{C2}|$, $Q_M = R_S / |X_{C1}|$ if $R_S \geq R_L$ or $R_L / |X_{C2}|$ if $R_S < R_L$, and $Q_{BW} = f_0 / BW$, where $f_0 =$ Design Frequency and $BW = 3$ dB Bandwidth.

Resistance (Ω)		Reactance (Ω)			Q_T	Q_W	Q_M	Q_{BW}
R_S	R_L	X_{C1}	X_L	X_{C2}				
5	50	1.03	4.19	3.21	4.8	20.4	15.6	10.0
50	50	4.91	9.73	4.91	10.2	20.4	10.2	10.0
500	50	32.1	41.9	10.3	15.6	20.4	15.6	10.0
5000	50	264	285	31.0	19.0	20.6	19.0	10.0

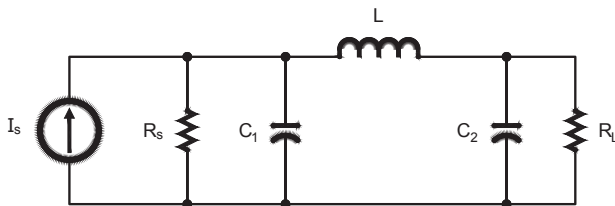
$$Q_{new} = \frac{Q_W}{2} = \frac{1}{2} \left(\frac{R_S}{|X_{C1}|} + \frac{R_L}{|X_{C2}|} \right) \quad [\text{Eq 6}]$$

To test this hypothesis, I used the computer program described earlier to determine the error estimating bandwidth using Q_{new} defined by Equation 6. I did this for a fixed load resistance of 50 Ω and source resistances of 5, 50, 500, and 5000 Ω . I found that the errors using Q_{new} to estimate bandwidth were reasonably similar across all the load resistances, so I selected the maximum error across all source resistances. The result is shown in Figure 3. Q_{new} is plotted on the horizontal axis and the vertical axis is the error using Q_{new} to estimate bandwidth. The error estimating bandwidth using Q_{new} is about -31% for $Q_{new} = 3$. As Q_{new} is increased, the maximum error decreases



QX1509-Kaune03

Figure 3 — This graph estimates the error in the predicted bandwidth using the quantity Q_{new} , as defined in the text.



QX1509-Kaune04

Figure 4 — This schematic diagram shows a pi network with a Norton Equivalent current source replacing the voltage source shown in Figure 1.

rapidly, falling to -8.6% when $Q_{new} = 5$ and -2.2% when $Q_{new} = 10$. These results show that Q_{new} is a good measure of the true bandwidth of a pi network, certainly for $Q_{new} \geq 5$. Q_{new} is a better indicator of bandwidth than any of the three Q equations that appear in *The ARRL Handbook*.

Of course, it would be desirable to also have a confirmation, based in theory, of this definition of Q [Equation 6]. In the next section, I present such a derivation.

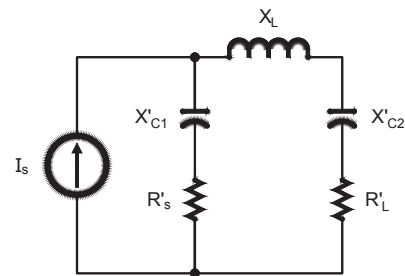
Theoretical Derivation of Q_{new}

Various textbooks on circuit analysis show (Norton’s Theorem) that a voltage source, characterized by an open-circuit voltage, V_S , and a series impedance, R_S , can be replaced by a current source, I_S , shunted by an impedance R_S , where $I_S = V_S / R_S$. Thus, the pi network drawn in Figure 4 is equivalent to the pi network in Figure 1. Next, convert the parallel combination R_S and X_{C1} in Figure 4 into a series combination R'_S and X'_{C1} , and similarly convert X_{C2} and R_L into X'_{C2} and R'_L , resulting in the circuit configuration shown in Figure 5. The relation between the original and converted quantities is given in Equations 7 and 8.

$$R'_S = R_S \frac{X_{C1}^2}{R_S^2 + X_{C1}^2} \quad \text{and} \quad X'_{C1} = X_{C1} \frac{R_S^2}{R_S^2 + X_{C1}^2} \quad [\text{Eq 7}]$$

$$R'_L = R_L \frac{X_{C2}^2}{R_L^2 + X_{C2}^2} \quad \text{and} \quad X'_{C2} = X_{C2} \frac{R_L^2}{R_L^2 + X_{C2}^2} \quad [\text{Eq 8}]$$

At first sight, Figure 5 appears to be a simple series RLC circuit, and, this is true so long as only one frequency is considered. Things become more complicated, however, as frequency is varied, because the resistances, R'_S and R'_L , and the capacitances, C'_1 and C'_2 vary with frequency according to Equations 7 and 8. We can use Figure 5 as long as we restrict ourselves to the design frequency.



QX1509-Kaune05

Figure 5 — Here is a redrawn version of the pi network shown in Figure 4, obtained by converting parallel resistor and capacitor combinations into equivalent series combinations.

In a matched system, the power transferred to the load resistance, R_L' in Figure 5, is maximized. It is easy to show (and is well known) that Equation 9 expresses the conditions for maximum power transfer.

$$\begin{aligned} X_L + X'_{C1} + X'_{C2} &= 0 \\ R'_S &= R'_L \end{aligned} \quad [\text{Eq 9}]$$

These two equations determine the values of two of the three adjustable components (C_1 , L , and C_2) in a pi network. We are thus free to choose the value of the remaining component. (Ultimately, we will use a specification of Q to determine the value of this component.) Thus, for the time being, assume that a value for X_{C1} has been specified. We will determine X_L and X_{C2} as functions of X_{C1} . Use the second equation in each set shown as Equations 7, 8 and 9.

$$R'_S = R'_L \Rightarrow R_S \frac{X_{C1}^2}{R_S^2 + X_{C1}^2} = R_L \frac{X_{C2}^2}{R_L^2 + X_{C2}^2} \quad [\text{Eq 10}]$$

Solve this equation for X_{C2} , yielding Equation 11.

$$X_{C2} = -R_L \sqrt{\frac{R_S X_{C1}^2}{R_L R_S^2 + (R_L - R_S) X_{C1}^2}} \quad [\text{Eq 11}]$$

Then, the first equation in each set shown as Equations 7, 8 and 9 can be combined to yield Equation 12 for X_L .

$$X_L = -(X'_{C1} + X'_{C2}) = -X_{C1} \frac{R_S^2}{R_S^2 + X_{C1}^2} - X_{C2} \frac{R_L^2}{R_L^2 + X_{C2}^2} \quad [\text{Eq 12}]$$

What is the Q of the circuit in Figure 5? Treating it as a simple series RLC circuit with total resistance $R'_S + R'_L$ and inductive reactance X_L , we get Equation 13.

$$Q = \frac{X_L}{R'_S + R'_L} \quad [\text{Eq 13}]$$

Then, using Equations 7, 8, and 12, we get Equation 14.

$$Q = \frac{-X_{C1} \frac{R_S^2}{R_S^2 + X_{C1}^2} - X_{C2} \frac{R_L^2}{R_L^2 + X_{C2}^2}}{R_S \frac{X_{C1}^2}{R_S^2 + X_{C1}^2} + R_L \frac{X_{C2}^2}{R_L^2 + X_{C2}^2}} \quad [\text{Eq 14}]$$

Equation 10 can be rearranged to yield the identity shown as Equation 15.

$$\frac{R_L^2}{R_L^2 + X_{C2}^2} = \frac{R_L}{X_{C2}} \frac{X_{C1}^2}{R_S} \frac{R_S^2}{R_S^2 + X_{C1}^2} \quad [\text{Eq 15}]$$

Placing this expression into Equation 14, we obtain Equation 16.

$$Q = \frac{-X_{C1} \frac{R_L}{R_S} \frac{X_{C1}^2}{X_{C2}}}{2 \frac{X_{C1}^2}{R_S}} = \frac{1}{2} \left(\frac{R_S}{|X_{C1}|} + \frac{R_L}{|X_{C2}|} \right) \quad [\text{Eq 16}]$$

This is just the expression for Q that we earlier identified as Q_{new} in Equation 6. We previously found that Q_{new} is a better predictor of the bandwidth of a pi network than other definitions of Q that have been given in the Amateur Radio literature, and we have now shown that there is theoretical plausibility for this form of Q .

Calculation of Components of a Pi Network

Now I will show how to calculate X_{C1} given a value of Q . Equation 16 can be rewritten as Equation 17.

$$\left(2Q - \frac{R_S}{|X_{C1}|} \right)^2 = \frac{R_L^2}{X_{C2}^2} \quad [\text{Eq 17}]$$

Use Equation 11 to eliminate X_{C2} in the denominator on the right-hand side of Equation 17. This gives an equation that involves only R_S , R_L , X_{C1} , and Q . Solving for X_{C1} gives the result shown in Equation 18.

$$X_{C1} = -R_S \left[\frac{2QR_S + \sqrt{4Q^2 R_S R_L - (R_S - R_L)^2}}{R_S (4Q^2 + 1) - R_L} \right] \quad [\text{Eq 18}]$$

There is actually a second solution, obtained by replacing the plus sign in front of the square root symbol with a minus sign. I have been able to show, however, that this solution always leads to values of X_{C2} and/or X_L that have the wrong sign.

Once X_{C1} is determined, the values of X_{C2} and X_L can be calculated using Equations 11 and 12. In order for X_{C1} to be real and negative, the quantity in Equation 18 under the square root sign must not be negative and the denominator must be positive. In addition, for X_{C2} , defined by Equation 11, to be a real number, the denominator of the fraction under the square root sign must be a positive number. Analysis shows that these three conditions are met if the following inequalities are satisfied

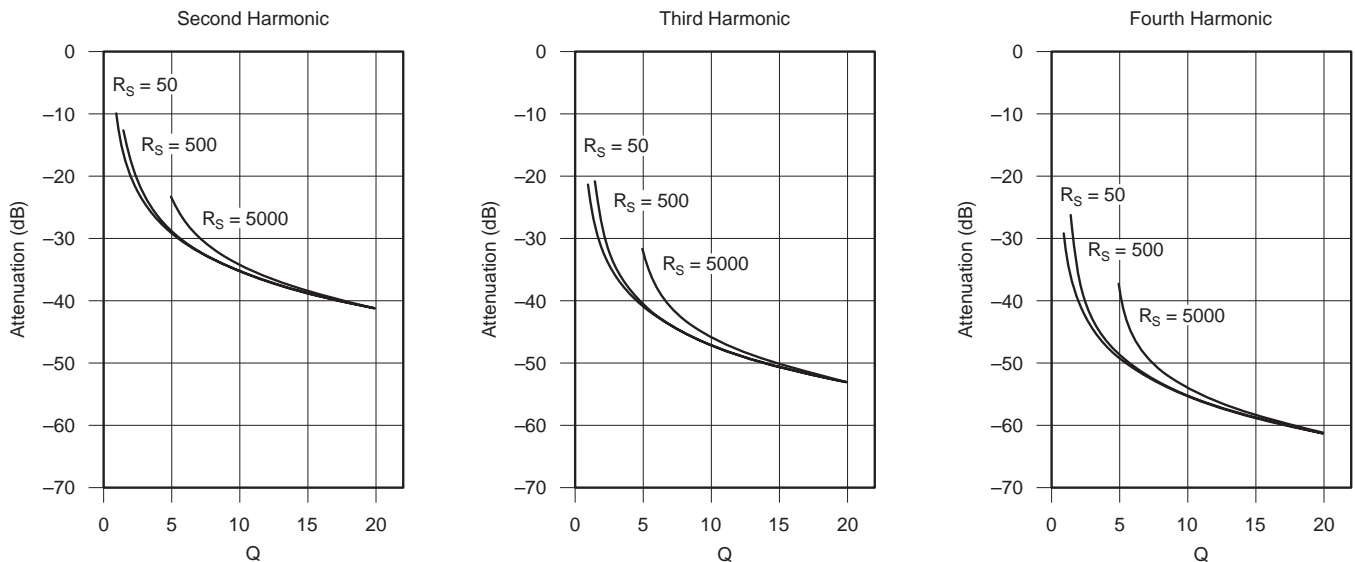
$$Q > \frac{1}{2} \sqrt{\frac{R_S}{R_L} - 1} \quad \text{if } R_S > R_L \quad [\text{Eq 19}]$$

$$Q > \frac{1}{2} \sqrt{\frac{R_L}{R_S} - 1} \quad \text{if } R_S < R_L$$

Harmonic Attenuation of Pi Networks

Figure 2 shows that pi networks provide substantial attenuation of the harmonics of the design frequency. Indeed, impedance matching and harmonic attenuation are the usual reasons for employing a pi network. I used the computer program described earlier to calculate the attenuation of the second through tenth harmonics of the design frequency of the network. The results for the second, third, and fourth harmonics are shown graphically in Figure 6 for values of Q defined by Equation 6, ranging from 1 to 20, and for source impedances of 50, 500, and 5000 Ω . Because of the reciprocal nature of pi networks, harmonic attenuation for a network with a given *ratio* of source to load resistances will be the same as network whose *ratio* of source to load resistances is the inverse of the first. Thus, for example, the harmonic attenuation of a network with source and load resistances of, say, 500 and 50 Ω , respectively, will be the same as that of a network with source and load resistances of 5 and 50 Ω , respectively.

The data in Figure 6 show that harmonic attenuation increases as Q increases, but also that the rate of this increase decreases for larger values of Q . For a Q of 10, the second, third, and fourth harmonics

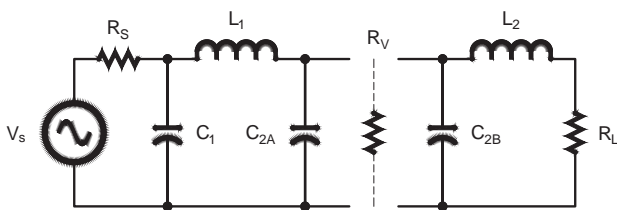


QX1509-Kaune06

Figure 6 — These graphs plot the attenuation of second, third and fourth harmonics by a pi network as a function of Q . Data are shown for load resistance of $50\ \Omega$ and source resistances, R_S , of 50, 500, and 5000 Ω .

Table 2
Fitted Values for Parameters in Equation $A_N = a_0 + a_1Q + a_2Q^2$

Harmonic	a_0 (dB)	a_1 (dB)	a_2 (dB)	Accuracy (dB)
2	-22.4	-1.58	0.0316	± 0.4
3	-34.0	-1.62	0.0328	± 0.5
4	-41.8	-1.64	0.0333	± 0.5



QX1509-Kaune07

Figure 7 — Here, the pi-L network is divided into a pi network followed by an L network. The resistance looking into the input of the L network is R_V ; this is also the load resistance for the pi network.

of the design frequency are attenuated by about $-35\ \text{dB}$, $-47\ \text{dB}$, and $-54\ \text{dB}$, respectively, and are nearly the same for all three source resistances. The data for $Q \geq 7.5$ are described with an accuracy of $\pm 0.5\ \text{dB}$ or better by the form $A_N = a_0 + a_1Q + a_2Q^2$, where A_N is the attenuation of the N^{th} harmonic, and values for the constants a_0 , a_1 , and a_2 are listed in Table 2.

More Complex Networks

When I started this investigation, I had little idea how to *simply* analyze a pi network, and my first efforts led to quite complicated equations that were not very illuminating. It was only when I happened on the idea of transforming parallel resistances and reactances into an

equivalent series pair that I was able to make progress. In this way, I was able to deduce a value for the Q of a pi network that effectively predicted bandwidth and harmonic attenuation, at least for larger values of Q . I began to wonder if the same approach would work for more complicated networks.

My first effort was to add a second inductor between the load resistor and the top of capacitor C_2 in Figure 1 to form a pi-L network. By dividing the capacitance C_2 into two parallel capacitors, C_{2A} and C_{2B} , the pi-L network can be transformed into a cascaded pair of networks, a pi network followed by a L network; this is illustrated in Figure 7. Furthermore, by selecting C_{2B} appropriately, the impedance looking into the input of the L network can be made a pure resistance, R_V ; this “virtual” resistance is drawn in dotted lines in Figure 7 and is the load resistance of the pi network and the source resistance for the L network. Analysis of the L network is simple, and we can use the results earlier in this paper for the pi network.

Let Q_2 be the quality factor for the L network. By transforming the series pair L_2 and R_L into an equivalent parallel pair, the L network is transformed into a simple parallel RLC network, from which we can show that the reactances of L_2 and C_{2B} , and the resistance of R_V are given by the expressions of Equation 20.

$$X_{L_2} = 2Q_2R_L, \quad X_{C_{2B}} = -\left(\frac{4Q_2^2 + 1}{2Q_2}\right)R_L, \text{ and}$$

$$R_V = (4Q_2^2 + 1)R_L \quad [\text{Eq } 20]$$

Next, let Q_1 be the quality factor for the pi network. Equations 11, 12 and 18, with L , C_2 , and R_L replaced by L_1 , C_{2A} , and R_V , respectively, can then be used to calculate X_{C_1} , $X_{C_{2A}}$, and X_{L_1} . X_{C_2} can then be calculated by combining $X_{C_{2A}}$ and $X_{C_{2B}}$ in parallel.

What, then, is the quality factor, Q , for the composite network? According to Equation 1, it is the sum of the energies stored in the pi and in the pi-L networks, divided by the power dissipated in the source and load resistors (assuming losses in C_1 , C_2 , L_1 , and L_2 are small enough to be neglected).

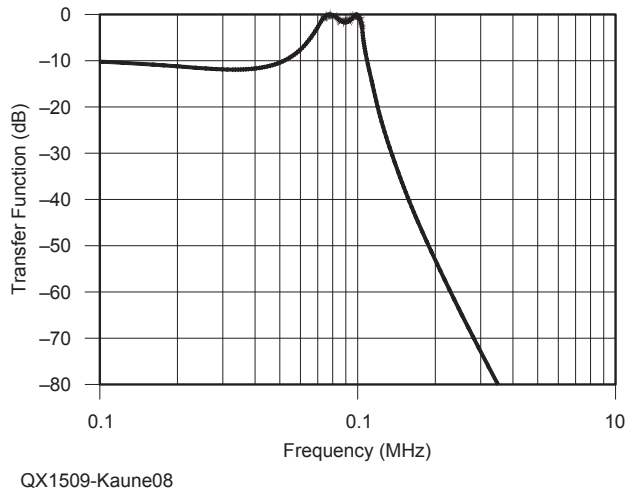


Figure 8 — This graph shows the transfer function for a cascade of two pi networks.

$$Q = 2\pi f_0 \frac{S_1 + S_2}{P_S + P_L} = 2\pi f_0 \frac{S_1}{P_S + P_L} + 2\pi f_0 \frac{S_2}{P_S + P_L} \quad [\text{Eq 20}]$$

where S_1 and S_2 are the average energies stored in the two networks, and P_S and P_L are the powers dissipated in the source and load resistances, respectively. Now look at each network separately. Network 1, the pi network, has as its load resistance R_V , which dissipates a power P_V . Then we obtain Equation 21.

$$Q_1 = 2\pi f_0 \frac{S_1}{P_S + P_V} \quad [\text{Eq 21}]$$

For network 2, the L network, we obtain Equation 22.

$$Q_2 = 2\pi f_0 \frac{S_2}{P_V + P_L} \quad [\text{Eq 22}]$$

Since R_V is matched to R_S by network 1, and R_L is matched to R_V by network 2, the powers dissipated in all three resistances are equal. With this result, we have proven Equation 23.

$$Q = Q_1 + Q_2 \quad [\text{Eq 23}]$$

I modified the computer program described earlier to model pi-L networks and found that Q calculated in this way is a good predictor of bandwidth (at least for larger values of Q). Q was not a good measure of harmonic attenuation, however, which varied significantly as the source resistance was varied.

I have explored even more complicated networks, such as two cascaded pi networks using the techniques described in this paper. With two pi networks, there are three independent parameters that have to be specified in order to uniquely define the network. For these three I chose Q_1 and Q_2 , the quality factors of the individual pi networks, and R_V , the “virtual” resistance looking into the input of the second network. Figure 8 shows the transfer function for one network where $R_L = 50 \Omega$, $R_S = 1800 \Omega$, $R_V = 300 \Omega$, $Q_1 = Q_2 = 5$, and with a design frequency of 1 MHz.

Note that there are now two peaks rather than one in the transfer function, leading to a considerably broadened response. In fact, the actual 3 dB bandwidth is 342 kHz. The overall Q of this network

is 10, so the predicted bandwidth would be 100 kHz, substantially less than the actual value. Each pi network, taken alone, would have had a single peak at 1 MHz, but the two together yield two peaks. Evidently, there are interactions between the two pi networks as the frequency is varied away from 1 MHz. From this and other examples I have worked out, I conclude that, in general, Q is no longer related in any simple way to the network bandwidth and level of harmonic attenuation. This is consistent with the comments of Wes Hayward quoted earlier in this paper.

Discussion and Conclusions

This article has found that three existing definitions for the quality factor of pi networks found in the Amateur Radio literature are not good predictors of the bandwidths (and harmonic attenuations) of these circuits. Both empirical and theoretical analysis suggest that a better definition of Q , at least for predicting bandwidth and harmonic attenuation, is given by Equation 24.

$$Q = \frac{1}{2} \left(\frac{R_S}{|X_{C1}|} + \frac{R_L}{|X_{C2}|} \right) \quad [\text{Eq 24}]$$

where R_S and R_L are the source and load resistances, respectively, and X_{C1} and X_{C2} are the input and output capacitive reactances of the pi network, respectively.

It appears to me that the methods employed in this paper can be extended to all networks containing three reactive components, with good results.

I was able to extend my analysis to pi-L networks with good results for bandwidth prediction but not harmonic attenuation. Analysis of networks more complex than pi-L networks yielded values for Q that were not predictive of bandwidth; I am not sure that Q has much significance for these more complex networks.

There are, of course, limitations to what is presented in this paper. The two main limitations are:

1) My analysis assumes that the reactive elements are lossless, but all real inductors and, to a lesser extent, capacitors have loss.

2) The source and load resistances are assumed to be constant independent of frequency, but this is probably seldom the case. For example, pi networks are often used in power amplifiers to match the output impedance of the amplifier to an antenna, and antenna impedances vary with frequency.

It would be well in any actual design to check the performance of circuits that include pi networks using one of the modern sophisticated computer circuit modeling programs, such as SPICE.

During the process of the work reported here, I could not perform an exhaustive search of the technical literature on pi networks. The material in this paper is new to me, but I would not be surprised to find a paper somewhere that made similar remarks to the ones here. I hope the results are of interest to hams and other electronics experimenters.

Finally, I would like to express my appreciation to the hams that reviewed an earlier version of this paper. They identified several errors and made very helpful suggestions.

Bill Kaune, W7IEQ, is a retired physicist (BS, PhD). He is married and has two grown daughters and four grandchildren. Bill spent most of his career collaborating with biologists and epidemiologists researching the biological effects of power-frequency electric and magnetic fields. Along with Amateur Radio, Bill spends his time hiking, backpacking, and doing some volunteer work. Bill was first licensed in 1956 as a novice and then a general, but became inactive while in college. He was licensed again in 1998 and upgraded to the Amateur Extra class in 2000. Bill is a member of the Jefferson County Amateur Radio Club and the ARRL.

Notes

- ¹Wes Hayward, W7ZOI, Rick Campbell, KK7B, and Bob Larkin, W7PUA, *Introduction to Radio Frequency Design*, ARRL, Newington CT, 1996, p 139.
- ²Elmer A Wingfield, "New and Improved Formulas for the Design of Pi and Pi-L Networks," QST, August 1983, pp 23 – 29.
- ³ARRL, *The Radio Amateur's Handbook*, The American Radio Relay League, Inc., The Rumford Press, Concord, NH, p 51.
- ⁴Dana Reed, W1LC, Ed, *The 2003 ARRL Handbook for Radio Communications*, ARRL, 2002, Newington, CT, pp 13.6 – 13.7.
- ⁵Mark Wilson, K1RO, Ed, *The 2007 ARRL Handbook for Radio Communications*, ARRL, 2006, Newington, CT, pp 18.6 – 18.7.
- ⁶H. Ward Silver, NØAX, Ed, *The 2013 ARRL Handbook for Radio Communications*, ARRL, 2012, Newington, CT, pp 5.25 – 5.26.
- ⁷H. Ward Silver, NØAX, Ed, *The 2015 ARRL Handbook for Radio Communications*, ARRL, 2014, Newington, CT, pp 5.25 – 5.26.

We Design And Manufacture To Meet Your Requirements

*Prototype or Production Quantities

800-522-2253

This Number May Not Save Your Life...

But it could make it a lot easier! Especially when it comes to ordering non-standard connectors.

RF/MICROWAVE CONNECTORS, CABLES AND ASSEMBLIES

- Specials our specialty. Virtually any SMA, N, TNC, HN, LC, RP, BNC, SMB, or SMC delivered in 2-4 weeks.
- Cross reference library to all major manufacturers.
- Experts in supplying "hard to get" RF connectors.
- Our adapters can satisfy virtually any combination of requirements between series.
- Extensive inventory of passive RF/Microwave components including attenuators, terminations and dividers.
- No minimum order.

NEMAL

Cable & Connectors
for the Electronics Industry

NEMAL ELECTRONICS INTERNATIONAL, INC.

12240 N.E. 14TH AVENUE
NORTH MIAMI, FL 33161
TEL: 305-899-0900 • FAX: 305-895-8178
E-MAIL: INFO@NEMAL.COM
BRASIL: (011) 5535-2368

URL: WWW.NEMAL.COM

Down East Microwave Inc.

We are your #1 source for 50MHz to 10GHz components, kits and assemblies for all your amateur radio and Satellite projects.

Transverters & Down Converters, Linear power amplifiers, Low Noise preamps, coaxial components, hybrid power modules, relays, GaAsFET, PHEMT's, & FET's, MMIC's, mixers, chip components, and other hard to find items for small signal and low noise applications.

We can interface our transverters with most radios.

Please call, write or see our web site
www.downeastmicrowave.com
for our Catalog, detailed Product descriptions and interfacing details.

Down East Microwave Inc.
19519 78th Terrace
Live Oak, FL 32060 USA
Tel. (386) 364-5529



Bring Your Ideas to Us

M² brings your antenna designs to life!

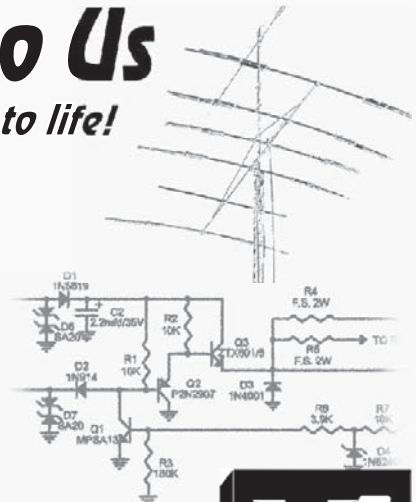
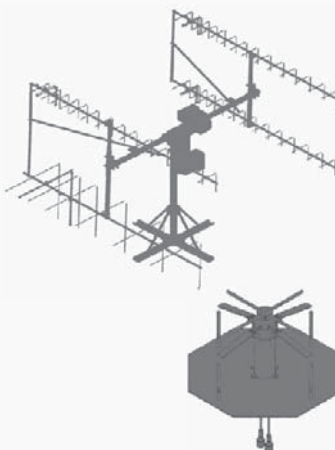
M² makes more than just high quality off-the-shelf products. We also build custom antenna systems using innovative designs to meet our customers' demanding specifications.

Our high-performing products cover high frequency, VHF, UHF and microwave. Ask us about our custom dish feeds.

From simple amateur radio installations to complete government and commercial projects, we have solutions for nearly every budget.

Directional HF and small satellite tracking stations are our specialties.

Contact us today to find out how we can build a complete antenna system to meet your needs!



WORLD CLASS PRODUCTS

M² offers a complete line of top quality amateur, commercial and military grade antennas, positioners and accessories. We produce the finest off-the-shelf and custom radio frequency products available.

For high frequency, VHF, UHF and microwave, we are your source for high performance RF needs. M² also offers a diverse range of heavy duty, high accuracy antenna positioning systems.

For communications across town, around the world or beyond, M² has World Class Products and Engineering Services to suit your application.

M² products are proudly 'Made in the USA'

4402 N. Selland Ave.
Fresno, CA 93722
Phone (559) 432-8873
<http://www.m2inc.com>
sales@m2inc.com

ANTENNAS POSITIONERS ACCESSORIES

SDR Simplified

Step Two towards a working SDR.

A Place for Updates

I have had the URL dsp-radio-resources.info set aside for several years, so that I could give readers a place to get updates, error corrections, and file downloads for this column. The site has been there but without useful content. I am happy to report that I now have the site populated with files for my May/June column. It also has additional instructions for using *Linux* on the BeagleBone Black computer.

Those who have used *Linux* will understand that *Linux* builds and installations can be quite an adventure. Fortunately, Ron Bassett is a neighbor who works for Canonical (the Ubuntu people). He has been quite helpful and obtained his own BeagleBone Black to work with me on this project. We have an image for 8 GB SD cards that is Ubuntu 14.04 LTS (Long Term Stability) for the BeagleBone Black, a 4 GB image with the TI EVM demonstration, and a 4 GB image for SDR development. We also have all of the libraries and header files, so that it is possible to build loadable modules on a computer for use with tasks such as the rotary encoder. Those files are all on the dsp-radio-resources.info web site.

As time away from writing SDR: Simplified allows, I will put older information on the site, too. Of course, each new edition of the column will be supported on the site.

Hardware News

The BeagleBone-X15 is a new project that is on the cusp of being available. There were announcements late last year about the development work. BeagleBoard.org has announced that the first 50 boards are in manufacturing and they expect general availability by November. The board uses the AM5728 Sitarra, which is an ARM A15 device. What makes this board interesting is that the main IC actually contains four

CPUs: two ARM cores and two C66X cores. It also contains all of the display and peripheral support contained in BeagleBone Black. My experience with support on brand new designs is that it is much like early versions of *Windows* or a new car model: don't buy the first ones off the assembly line. The early adopters will find the issues, and in a year or so we can probably start looking at this as a possible SDR platform. My initial impression is that the C66X DSP cores are similar to the DaVinci cores used in the Flex 6000 series of radios. The \$199 suggested price makes this an incredible potential for a *Linux* SDR computer. Imagine an entire *Linux* computer on a 4 x 4.2 inch board! I hope to be one of the first folks to look at it and will keep you updated.

The second bit of news is that the BeMicro CV A9 FPGA development kit is now shipping from Arrow. We have been anxiously awaiting its release because it is perfect for medium capability SDR filtering, up conversion, and down conversion. The price is \$149. It is just as important that Altera has included support for the A9 FPGA in the web version of Quartus II. Scotty Cowling is planning on covering this evaluation kit in his Hands-On SDR column in the next issue of *QEX*.

BeagleBone Black Issues

I found one hardware issue with the latest BeagleBone Black (revision C). The full size "Type A" USB host port does not play well with powered USB hubs. This issue likely affects older board revisions, too. I needed a powered hub to attach a USB powered mouse and USB powered keyboard. The issue is that the USB hardware and software do not handle power going both directions on the USB cable. The solution is to use low power devices on the hub and not use external power for the hub. That means I

plug nothing into the hub except a wireless mouse/keyboard combination and flash drives.

If you really need to use the USB hub in powered mode, you can do one of two procedures. The first is to open the jacket on the cable between the BeagleBone and the hub so you can cut the red wire. That stops the hub from sending power back towards the computer. The other alternative is to wait for the system to boot before plugging the hub cable into the computer. (This works, but is very inconvenient.)

Step Two

Last time we set up an optical encoder to control user input especially for frequency control. My goal for this issue was to be able to load an SDR program and connect our encoder to the program.

The first step is to choose a *Linux* based SDR program. There are many. The first one I looked at that was promising is *Quisk* as done by Jim Ahlstrom, N2ADR. Jim wrote a couple of awesome articles for *QEX* quite a while ago using FPGAs to implement a transceiver for HF.^{1,2} Jim was doing his initial work starting back in 2004 and developed his FPGA based exciter in 2007. FPGAs were not especially large that far back. The CV-A9 FPGA development kit is likely half the cost and at least 40 times the capability (113560 logic elements and 684 multipliers) of the EP2C8T144C7 in that original design (only 18 multipliers and 8000 logic elements.) Jim's design has progressed and you can build the HiQSDR board from his Eagle design files if you are looking for something that is already proven.³

My hardware to implement our desktop radio is in process. I am using

¹Notes appear on page 39.

the BeagleBone Black for control and user interface, the TI 5535 Launchpad for DSP (demodulation, modulation, audio in and out), BeMicro CV-A9, and a high speed ADC. My inclination is to use an evaluation board from Linear Technology. The LTC2208 that is used by TAPR is a 130 million samples per second (MSPS), 16 bit single channel converter. An alternate ADC is the LTC2182 giving 65 MSPS with two channels for I/Q operation. The evaluation boards are \$200 for either. Given that the LTC2182 is \$93 in single quantities, \$200 is a very good price.

Linux Adventures

I had mentioned the goal of trying to have a minimal system to listen to the Andersen Alternator in my May/June QEX column. It didn't take long to see that goal evaporate due to issues just getting Linux running. My friend Ron Bassett put together an image with Ubuntu long term stability release

14.04 for BeagleBone Black and pointed me to the only truly useful sites I have found so far for getting an SD card loaded with Linux.^{4,5} I found at least 60 different kernel and rootfs images all over the web. The one that eventually gave me a system that would allow me to build *Quisk* is the latest stable version of the lxde interface available from beagleboard.org.⁶

We have two options for compiling applications: native on BeagleBone, or cross compiling on an x86 Linux platform. I have installed both, but it is easier in general to compile and run on the target. I have images with various configurations on dsp-radio-resources.info so you can just download an image instead of building a system yourself. I discovered that the best course is a mixture. Loadable modules are best developed and compiled on an x86 Linux machine and Python and C user mode programs are best developed and compiled on the target.

It took a while, but I finally realized

that the Sitarra EVK comes with Linux and drivers for an LCD. The TI Sitarra support pages are an extra resource for getting a workable system running.⁷ The Sitarra EVK is very similar to the BeagleBone with input devices, connectors for USB, keyboards, and other devices, and a direct connection to a TFT LCD. TI supports BeagleBone Black, too, so we have fairly up to date resources from them. The TI Linux SDK is a bare bones system (no C compiler, no Python, or other compilers) aimed at allowing us to use the Qt graphics tools for displays.

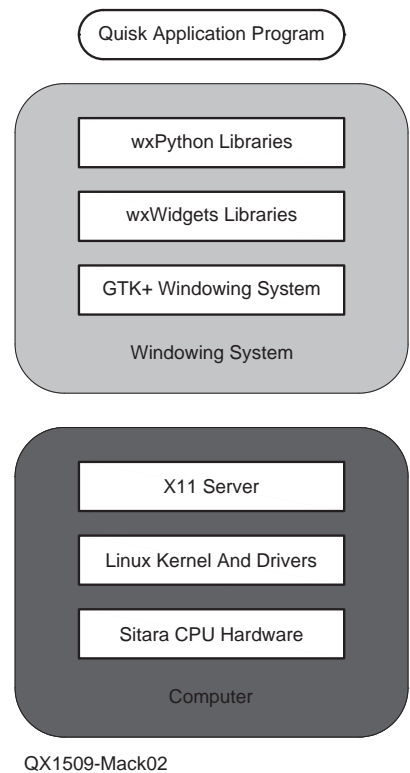
Figure 1 is a list of the steps that you need to take to build a development image from the ground up.

Getting Quisk Running

Quisk is a user mode application program written in C and Python. Figure 2 shows the layers of software and hardware in the system when it runs *Quisk*. It is very much like an onion with layers upon layers of software. All of the binary resources for *Quisk* are intended to run on an x86 computer, with Windows, Mac OSX, or Linux. No Armhf resources are available, so we need to build the system from source.⁸ As a practical matter, our radio is enough different that we will want to build from source files anyway. Figure 3 shows the display of *Quisk* running on my Linux development computer. The

Linux Commands to Build an Image

- 1) Download the bootable image from the web page. From dsp-radio-resources.info get **bbb-gui-wheezy-quisk-3-aug-2015.img.gz**. Say yes if the browser wants to open the archive manager. Save the file in your home directory. My home directory is **/home/ray**. The file in your home directory will be **bbb-gui-wheezy-quisk-3-aug-2015.img**
- 2) Open a terminal. In Ubuntu 14.04, it is in the utilities menu. Type "df -h" to display the various file systems that are mounted. Insert the 8GB microSD card in its adapter and install it in your computer. Your microSD card is likely the last one in the list, but you can tell which one it is because it is the new one in the list. Make note of the device for the SD card. Mine always show up as **/dev/mmcblk0p1** and **/dev/mmcblk0p2**. The "dd" command will copy an entire bit image from your hard drive and wipe out any existing data on the SD card. Make sure you back up any information on the SD card at this point.
- 3) You need to unmount these file systems. Type "sudo umount /dev/mmcblk0p1" and "sudo umount /dev/mmcblk0p2". Be sure to use the names appropriate to your system and all of the partitions on the device. Most will only have p1 and p2.
- 4) You are ready to copy your new image. It is imperative that you use the correct name in this next step so you do not overwrite other useful data. Type "sudo dd bs=4M if= bbb-gui-wheezy-quisk-3-aug-2015.img of=/dev/mmcblk0"
- Note that you use just the base part of the device. In this case it is mmcblk0. The p1 and p2 will show up once the disk image is written to the card. The copy process takes perhaps five or ten minutes and gives you no progress indication, so get a cup of coffee while you wait. It is unlikely it will fail, but if it does change the block size from "4M" to "1M" and retry the command. This **really** makes the copy process take a while if you should need it.
- 5) Type the command "sync" to force Linux to flush all of its data to the SD card.
- 6) Now you can eject the SD card and install it in the BeagleBone Black. Plug in power or press the power button to turn on the BeagleBone Black. You will see the penguin in the upper corner indicating that uboot has operated. Then you will see a fair number of lines of text indicating progress of the kernel loading. Shortly, you will see the mouse pointer and then the GUI will display. The display always flashes once while the process is proceeding. You now have a full Linux system ready to do work.



QX1509-Mack02

Figure 2 — A description of the layers of software components necessary for *Quisk* to operate.

Figure 1 — Linux commands to build an SD card image for BeagleBone Black.

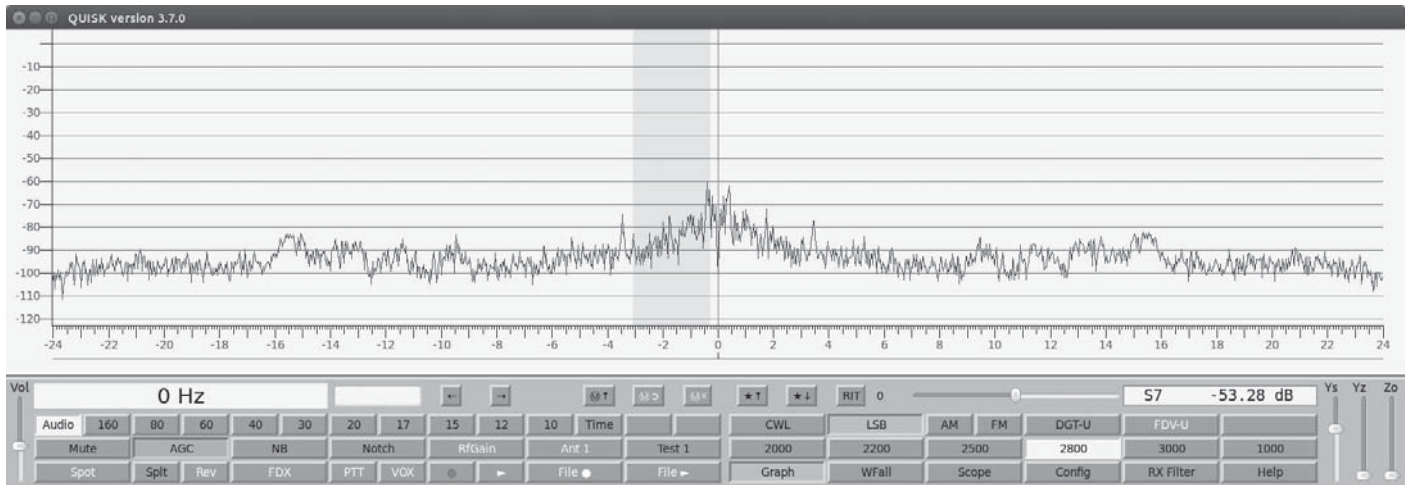


Figure 3 — A screenshot of *Quisk* running on a *Linux* computer.

display shows the frequency spectrum picked up using the computer's microphone.

The top level package is *wxPython*. This is a Graphical User Interface (GUI) toolkit for use in *Python* programs. The user interface in *Quisk* relies entirely on *wxPython*. As you can see from the block diagram, *wxPython* is built on top of *wxWidgets* which is in turn built on *GTK+* which runs on top of the *X11* system. Each library layer is intended to provide abstraction so that a program based on the library can run on multiple platforms by simply recompiling for the new system.

X11 is at the bottom of the stack and is the oldest of the libraries. Its job is to provide a common set of functions for displaying a primitive graphical interface on a display. Originally, *X11* was used to communicate with stand-alone terminals connected to mainframe computers in the late 70s and early 80s. Early CAD programs relied heavily on *X11* terminals connected to *Unix* systems. In modern computers, an *X11* server provides a software connection between application programs and the display hardware; it is completely computer specific code. *GTK+* is the next level up and provides a set of libraries for a uniform look and feel for a graphical user interface. It is the equivalent of the *Windows* API for computers. The next level of abstraction is provided by *wxWidgets* and provides the interfaces necessary to implement features like buttons, radio controls, scroll bars, and so on. Since *wxWidgets* is written entirely in *C++*, using it in an application program would require writing the program in *C++*. *wxPython* was written to provide a translation layer between a *Python* program and the *wxWidgets* library.

The waterfall and spectrum displays are based on the package *FFTW3*. It provides a very efficient fast Fourier transform library.

Figure 4 is a list of the sequence of

Linux Commands to Build *Quisk*

These instructions assume you are using an SD card that did not come from dsp-radio-resources.info with *Quisk* already installed and built. The instructions also apply if you want to build *Quisk* to run on your computer. (Start at step 3 and omit steps 4 and 5 for building for your computer)

- 1) Turn off power to your BeagleBone Black. Eject the SD card and put it in its adapter. Insert the SD card into your *Linux* computer. Open a terminal window on your computer.
- 2) Verify the name of your SD card by typing "df -h". For the target file system, the first string will likely be /dev/mmcblk0p2 and the last string will be something like /media/ray/rootfs. You can do a second verification by looking at the total size to verify that it is 4 GB for the stock image from Beagleboard.org.
- 3) Open a browser and get the *Quisk* distribution from "james.ahlstrom.name/quisk", and select "quisk-3.7.2.tar.gz" to download the package. Firefox on Ubuntu will ask if you want to open the package with the archive manager. Say "Yes". Save the decompressed image to your SD card home directory (/media/ray/rootfs/home/debian).
- 4) Type "sudo mount /dev/mmcblk0p1" and "sudo mount /dev/mmcblk0p2" in the terminal.
- 5) Place the SD card back in the BeagleBone Black and turn on the power. Open a terminal window.
- 6) Type "tar xJvf quisk3.7.0.tar". This will unpack the *Quisk* directory.
- 7) Type the following commands:

```
sudo apt-get install python-dev
sudo apt-get install python-wxgtk2.8 python-wxtools wx2.8-i18n
sudo apt-get install fftw3
sudo apt-get install fftw3-dev
sudo apt-get install libasound2-dev
sudo apt-get install libpulse-dev
sudo apt-get install portaudio19-dev
```

This process installs all of the header files and the packages necessary to build *Quisk*.
- 8) Be sure you are in the quisk-3.7.0 directory. Type "make". This will build a file called "quisk" in the quisk-3.7.0 directory. You cannot run this program just yet. You have to tell Linux that it is a program. Type "chmod 666 quisk" to make it a program that can run.
- 9) Type "./quisk &" to run *Quisk*. The shell will display a number as it starts *Quisk* that looks something like "[1] 2564". You can stop the program by typing "kill -9 2564" should it be necessary.

Figure 4 — The set of commands to get all of the pieces for use with *Quisk*.

commands that you need to run on the BeagleBone Black to install the *Quisk* source code and all of the other packages necessary for building our radio. The first step after downloading all of the resources is to build *Quisk* as delivered. Simply typing the command “make” is all that is necessary to build the system. *Quisk* runs on the BeagleBone Black but does nothing useful at this point because the hardware is enough different from a computer. At least it does not “crash and burn.” By the time you read this, I anticipate having it doing a minimal amount of display work. Another change I will be making is to move many of the buttons from Jim’s version into lower menus. With a change from mouse/touchpad to dedicated buttons, we will not have enough buttons to keep all functions at the top level menu. If you buy the touchpad version of the LCD, however, there is no reason not to keep Jim’s layout. The only reason you might not want to use the touch screen is that the buttons may be too small if you have “fat fingers” and bad eyesight, like me.

Notes

- ¹James Ahlstrom, N2ADR, “An All-Digital SSB Exciter for HF,” *QEX*, May/June 2008, pp 3 – 10.
- ²James Ahlstrom, N2ADR, “An All-Digital Transceiver for HF,” *QEX*, Jan/Feb 2011, pp 3 – 8.
- ³You can download the Eagle circuit board design files for Jim Ahlstrom’s HiQSDR transceiver at james.ahlstrom.name/transceiver/eagleboard.zip.
- ⁴One of the websites that I have found helpful for loading a Linux image to an SD card is: www.armhf.com/boards/beaglebone-black/#wheezy.
- ⁵The other website that I have found helpful for loading a Linux image to an SD card is: elinux.org/Beagleboard:BeagleBoneBlack_Debian.
- ⁶Download the latest stable version of the Ixde interface from: rcn-ee.com/rootfs/bb.org/release/2015-07-17/ixde-4gb/bone-debian-7.8-4gb-armhf-2015-07-17-4gb.img.xz.
- ⁷The TI Sitarra support pages are an extra resource for getting a workable system running: processors.wiki.ti.com/index.php/Sitara_Linux_Software_Developer%E2%80%99s_Guide, processors.wiki.ti.com/index.php/Processor_SDK_Linux_Getting_Started_Guide.
- ⁸You can download James Ahlstrom’s *Quisk* files at: james.ahlstrom.name/quisk. Select “quisk-3.7.2.tar.gz” to download the source.

2015 ARRL / TAPR

Digital Communications Conference

October 9-11
Chicago, Illinois



Make your reservations now for three days of learning and enjoyment at the DoubleTree by Hilton Chicago – Arlington Heights hotel. The Digital Communications Conference schedule includes technical and introductory forums, demonstrations, a Saturday evening banquet

and an in-depth Sunday seminar. This conference is for everyone with an interest in digital communications—beginner to expert.

Call Tucson Amateur Packet Radio at: 972-671-8277, or go online to www.tapr.org/dcc

From MILLIWATTS
To KILOWATTSSM
More Watts per DollarSM

In Stock Now! Semiconductors for Manufacturing and Servicing Communications Equipment

- **RF Modules**
- **Semiconductors**
- **Transmitter Tubes**

Se Habla Español • We Export

Phone: **760-744-0700**
Toll-Free: **800-737-2787**
(Orders only) **800-RF PARTS**
Website: **www.rfparts.com**
Fax: **760-744-1943**
888-744-1943
Email: **rfp@rfparts.com**



RF PARTS
COMPANY
From Milliwatts to KilowattsSM

Letters to the Editor

Octave for SWR (Jan/Feb 2009) and More Octave for SWR (Jan/Feb 2014)

Hi Larry,

My QEX articles “Octave for SWR” (Jan/Feb, 2009) and “More Octave for SWR” (Jan/Feb, 2014) make reference to a figure that has appeared in the *ARRL Handbooks* and *ARRL Antenna Books* for many years.^{1,2} The figure appears as Figure 20.4 in the 2013 *ARRL Handbook* and as Figure 23.14(A) in the 22nd Edition of *The ARRL Antenna Book*. The figure relates SWR and matched line loss to the additional loss caused by an SWR of greater than 1:1 at the load.

In the 2014 and later *ARRL Handbook*, the figure was replaced by one that yields total line loss, including matched loss, plus the additional loss caused by SWR, rather than just the added line loss. The revised Figure appears as Figure 20.4 in the 2015 *ARRL Handbook*.

The new figure requires no changes in the text or math in the QEX articles, and the old figure as reprinted in the two articles is still a valid tool. Just be aware that the figure in the current *ARRL Handbook* yields the same information, but in a slightly different form.

The new figure has the advantage that it yields a quantity — total line loss — that is in accord with the text and math in *The ARRL Handbook*.

I do have some concerns about the labels in the new *Handbook* Figure. For many years, dating as far back as 1952 or earlier, *The ARRL Handbooks* have included a figure that yields the loss that is added to the matched line loss when a transmission line is terminated in other than its characteristic impedance. In the 2013 and older *Handbooks*, the figure caption begins: “Fig. 20.4 — Increase in line loss due to standing waves (SWR) ...” The abscissa of the figure is labeled “Line Loss in dB When Matched” and the ordinate is labeled “Additional Loss in dB Caused by Standing Waves.”

The figure has been very useful, but it yields only the *increase* in line loss caused by SWR while the accompanying equation (Equation 11 on Page 20.5 of the 2013 *Handbook*) and the text deal with the total line loss, which is equal to the matched line loss plus the added loss due to SWR.

In the 2014 *Handbook*, and continuing with the 2015 Edition, the figure has been revised to yield the total line loss, rather than the additional line loss due to SWR. This change brings the figure into conformance with the accompanying text and math.

There are two problems with the new figure, though: the ordinate is labeled “Line Attenuation (dB)” and the caption begins with “Figure 20.4 — Total insertion loss ...”

There are several measures of loss that are commonly used in connection with transmission lines: insertion loss, transducer loss, attenuation, and line loss. All four are carefully defined in various references, including the *IEEE Dictionary of Electrical and Electronics Terms*, where “line loss” is termed “power loss,” as it is sometimes called elsewhere.³ I’ll summarize the definitions here, particularizing them to the case of a transmitter (source), transmission line and antenna (load):

Insertion loss: the ratio between the power delivered by the source to the load when the two are connected directly and the power delivered to the same load when a particular transmission line is interposed between the source and the load.

Transducer loss: the ratio between the maximum power that a particular source can deliver to a load selected to maximize the power absorbed (conjugate match) and the power that is delivered to a specified load by the same source through a particular transmission line.

Attenuation: the ratio between either voltages or currents at two points along a transmission line, usually a line with no reflections. When divided by the distance between the two points, this measure is the real part of the complex propagation constant.

Line loss: the ratio between the power delivered by the source to the transmission line and the power delivered by the transmission line to the load.

All these measure of loss are generally expressed in dB, but sometimes in nepers. Note that, for perfectly matched resistive sources, lines, and loads (SWR = 1:1 at all points), the various measures converge to the same value when the points measured for attenuation are at the source and the load.

I presented mathematical comparisons of insertion loss, transducer loss, and line loss in “Octave for SWR”. (See Note 1.) I showed that the equation and figure in the *Handbook* and the *Antenna Book* treat line loss rather than insertion loss or transducer loss. This is an important distinction because insertion loss and transducer loss are functions of the impedance of the source, the characteristic impedance of the line, and the impedance of the load. Line loss involves only the characteristic impedance of the line and the impedance of the load. Line loss “sees” the power from the source, but doesn’t care about the impedance of the source.

Using *line loss* makes possible the use of a relatively simple graph to relate matched line loss to total line loss in the presence of an SWR greater than 1:1. Pages 569 through 573 of *Reference Data for Radio Engineers*, on the other hand, provide equations and alignment charts for

calculating transducer loss and, along with it, line loss.⁴ The alignment chart on page 573 duplicates the functionality of the older added loss graph in the pre-2014 *Handbooks* and the current (22nd Edition) *Antenna Book*. The legend for the alignment chart notes that it disregards the impedance of the source, as should be the case for line loss.

The text and equations in *Reference Data for Radio Engineers* show that the mathematical or graphical procedures for determining insertion loss or transducer loss are more complicated than are the corresponding determinations of line loss.

Insertion loss and transducer loss are heavily used in telecommunications engineering, where the source and load impedances are generally known and are well controlled where accuracy of information transfer is the objective. For radio transmitters, though, where power efficiency is important, the source impedance is generally not well known and must be below the value of the “50 Ω” label on the output connector or the transmitter’s final amplifier will not be capable of reasonable Class AB1, AB2, or C performance. A 50 Ω resistive output impedance would yield an amplifier efficiency of exactly 50%. The transmitter expects to see a 50 Ω load to establish the load line for its final transistors or tubes, but its actual output impedance will generally be below 50 Ω.⁵

A tuner may, in addition, alter that output impedance significantly as it attempts to reflect as much returned energy as possible back toward the antenna. The equations and the figure in the *Handbook* would thus have to be made more complex so as to include the source impedance of the transmitter if they were to be used for insertion loss or transducer loss, and various different transmitters would cause the loss to change, making comparisons of lines and antennas difficult.

Insertion loss and transducer loss are also generally difficult to measure in the radio environment, as I pointed out in “Octave for SWR.” Line loss is thus the best measure of SWR performance for Amateur Radio transmission lines, and the new figure in the *Handbook* yields total line loss, not insertion loss or attenuation.

Attenuation is generally used to describe the reduction in voltage or current along a line when the impedances are matched so that there are no reflections. Attenuation is thus formally described as a simple voltage or current ratio, usually expressed in nepers or dB, and is often used to express the loss per unit length — in the matched case — of a transmission line.⁶

I suggest that the ordinate of the new *Handbook* figure should read “Total line loss (dB)” and the caption should begin with

"Figure 20.4 — Total line loss ..." Note that the text discusses line loss and is already in agreement with these recommendations. Because Figure 20.4 includes the matched case (SWR = 1:1) at its left margin, "...Total line loss ..." would be better than "...Total mismatched line loss ...," although the latter is appropriate in the text.

— 73, Maynard Wright, W6PAP, 6930
Enright Dr, Citrus Heights, CA 95621;
w6pap@arri.net

Octave for Transmission Lines (Jan/Feb 2007)

Hi, Larry,

In "Octave for Transmission Lines," I introduced a GNU Octave expression for the input impedance of a transmission line in terms of the length of the line, its electrical characteristics, and the terminating impedance at the far end.^{7,8,9}

$Z_d = Z_o \cdot \tanh((a + j \cdot B) \cdot d + \operatorname{atanh}(Z_t / Z_o));$

There is a degenerative case that may not be of much practical value, but that should probably yield a valid result for the sake of consistency: $Z_t = Z_o$. In that case, there are no reflections, the line is "flat," and Z_d (the input impedance) is equal to Z_o and Z_t . The Octave code in that case reduces to:

$Z_d = Z_o \cdot \tanh((a + j \cdot B) \cdot d + \operatorname{atanh}(1))$

but $\operatorname{atanh}(1)$ is mathematically undefined in that the limit of $\operatorname{atanh}(x)$, as x approaches 1, is infinity.

Octave accordingly returns Inf from a call to $\operatorname{atanh}(1)$, indicating that the value is too large to be represented by the IEEE floating point format for numbers.¹⁰ Octave does, though, allow certain operations involving Inf.¹¹ In this case, the hyperbolic tangent of an argument approaching infinity approaches 1, so the value 1 is returned by $\tanh((a + j \cdot B) \cdot d + \operatorname{Inf})$ and the result is $Z_d = Z_o = Z_t$ as we would expect of an actual implementation of this particular circumstance.

When we implement the same expression in Python, we get:¹²

```
import math
import cmath
```

```
....
Zd = Zo * cmath.tanh((a + B * 1j) * d +
cmath.atanh(Zt / Zo))
```

which, when $Z_t = Z_o$, reduces to:

```
Zd = Zo * cmath.tanh((a + B * 1j) * d +
cmath.atanh(1))
```

The call to the Python function $\operatorname{cmath}.\operatorname{atanh}(1)$ returns "Value error: math domain error" and halts execution if a script is being run.

Although we highlighted compatibilities in "Alternatives to Octave," Octave and Python behave differently in this case.¹³ Octave conveniently allows continuation of the

computation and yields a correct result, while Python flags an error and halts execution. It seems that neither Octave nor Python is incorrect in this matter, as the IEEE floating point standard allows several different behaviors as optional methods of exception handling, but the Octave result is probably more convenient for our purposes.

The exception in Python could be handled using the Python exception handling mechanism, which would allow continuation of the computation. Other alternatives, such as C or C++, should be tested for this anomaly and should be subjected to exception handling when appropriate.

— 73, Maynard Wright, W6PAP, 6930
Enright Dr, Citrus Heights, CA 95621;
w6pap@arri.net

Optimizing Magnetically Coupled Loop Antennas (Jan/Feb 2015)

Hi John,

I have several questions concerning your article "Optimizing Magnetically Coupled Loop Antennas," which appeared in the January/February 2015 issue of QEX.

Question 1: On Page 21, on the 5th line of the paragraph above the "Examples of Improved AM Broadcast Band Reception" heading, The sentence reads, "...and a = 15 inches × 0.0254 inches/cm/2 = 0.1635 m. Shouldn't the results be 0.1905 m?"

Question 2: I also wonder if equation A-27 is correct. I have used the values given in the text, and try as I might, I cannot calculate the values of inductance shown in Table A-1. Nor can I verify this equation, since it doesn't seem to appear anywhere else in the articles I've found on the Internet. The primary problem appears to be the $\sinh(x)$ hyperbolic function. Using the terms $(\pi)^{a/b}$ returns values that are extremely large. Other references seem to use the inverse of this ratio when the coil is of large diameter and has few turns. I wonder if there is a typo.

I enjoyed the article, as I do all the others you have in QEX and am interested in this subject area. Thanks for your continued excellence and please keep up the good work.

— Thanks, and 73, Richard Corey,
W8IMA, 7652 Lilac Dr, Jenison, MI,
49428; w8ima.richard@sbcglobal.net


Hi Richard,

Thank you for your questions and the diligence that they reflect.

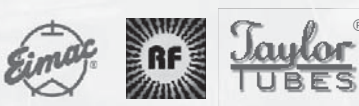
For your Question 1: Rechecking the calculation gives 0.1905 m instead of 0.1635 m. This was apparently a typo in the manuscript for that distance, but not an error in the overall inductance calculation because I'm still getting 3.7 μH for the calculated mutual inductance for the 15 inch loop, as I reported in the article.

For your Question 2: This error occurred between my original submission and the edited version of the manuscript and I didn't catch it. Equation A-27 is calling for the

From **MILLIWATTS**
To **KILOWATTS**
More Watts per Dollar



Transmitting & Audio Tubes



**COMMUNICATIONS
BROADCAST
INDUSTRY
AMATEUR**

Immediate Shipment from Stock

3CPX800A7	4CX1000A	810
3CPX1500A7	4CX1500B	811A
3CX400A7	4CX3500A	812A
3CX800A7	4CX5000A	833A
3CX1200A7	4CX7500A	833C
3CX1200D7	4CX10000A	845
3CX1200Z7	4CX15000A	6146B
3CX1500A7	4CX20000B	3-500ZG
3CX3000A7	4CX20000C	3-1000Z
3CX6000A7	4CX20000D	4-400A
3CX10000A7	4X150A	4-1000A
3CX15000A7	572B	4PR400A
3CX20000A7	805	4PR1000A
4CX250B	807	...and more!

Se Habla Español • We Export


Phone: **760-744-0700**

Toll-Free: **800-737-2787**
(Orders only) **RF PARTS**

Website: **www.rfparts.com**

Fax: **760-744-1943**
888-744-1943

Email: **rpf@rfparts.com**



RF PARTS COMPANY

inverse hyperbolic sine, \sinh^{-1} , or asinh . Specifically, the Equation should read:

$$L = \mu_0 n^2 a \left[0.48 \ln \left(1 + \pi \frac{a}{b} \right) + 0.52 \operatorname{asinh} \left(\pi \frac{a}{b} \right) \right]$$

[Eq A-27]

— 73, John E. Post, KA5GSQ, Embry-Riddle Aeronautical University, 3700 Willow Creek Road, Prescott, AZ 83630; john.post.erau.edu

Hi Richard and John,

The error in typesetting Equation A-27 was mine. When I created the *MathType* equation in Microsoft *Word* to format it for the typesetting process, I did not notice that the program automatically inserted a space between the a and the sinh abbreviation for the hyperbolic sine function. *MathType* interpreted the “a” as a variable along with the sinh function. I should have recognized that error, and defined the asinh term as a

function, as I did for the equation given above. I apologize for that error, and for the confusion that it caused.

I should also have double checked the calculations in that example on page 21 before we published the article, but I did not. — 73, Larry Wolfgang, WR1B, QEX Editor; lwolfgang@arrrl.org

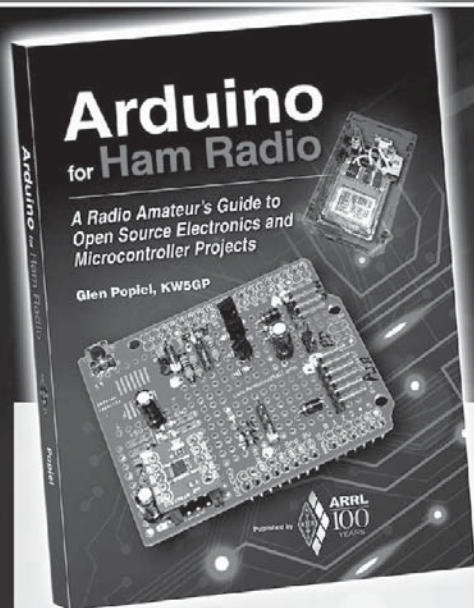
Notes

- ¹Maynard Wright, W6PAP, “Octave for SWR,” *QEX*, Jan/Feb, 2009, pp 37 – 40.
- ²Maynard Wright, W6PAP, “More Octave for SWR,” *QEX*, Jan/Feb, 2014, pp 31 – 33
- ³*IEEE Dictionary of Electrical and Electronics Terms*, Fourth Edition, IEEE, 1988.
- ⁴*Reference Data for Radio Engineers*, Fourth Edition, ITT, 1956.
- ⁵This does not violate the conditions for maximum power transfer because matching the load to the source yields maximum power transfer (conjugate match) only when the load is adjustable and the source is fixed. When the source is adjustable, maximum power is transferred by making the source

impedance as low as possible.

- ⁶B. Whitfield Griffith, Jr., *Radio-Electronic Transmission Fundamentals*, McGraw-Hill, 1962, pp 203 – 204.
- ⁷Maynard Wright, W6PAP, “Octave for Transmission Lines,” *QEX*, Jan/Feb, 2007, pp 3 – 8.
- ⁸For more information about *Octave*, or to download a copy of the software (Revision 3.8.1), go to the official *Octave* website: www.octave.org
- ⁹Robert A. Chipman, *Schaum's Outline Series Theory and Problems of Transmission Lines*, McGraw-Hill, Inc., 1968, p 130
- ¹⁰IEEE 754-2008, *IEEE Standard for Floating-Point Arithmetic*, The Institute of Electrical and Electronics Engineers, Inc.
- ¹¹Be careful, though: although Inf is accepted as an argument or returned from certain trigonometric or hyperbolic functions in *Octave*, the use of Inf in arithmetic computations will lead to unexpected and incorrect results. $\operatorname{isfloat}(\operatorname{Inf})$ returns true, but $\operatorname{Inf} - \operatorname{Inf}$ returns NaN rather than 0.
- ¹²For the latest version of *Python* (Revision 2.7.6) go to: www.python.org.
- ¹³Maynard Wright, W6PAP, “Alternatives to Octave,” *QEX*, Jul/Aug, 2009, pp 25 – 27.

Arduino Microcontroller Projects You Can Build Today!



Arduino for Ham Radio

A Radio Amateur's Guide to Open Source Electronics and Microcontroller Projects
By Glen Popiel, KW5GP

The Arduino has become widely popular among hobbyists and ham radio operators. **Hams are exploring these powerful, inexpensive microcontrollers, creating new projects and amateur station gear. With its Open Source model, the Arduino community freely shares software and hardware designs, making projects easier to build and modify.**

Arduino for Ham Radio introduces you to the exciting world of microcontrollers and Open Source hardware and software. It starts by building a solid foundation through descriptions of various Arduino boards and add-on components, followed by a collection of ham radio-related practical projects. Beginning with simple designs and concepts and gradually increasing in complexity and functionality, there is something here for everyone. Projects can be built quickly and used as-is, or they can be expanded and enhanced with your own personal touches.

Arduino for Ham Radio
ARRL Order No. 0161
Special Member Price! Only \$29.95* (retail \$34.95)
Order Online www.arrrl.org/shop
Call Toll-Free **1-888-277-5289** (US)



ARRL The national association for AMATEUR RADIO®

*Shipping and Handling charges apply. Sales Tax is required for all orders shipped to CT, VA, and Canada. Prices and product availability are subject to change without notice.

QEX 10/2015

Upcoming Conferences

The 34th Annual ARRL and TAPR Digital Communications Conference

Chicago, Illinois
October 9 – 11, 2015
DoubleTree by Hilton Chicago -
Arlington Heights
75 West Algonquin Road,
Arlington Heights, IL 60005
Reservation Phone: 847-364-7600

Reservation Website: doubletree.hilton.com/en/dt/groups/personalized/C/CHIARDT-DCC-20151007/index.jhtml

It is not too late to make plans to attend the premier technical conference of the year, the 34th Annual ARRL and TAPR Digital Communications Conference. This year's DCC will be held October 9 – 11, 2015 in Chicago, Illinois, at the DoubleTree by Hilton Chicago, in Arlington Heights, IL. Regular attendees will note that the conference is a couple of weeks later than normal this year. It is the Columbus Day Weekend.

The ARRL and TAPR Digital Communications Conference is an international forum for radio amateurs to meet, publish their work, and present new ideas and techniques. Presenters and attendees will have the opportunity to exchange ideas and learn about recent hardware and software advances, theories, experimental results, and practical applications.

Topics include, but are not limited to: Software defined radio (SDR), digital voice (D-Star, P25, WinDRM, FDM DV, G4GUO), digital satellite communications, Global Position System (GPS), precision timing, Automatic Packet Reporting System® (APRS), short messaging (a mode of APRS), Digital Signal Processing (DSP), HF digital modes, Internet interoperability with Amateur Radio networks, spread spectrum, IEEE 802.11 and other Part 15 license-exempt systems adaptable for Amateur Radio, using TCP/IP networking over Amateur Radio, mesh and peer to peer wireless networking, emergency and Homeland Defense backup digital communications, using Linux in Amateur Radio, updates on AX.25 and other wireless networking protocols and any topics that advance the Amateur Radio art.

This is a three-Day Conference (Friday,

Saturday, and Sunday). Technical sessions will be presented all day Friday and Saturday. In addition there will be introductory sessions on various topics on Saturday.

Join others at the conference for a Friday evening social get together. A Saturday evening banquet features an invited speaker and concludes with award presentations and prize drawings.

The ever-popular Sunday Seminar has not been finalized yet, but is always an excellent program. This is an in-depth four-hour presentation, where attendees learn from the experts. Check the TAPR website for more information: www.tapr.org.

Plan to bring a project or two to display and talk about in the popular Demonstration Room, or "Play Room" as it is commonly known.

Microwave Update

October 15 – 18, 2015
San Diego, California
Crowne Plaza San Diego
2270 Hotel Circle North
San Diego, CA 92108
Reservation Phone: 888-233-9527

Microwave Update (MUD), the paramount international conference on Amateur Radio experimentation above 1,000 MHz, will take place on Thursday, October 15 to Sunday, October 18, 2015 at the Crowne Plaza San Diego.

MUD 2015 will include technical programs, a banquet and the opportunity to network with fellow microwave ham radio enthusiasts from around the world. This year's event is sponsored jointly by the San Bernardino Microwave Society (SBMS) and the Microwave Group of San Diego (MGSD). MUD 2015 has been approved as an official ARRL Specialty Convention.

Special hotel rates are available to MUD 2015 attendees if booked by September 14. Be sure to mention the Microwave Update 2015 when making hotel reservations.

Call for Papers and Presentations

MUD is a great opportunity to share your ideas by presenting and writing papers. If you are interested in writing and/or presenting a topic for the 2015 MUD, send an e-mail message to mud2015-presentations@ham-radio.com with an abstract or

a general idea. This will help the conference planning and scheduling team organize the event.

Presentation and paper guidelines are posted at www.ham-radio.com/sbms/mud2015/mud2015_call_for_Papers.pdf. The deadline for *Proceedings* submissions is September 1 and deadline for presentations is September 25.

This conference features a full schedule of presentations, with a special EME track on Sunday. The keynote speaker at the Saturday evening banquet will be Jim Lux, W6RMK, the project manager for JPL's FINDER rescue radar.

For more information and the latest updates on MUD 2015, go to: www.ham-radio.com/sbms/mud2015/. If you need any additional information, please contact MUD 2015 chairman Pat Coker, N6RMJ, at n6rmj@sbcglobal.net.

AMSAT Symposium

Dayton, Ohio
October 16 – 18, 2015
Crowne Plaza
33 East 5th Street
Dayton, OH
Hotel Reservation Phone:
877 270 1393

The 2015 AMSAT Space Symposium will be held on Friday through Sunday, Oct 16, 17, 18, 2015 in Dayton, Ohio. The location is the Crowne Plaza, 33 East 5th Street, in Downtown, Dayton. The Crown Plaza has been recently renovated.

The annual AMSAT Space Symposium features:

Space Symposium with Amateur Satellite Presentations.

Operating Techniques, News, & Plans from the Amateur Satellite World.

Board of Directors Meeting open to AMSAT members.

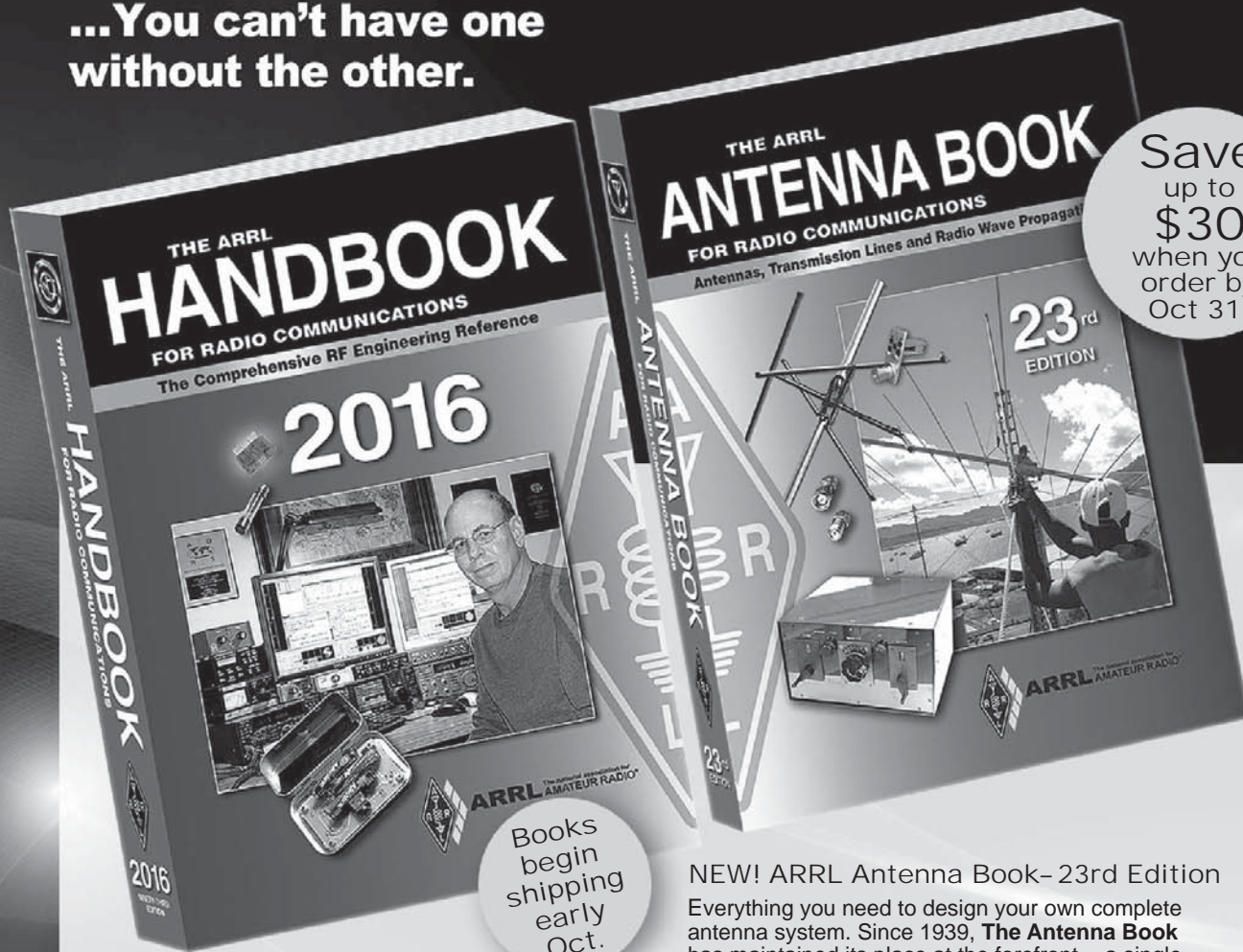
Opportunities to Meet Board Members and Officers.

AMSAT-NA Annual General Membership Meeting.

Annual Banquet, Keynote Speaker and Door Prizes!

For updates and further information, check the AMSAT website: www.amsat.org.

Radios and Antennas: ...You can't have one without the other.



Books begin shipping early Oct.

NEW! ARRL Handbook – 2016 Edition
THE standard reference for electronic fundamentals, radio design, and wireless communication. Since 1926, **The Handbook** has kept radio amateurs immersed in applied theory and do-it-yourself projects.
Fully searchable CD-ROM inside!

NEW! ARRL Antenna Book– 23rd Edition
Everything you need to design your own complete antenna system. Since 1939, **The Antenna Book** has maintained its place at the forefront—a single resource covering antenna theory, design and construction, and practical treatments and projects.
Fully searchable CD-ROM inside!

System Requirements: Windows® 7, Windows Vista®, or Windows® XP, as well as Macintosh® systems, using Adobe® Acrobat® Reader® software. The Acrobat Reader is a free download at www.adobe.com. PDF files are Linux readable. The ARRL Antenna Book utility programs are Windows® compatible, only.

Special Offer! Get the **HARDCOVER** editions for the **softcover** price when you order now or while supplies last. Save an additional \$10 when you Double-Up and order both books online by **October 31**. Enter Coupon Code **QEX** at www.arrl.org/shop.

Hardcover Handbook 2016 Edition. Retail ~~\$59.95~~
Special Offer! Save \$10 Only \$49.95*
ARRL Item No. 0420

Hardcover Antenna Book 23rd Edition. Retail ~~\$59.95~~
Special Offer! Save \$10 Only \$49.95*
ARRL Item No. 0390

Softcover Handbook 2016 Edition. Retail \$49.95*
ARRL Item No. 0413

Softcover Antenna Book 23rd Edition. Retail \$49.95*
ARRL Item No. 0444

Get this exclusive offer when you order both books in **hardcover, softcover or combination of both**, online, now through October 31, 2015. When prompted for a Coupon Code type **QEX** (one coupon code per order). The additional \$10 savings will automatically be applied. Valid on retail orders from ARRL, only.

*Actual dealer prices may vary. Shipping and handling charges apply. Sales Tax is required for all orders shipped to CT, VA, and Canada. Prices and product availability are subject to change without notice.



Toll-Free US 888-277-5289,
or elsewhere +1-860-594-0355



EXPERT LINEARS *America* LLC

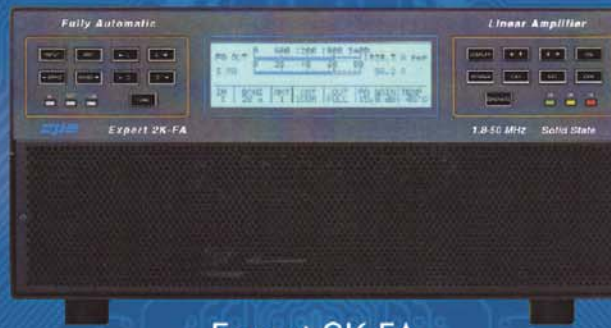
281-259-7877

Authorized Distributor for  Linear Amplifiers

**FULLY AUTOMATIC SOLID STATE LINEAR POWER AMPLIFIERS
MOST TECHNOLOGICALLY ADVANCED IN THE WORLD!**



Expert 1.3K-FA



Expert 2K-FA



Expert 1K-FA

SUPERIOR OPERATING CAPABILITIES

Includes Power Supply & Automatic Antenna Tuner
Follows Transceiver & Fully Remoteable!

Automatically Changes Bands, Antennas & Stores in Memory

The CPUs intelligently protect & control the linears plus produce warning & alarm messages.

Expert Linears America, LLC Offers SALES & EXPERT SERVICE

- ★ On-Site SPE Factory-Trained with over 3½ years Servicing & Repairing Expert Amps
- ★ Fast Turnaround Service
- ★ Enhanced Warranty *see website for details*
- ★ Over 50 years RF Experience
- ★ Over 60 years Ham Radio experience



EXPERT LINEARS AMERICA, LLC
PO Box 1224, Magnolia, TX 77355 | 281-259-7877 | 281-725-2113
Contact: Bob Hardie W5UQ | Bob@ExpertLinears.com

ExpertLinears.com

Quicksilver Radio

Test Equipment

USB Microscope



Up to 500X magnification. Captures still images and records live video. Built in LED Lighting. A must for working on surface mount components.

Wireless Relay Switch



200'+ Range. We have single, four, and eight channel models.

GO-PWR Plus™



Portable power to go or backup in the shack. Includes Powerpoles, bright easy to read meter, and lighted switch. For U1 size (35 ah) and group 24 (80 ah) batteries.



Digital Voltmeter/Ammeter

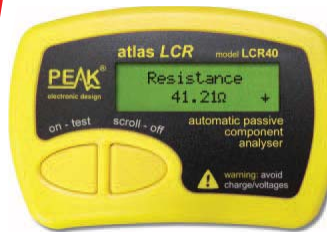
Two line display shows both current and voltage. Included shunt allows measurement up to 50A and 99V. Snaps into a panel to give your project a professional finish.

LCR and Impedance Meter



Newest Model. Analyzes coils, capacitors, and resistors. Indicates complex impedance and more.

Automatic Passive Component Analyzer



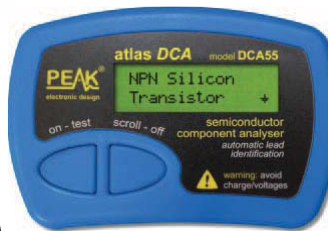
Analyzes coils, capacitors, and resistors.

Advanced Semiconductor Component Analyzer



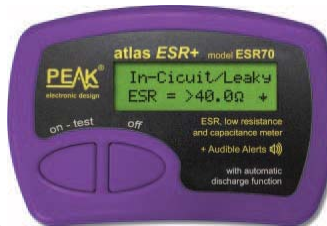
Analyzes transistors, MOSFETs, JFETs, IGBTs, and more. Graphic display. Enhanced functionality with included PC software.

Semiconductor Component Analyzer



Analyzes transistors, MOSFETs, JFETs and more. Automatically determines component pinout.

Capacitance and ESR Meter



Analyzes capacitors, measures ESR.

Get All Your Ham Shack Essentials at Quicksilver Radio Products. Safe and Secure Ordering at:

www.qsradio.com

